



# Structural and Functional Organization of Synaptic Proteins in *Drosophila melanogaster*

**Thesis for a doctoral degree**

**Faculty of Biology, Julius-Maximilians-Universität**

**Würzburg,**

**Submitted by**

**Rui Tian**

**From Peking**

**Würzburg 2011**

**Submitted on:**

**Office stamp**

**Members of the *Promotionskomitee*:**

**Chairperson: Prof. Dr. Thomas Dandekar**

**Primary Supervisor: Prof. Dr. Stephan Sigrist**

**Supervisor (Second): Prof. Dr. Erich Buchner**

**Date of Public Defence:**

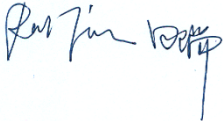
**Date of receipt of Certificates:**

## **Erklärung**

Erklärung gemäß § 4 Absatz 3 der Promotionsordnung der Fakultät für Biologie der Bayerischen Julius-Maximilians-Universität Würzburg vom 15. März 1999.

Hiermit erkläre ich, dass ich die vorliegende Dissertation selbständig verfasst habe und keine anderen als die von mir angegebenen Quellen und Hilfsmittel verwendet habe. Alle aus der Literatur entnommenen Stellen sind als solche gekennzeichnet. Die Dissertation wurde weder in gleicher noch in ähnlicher Form bereits in einem anderen Prüfungsverfahren vorgelegt. Zuvor habe ich keine akademischen Grade erworben oder zu erwerben versucht.

Rui Tian

A handwritten signature in blue ink, appearing to read 'Rui Tian', is placed over a light blue rectangular background.

Würzburg, den 15.03.2011

# **Acknowledgements**

**I would like to thank my instructor and supervisor Prof. Dr. Stephan Sigrist for giving me the opportunity to conduct exciting cutting-edge scientific studies in his research group. During my whole thesis period, I was encouraged by our extensive and enthusiastic discussion, from which I really have learned a lot. His talent and passion in science impressed me really. I would also like to thank my supervisor Prof. Dr. Erich Buchner, Prof. Dr. H. Hilger Ropers, Dr. Andreas W. Kuss and Prof. Dr. Volker Haucke for sharing their experience in discussions and supporting me on my project. Prof. Dr. Erich Buchner gave me deep impression of his kindness and nice personality.**

**I am appreciating the nice cooperation with Jasmin Podufall, Till Andlauer, Dr. Carolin Wichmann, Dr. Wernher Fouquet, Karen Liu, Omid Khorramshahi, Harald Depner and Sara Mertel. I also thank Dr. Tobias Schwarz, Frauke Christiansen-Engelhart, David Oswald, Dr. Robert Kittel, Dr. Carola Sigrist, Dr. Birgit Greiner and Christian Werner for the nice working atmosphere, their contributions to this work, and constant support. In addition, I thank Christine Quentin, Claudia Wirth and Franziska Zehe for the indispensable and excellent technical assistance, and Eva Albero for friendly and reliable coordination.**

**Thank you to my friends, particularly YuMei, DongJiao, HaiMing and Xue for supporting me in difficult times, while always letting me feel positive and happy. I would like to thank my parents MeiYe and HaoYi and my family, which always encouraged me in my life. Sincerely, I thank my husband, Zhen Liang, who supported me spiritwise always during these years. Specially, I thank my dear son, Jia Hui for bringing me a wonderful life and encouraging me in my life.**



# Contents

CONTENTS.....	2
1. ZUSAMMENFASSUNG .....	4
1. SUMMARY .....	7
2. INTRODUCTION .....	9
2.1 SYNAPSE .....	9
2.2 PRESYNAPSE .....	10
2.2.1 Exocytosis and endocytosis .....	10
2.2.2 $Ca^{2+}$ ions in synaptic transmission.....	11
2.2.3 Structural and molecular organization of the AZ .....	11
2.2.4 ELKS/CAST/ERC/Brp proteins .....	13
2.3 POSTSYNAPTIC SPECIALIZATION .....	15
2.4 SYNAPTIC TRANSPORT .....	18
2.5 APOPTOTIC DEATH OF NEURONS .....	20
2.5.1 Cell death intracellular effectors .....	21
2.6. FUNCTIONAL ANALYSIS OF SYNAPTIC AND NEURONAL PROTEINS IN <i>DROSOPHILA MELANOGASTER</i> .....	23
2.6.1 <i>Drosophila melanogaster</i> as a model organism for genetic analysis.....	23
2.6.2 The Neuromuscular junction of <i>Drosophila</i> .....	24
2.6.3 Organization and development of <i>Drosophila</i> NMJ synapses.....	26
2.7 OBJECTIVES .....	27
2.7.1 DREP proteins.....	27
2.7.2 GIT .....	28
2.7.3 DJM-1 .....	32
3. MATERIALS AND METHODS .....	33
3.1 MOLECULAR BIOLOGY .....	33
3.1.1 Materials.....	33
3.1.2 Buffer solutions .....	34
3.1.3 Construction of fluorophore tagged proteins.....	35
3.1.4 In situ hybridization.....	40
3.1.5 Production of DREP-2 antibody .....	44
3.2 <i>DROSOPHILA MELANOGASTER</i> .....	49
3.2.1 Fly culturing.....	49
3.2.2 Transgenesis.....	49
3.2.3 The UAS/Gal4 system and drivers .....	49
3.2.4 FLP-FRT recombination deletion .....	51
3.2.5 P-element imprecise excision screen .....	52
3.3 YEAST TWO-HYBRID .....	53
3.4 CELL CULTURE AND CoIP .....	54
3.4.1 Cell culture .....	55
3.4.2 Cell lysis.....	55
3.4.3 Immunoprecipitation.....	55
3.4.4 Western blot.....	56
3.5 NMJ IMMUNOHISTOCHEMISTRY .....	56
3.5.1 Material.....	56
3.5.2 Larval body wall preparation .....	56
3.5.3 Fixation and staining procedures .....	57
3.6 IMAGE ACQUISITION .....	59
3.6.1 Procedures for fixed samples imaging .....	59
3.6.2 In vivo imaging .....	59
3.7 IMAGE PROCESSING AND ANALYSIS .....	61

3.7.1 Software .....	61
3.7.2 Image quantifications .....	61
3.7.3 Statistical analysis .....	62
3.8 EM .....	62
3.8.1 Image acquisition .....	62
3.8.2 Statistics of the EM images .....	63
3.9 BEHAVIORAL ASSAYS .....	63
<b>4. RESULTS PART1: FUNCTIONAL ANALYSIS OF DREP-2, A NOVEL SYNAPTIC PROTEIN OF <i>DROSOPHILA</i></b> .....	<b>65</b>
4.1 IDENTIFICATION OF DREP-2 WITHIN BRP IMMUNOPRECIPITATES .....	65
4.2 DREP-2 - STRUCTURAL CONSIDERATIONS .....	67
4.3 DREP-2 IS SPECIFICALLY EXPRESSED IN THE NERVOUS SYSTEM .....	69
4.4 GENERATING TOOLS FOR ANALYSIS OF DREP-2: MUTANTS AND ANTIBODIES .....	70
4.4.1 Generation of a <i>drep-2</i> deletion mutant .....	70
4.4.2 Generating a polyclonal anti-DREP-2 antibody and transgenic flies of full length DREP-2 .....	72
4.5 DREP-2 AND DREP-4 LOCALIZE AT SYNAPSES OF THE FLY CNS .....	75
4.5.1 DREP-2 is a <i>neuroligin</i> specific protein .....	75
4.5.2 Synaptic localization of DREP-4 in the fly CNS .....	77
4.6 <i>DROSOPHILA</i> DREP-2 MUTANTS POTENTIALLY SHOW A NMJ MORPHOLOGICAL PHENOTYPE .....	80
4.7 BIDIRECTIONAL AXONAL TRANSPORT OF DREP-2-CONTAINING COMPLEXES .....	82
4.8 DREP-2 MUTANT MIGHT SHOW AN ACCUMULATION OF FLOATING ELECTRON DENSE STRUCTURE AND LARGE SIZE VESICLES BY EM .....	83
4.9 DISCUSSION .....	85
4.9.1 DREP-2 interacts with <i>Brp</i> .....	85
4.9.2 Is DREP-2 involved in trafficking or anchoring of target proteins to the membrane? .....	86
4.9.3 DREP family and apoptosis .....	88
<b>5 RESULTS PART2: ANALYZING SYNAPTIC FUNCTIONS OF <i>DROSOPHILA</i> GIT</b> .....	<b>91</b>
5.1 MUTATIONAL ANALYSIS OF <i>DROSOPHILA</i> GIT .....	93
5.2 EXPRESSION OF <i>DROSOPHILA</i> GIT .....	94
5.3 DGIT ASSOCIATES WITH STNB .....	97
5.4 ACTIVE ZONES AND POSTSYNAPTIC DENSITIES OF DGIT MUTANT NMJs .....	99
5.5 REDUCTION IN STNB LEVEL AT DGIT MUTANT NMJs .....	101
5.6 ABNORMAL ULTRASTRUCTURE OF DGIT MUTANT NMJs .....	103
5.7 NERVOUS SYSTEM MEDIATED LOCOMOTION-DEFICITS IN DGIT MUTANTS .....	107
5.8 DISCUSSION .....	109
5.8.1 Synaptic vesicle recycling and endocytosis .....	109
5.8.2 Receptor internalization and membrane trafficking .....	110
<b>6. RESULTS PART3: FUNCTIONAL ANALYSIS OF <i>DJM-1</i></b> .....	<b>112</b>
6.1 EFFECT OF RNAi VERSUS DJM-1 ON FLY VIABILITY .....	113
6.2 TISSUE DISTRIBUTION FOR DJM-1 mRNA .....	114
6.3 GENERATING MUTANTS FOR DJM-1 .....	116
6.4 ANALYSIS OF LOCOMOTION ABILITIES DEFICITS OF DJM-1 MUTANTS .....	117
<b>7. REFERENCES</b> .....	<b>120</b>
<b>8. APPENDIX</b> .....	<b>145</b>
8.1 TABLE OF FIGURES .....	145
8.2 ABBREVIATIONS .....	147
8.3 PUBLICATIONS .....	152

# **1. Zusammenfassung**

Es wird angenommen, dass strukturelle und funktionale Änderungen an synaptischen Verbindungen („synaptische Plastizität“) die Grundlage für Lern- und Gedächtnisprozesse darstellen. Daher sind die molekularen Mechanismen des strukturellen und funktionalen Aufbaus von Synapsen wichtig für das Verständnis von neuronaler Entwicklung sowie von Lern- und Gedächtnisprozessen.

Synapsen werden durch eine asymmetrische Verbindung von zwei hochspezialisierten Membranen gebildet: An der präsynaptischen aktiven Zone fusionieren mit Transmittern gefüllte Vesikel, während Transmitterrezeptoren in der gegenüberliegenden postsynaptischen Dichte dieses Signal wahrnehmen. Durch genetische Analysen wurde gezeigt, dass Matrixproteine der aktiven Zone verschiedener Familien wichtig für die schnelle Vesikelfusion sind. Es wird angenommen, dass diese Proteine zu synaptischer Stabilität und dem Aufbau von Synapsen beitragen. Das Labor von Stephan Sigrist hat in einer Kollaboration mit dem Labor von Erich Buchner in der Vergangenheit gezeigt, dass das große Gerüstprotein Bruchpilot (Brp) essentiell für sowohl die strukturelle und funktionale Intaktheit von aktiven Zonen als auch für synaptische Plastizität in *Drosophila melanogaster* ist. Im Zuge dieser Doktorarbeit wurden mehrere Kandidatenproteine untersucht, die vermutlich eine Rolle in prä- und postsynaptischen Funktionen spielen, was folgendermaßen zusammengefasst werden kann:

1. DREP-2 (DFF45 related protein 2) wurde von Dr. Manuela Schmidt durch Koimmunpräzipitationen mit Anti-Brp Antikörpern gefunden (unveröffentlichte Daten). Mutanten und Antikörper für die weitere Untersuchung von DREP-2 wurden im Zuge dieser Doktorarbeit erzeugt.

Die Ergebnisse aus Hefe-Zwei-Hybrid Versuchen legen nahe, dass DREP-2 mit Dynein light chain 2 interagieren könnte, während *in vivo* Bildung darauf hindeutet, dass DREP-2 in bidirektionalen axonalen Transport involviert sein könnte.

2. Koimmunpräzipitations- und Pulldown-Experimente ließen den Schluss zu, dass das ARFGAP-Protein (ADP-ribosylation factor (ARF)-directed GTPase activating proteins (GAPs)) GIT (G-protein coupled receptor kinase interacting protein) mit dem mit Endozytose assoziierten Protein Stoned B (StnB) interagieren könnte.

Elektronenmikroskopie der neuromuskulären Synapse von Larven im dritten Larvalstadium, die mutant für das *dgut*-Gen sind, zeigte eine Akkumulation von großen Vesikeln und Membran-Zwischenprodukten sowie eine verringerte Vesikeldichte. Zwei der Phänotypen, die Akkumulation großer Vesikel und der Membran-Zwischenprodukte, konnten durch die Expression von *Drosophila* GIT (DGIT) oder menschlichem GIT im *dgut*-mutanten Hintergrund teilweise ausgeglichen werden. Darüberhinaus wurde über Immunofluoreszenz deutlich, dass die *dgut*-Mutante eine spezifisch reduzierte Menge an StnB enthält, was durch die Expression von DGIT teilweise ausgeglichen werden konnte. Diese Ergebnisse unterstützen die Vorstellung sehr, dass DGIT mit StnB interagiert.. StnB spielt eine Rolle bei der Regulierung von Vesikelgrößen, Endozytose und der Wiederverwertung von synaptischen Vesikeln. Darüberhinaus zeigen *dgut* Mutanten Hinweise auf eine fehlerhafte Lokalisierung des präsynaptischen Proteins Brp relativ zu dem postsynaptischen Protein GluRIID, was durch die Expression von DGIT oder menschlichem GIT im *dgut*-mutanten Hintergrund ausgeglichen werden konnte, nicht jedoch durch StnB. Diese Ergebnisse legen den Schluss nahe, dass GIT einerseits eine Rolle bei der Regulierung der

Endozytose synaptischer Vesikel spielt aber möglicherweise auch eine strukturelle Funktion beim Aufbau von Synapsen hat.

3. *Djm-1* ist ein genetischer Locus, der geistige Behinderung bei menschlichen Patienten hervorruft, wenn er mutiert vorliegt. Als ersten Schritt in Richtung eines Verständnisses der mechanistischen Rolle von DJM-1, wurde Genetik in *Drosophila* durchgeführt, um die Funktion von DJM-1 zu untersuchen. Die in dieser Doktorarbeit erzeugte *djm-1* Mutante zeigte jedoch bisher keinen anomalen Phänotyp im Nervensystem.

# **1. Summary**

Structural and functional modifications of synaptic connections (“synaptic plasticity”) are believed to mediate learning and memory processes. Thus, molecular mechanisms of how synapses assemble in both structural and functional terms are relevant for our understanding of neuronal development as well as the processes of learning and memory.

Synapses form by an asymmetric association of highly specialized membrane domains: at the presynaptic active zone transmitter filled vesicles fuse, while transmitter receptors at the opposite postsynaptic density sense this signal. By genetic analysis, matrix proteins of active zones from various families have been shown to be important for fast vesicle fusion, and were suggested to contribute to synapse stability and assembly. The Sigrist lab in collaboration with the Buchner lab previously had shown that the large scaffold protein Bruchpilot (Brp) is essential for both the structural and functional integrity of active zones and for synaptic plasticity in *Drosophila melanogaster*. The work described in this thesis investigated several candidate proteins which appear to be involved in pre- and postsynaptic function, as summarized in the following:

(1) DREP-2 (DEF45 related protein-2) had been found by co-immunoprecipitations with anti-Brp antibodies by Dr. Manuela Schmidt (unpublished data). Mutants and antibodies for the further study of DREP-2 were generated in this thesis. Yeast two hybrid results suggest that DREP-2 might interact with dynein light chain 2, while *in vivo* imaging indicates that DREP-2 might be involved in bidirectional axonal transport.

(2) Coimmunoprecipitation and pull down experiments suggested that the ARFGAP [ADP-ribosylation factor (ARF)-directed GTPase activating protein (GAP)] protein GIT (G-protein coupled receptor kinase interacting protein) could interact with the endocytosis associated molecule StnB (StnB). Mutants in the *digit* gene showed an accumulation of large size vesicles, membrane intermediates and decreased vesicle density at the 3<sup>rd</sup> instar larval neuromuscular junction (NMJ) by electron microscopy (EM). The phenotypes accumulation of large size vesicles and membrane intermediates could be rescued partially by expression of *Drosophila* GIT (DGIT) or human GIT in *digit* mutant background. Furthermore, by immunofluorescence the *digit* mutant shows specifically decreased levels of StnB, which could be restored partially by the expression of DGIT. These results strongly support the suggestion that DGIT interacts with StnB, which is involved in the regulation of vesicle size, endocytosis or recycling of synaptic vesicles (SVs). Furthermore, the *digit* mutants also showed signs of a mislocalization of the presynaptic protein Brp relative to the postsynaptic protein GluRIID, which could be rescued by expression of DGIT or human GIT in the *digit* mutant background, but not by StnB. These results suggest that GIT on one hand executes roles in the regulation of synaptic vesicle endocytosis, but potentially also has structural roles for synapse assembly

(3) *Djm-1* is a candidate locus to mediate mental retardation in human patients when it is mutated. As a first step towards an understanding of the mechanistic role of DJM-1, *Drosophila* genetics were used to address DJM-1 *function*. So far, however, the *djm-1* mutant generated in this thesis did not show a nervous system phenotype.

## **2. Introduction**

### **2.1 Synapse**

The adult human brain is estimated to contain  $1-5 \times 10^{14}$  synapses (Drachman, 2005). The word "synapse" originates from "synaptein", which was coined from the Greek "syn-" ("together") and "haptein" ("to clasp") by Sir Charles Scott Sherrington and his colleagues in 1897. Biological synapses include three different types: chemical, electrical and immunological synapses. In an electrical synapse, the membranes of the two communicating neurons are very close at the synapse and are linked together by a gap junction (Fig. 2.1A; Purves, 2001). Electrical synapses are found throughout the nervous system. The postsynaptic potential in electrical synapses is delivered by direct electrical coupling between both neurons, which therefore makes the transmission faster and more reliable than at chemical synapses. However, chemical synapses are more common than electrical synapses. Chemical synapses deliver information from a presynaptic cell to a postsynaptic cell directionally where the membranes of the two adjacent cells are held together by cell adhesion proteins (Fig. 2.1B; Purves, 2001). In response to a potential, synaptic vesicles containing neurotransmitters docked at the presynaptic plasma membrane in regions called active zones (AZ), fuse and release the transmitter. Immediately opposite to the AZ is a region of the postsynaptic cell called the postsynaptic density (PSD) specialized for anchoring and trafficking neurotransmitter receptors and modulating the activity of these receptors. Between the pre- and post-synaptic cells is the synaptic cleft, a gap of ~20 nm width, which allows the neurotransmitter concentration to raise and decrease rapidly (Fig. 2.1B, Purves, 2001; Kandel, 2000).



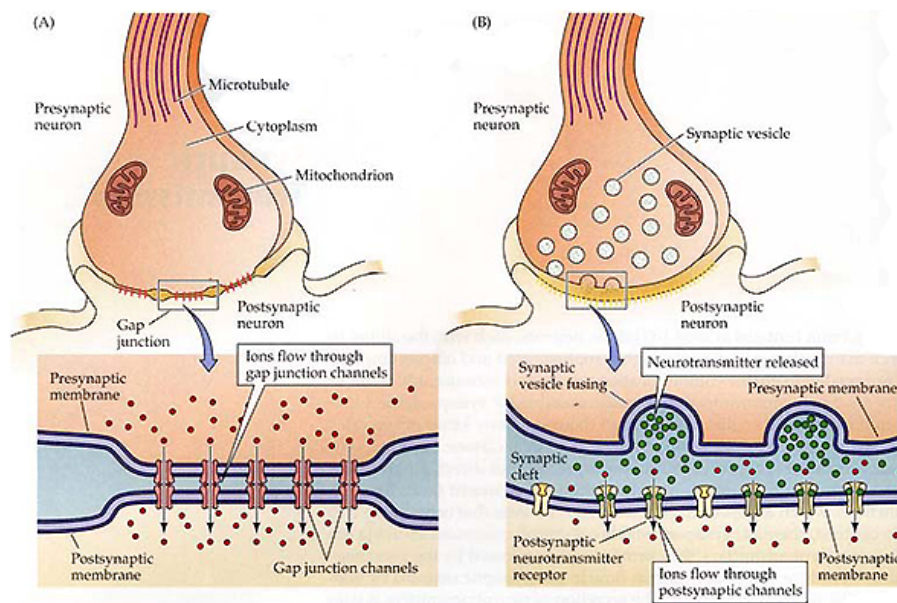


**Figure 2.1 Electrical and chemical synapses.** (A) At electrical synapses, synaptic currents flow through gap junctions between pre- and post-synaptic membranes, followed by initiating or inhibiting the generation of postsynaptic action potentials. (B) At chemical synapses, the secretion of neurotransmitters often provokes immediate opening of postsynaptic ion channels (transmitter receptor molecules), followed by the flow of postsynaptic current resulting in a change of the postsynaptic membrane potential (Adopted from Purves, 2001).

## 2.2 Presynapse

### 2.2.1 Exocytosis and endocytosis

Vesicles participate in a cycle of exocytosis at the active zone and endocytosis at the adjacent periaction zone for enabling their rapid reuse (Südhof, 2004). A popular model suggests that there are three different pools of synaptic vesicles (Sakaba and Neher, 2001; Zucker and Regehr, 2002; Schneggenburger and Neher, 2005; Rizzoli and Betz, 2005): the readily releasable pool where the vesicles are docked and primed to the

active zone membrane for release; the recycling pool where the vesicles maintain transmitter release during moderate physiological stimulation; and the reserve pool where the vesicles as a storage depot participate in release only during strong stimulation and when the recycling pool has been used up. The number of vesicles released at a synapse is dependent on the number of release-ready vesicles and the exocytotic probability of the individual vesicle. Low release probability of vesicles often results in facilitation and augmentation. However, high release probability synapses tend to exhibit paired-pulse and frequency-dependent depression (Zucker and Regehr, 2002).

### **2.2.2 $\text{Ca}^{2+}$ ions in synaptic transmission**

The divalent cation calcium ( $\text{Ca}^{2+}$ ) is essential for transmission of nerve impulses (Locke, 1894). The neurotransmitter release from synaptic vesicles is triggered by elevations of the  $\text{Ca}^{2+}$  concentration in the presynaptic terminal.  $\text{Ca}^{2+}$ -triggered neurotransmitter release requires a molecular coupling of  $\text{Ca}^{2+}$  influx with vesicle fusion at the protein level (Rosenmund, 2003). The vesicle fusion with the active zone membrane, which presumably follows binding of  $\text{Ca}^{2+}$  to the vesicle protein synaptotagmin (Geppert, 1994; Koh and Bellen, 2003), is mediated by SNARE [soluble N-ethylmaleimidesensitive factor attachment protein (SNAP) receptor] proteins, that include the synaptic vesicle protein Synaptobrevin and the plasma membrane protein SNAP-25 and Syntaxin (Jahn, 2003; Südhof, 2004).

### **2.2.3 Structural and molecular organization of the AZ**

The presynaptic active zone is the site where synaptic vesicles are clustered, docked, fused, and the neurotransmitter are released (Fig. 2.2).

By ultrastructural studies shown, the presynaptic active zone is aligned with the PSD, and the plasma membrane on both sides of the synaptic cleft displays electron-dense structures with a proteinaceous nature. Synapses in the central nervous system (CNS) by electron microscopy show that the presynaptic grid or CAZ (cytomatrix at the active zone) is in a web-like pattern by dense projections, which are interconnected by a meshwork of cytoskeletal filaments, and that long filamentous strands extend deeply into the presynaptic boutons (Phillips, 2001; Schoch, 2006). The extent of these electron-dense projections differs greatly amongst different synapse types, ranging from roughly 50 nm high pyramid-shaped particles in synapses of the mammalian CNS (Phillips, 2001), approximately 70 nm long T-shaped protrusions (T-bars) at the *Drosophila* NMJ (Atwood, 1993), to the spherical synaptic ribbons in vertebrate sensory synapses (Lenzi and von Gersdorff, 2001). The active zone is surrounded by the perisynaptic zone, where fused synaptic vesicles are retrieved by clathrin-mediated endocytosis (Gundelfinger, 2003).

A number of proteins involved in assembly of CAZ has already been identified (for reviews, see Dresbach, 2001; Gundelfinger and tom Dieck, 2000; Rosenmund, 2003; Ziv and Garner, 2004; Schoch and Gundelfinger, 2006): (1) cytoskeletal proteins, including tubulin, actin, myosin, spectrin and  $\beta$ -catenin; (2) proteins regulating synaptic vesicle fusion, including SNAP-25, syntaxin and Munc18; (3) scaffolding proteins, such as CASK, Mint, SAP97, and Veli/MALS; (4) voltage-gated calcium channels; and (5) cell adhesion molecules, including neurexins, cadherins, integrins and sidekicks (Fig. 2.2). Six CAZ-enriched protein families have been functionally analyzed: UNC13/Munc13 proteins, RIMs (Rab3-interacting molecule), Bassoon and Piccolo/aczonin, ELKS (ERC/CAST/Brp), and Liprin- $\alpha$ , which could form a scaffold at the active zone, and plays vital

roles in retrieval of fused synaptic vesicles and organizing the transmitter release and in regulating synaptic plasticity in response to short-term and long-term forms of potentiation (for review, see Schoch and Gundelfinger, 2006).

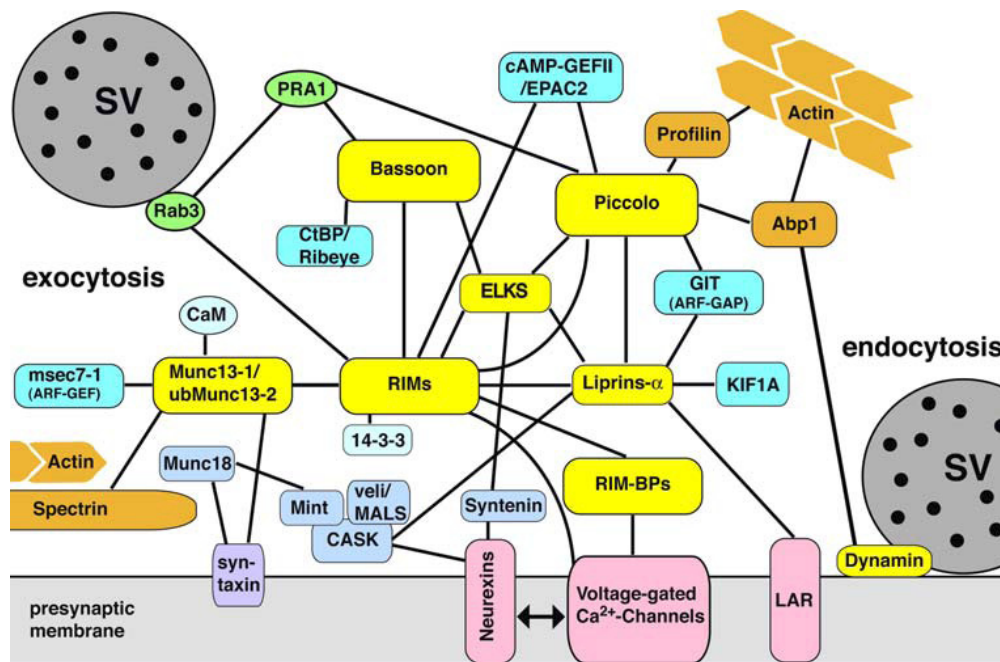


**Figure 2.2 Schematic diagram of interactions of CAZ proteins and the resulting network at the active zone** (Adopted from Schoch and Gundelfinger, 2006).

## 2.2.4 ELKS/CAST/ERC/Brp proteins

ELKS/CAST/ERC proteins, which are characterized by containing a high content in the amino acids glutamate (E), leucine (L), lysine (K) and serine (S), were isolated independently in a yeast two-hybrid screen for RIM binding proteins as ERC (ELKS/Rab6-interacting protein/CAST; Wang, 2002) and in a biochemical screen for proteins enriched in the postsynaptic density fraction as CAST (CAZ-associated structural protein; Ohtsuka, 2002). ELKS is also an essential regulatory subunit of the I $\kappa$ B kinase

complex in the nuclear factor-kappa B (NF- $\kappa$ B) signaling cascade (Ducut Sigala, 2004). Several isoforms of ELKS/CAST/ERC have been reported to be transcribed from two genes (Wang, 2002; Deguchi-Tawarada, 2004). Two isoforms, including CAST1/ERC2 and CAST2 $\alpha$ /ERC1b, contain several coiled-coil domains and a C-terminal IWA motif essential for binding the PDZ domain of RIM1 (Ohtsuka, 2002). ELKS/CAST/ERCs could interact with other CAZ proteins, including Munc-13, RIM1, Piccolo and Bassoon and forms a complex, which is involved in the molecular organization of presynaptic active zones (Ko, 2003), and in regulation of neurotransmitters release (Takao-Rikitsu, 2004).

*Drosophila* Brp shows homology to ELKS in its N-terminus, whereas for the large coiled-coil-rich C-terminus no direct vertebrate homolog has been detected (Kittel, 2006; Wagh, 2006). Different from the mammalian and *C. elegans* ELKS proteins, Brp does not contain a PDZ-interaction motif (IWA) for RIM-binding. Stimulated emission depletion fluorescence microscopy (STED, Hell, 1994) has shown that Brp is localized in donut-shaped structures centered at active zones of neuromuscular synapses (Kittel, 2006). Mutant animals, in which nearly the entire open reading frame is deleted, could form synapses but exhibit a loss of electron-dense projections (T-bars) at active zones and a reduction in the density of calcium channels. In the NMJ of *brp* mutant larvae, the amplitudes of excitatory junctional currents are drastically reduced, the nerve-evoked responses are delayed, and the initial release probability is decreased (Kittel, 2006). These observations suggest that Brp is involved in establishing a matrix essential for ensuring the correct localization of active zone components (e.g., calcium channels) and for the assembly of the T-bar.

## 2.3 Postsynaptic specialization

Glutamate is the major excitatory neurotransmitter in the mammalian central nervous system (Seeburg, 1993). At glutamatergic synapses, fast excitatory transmission acts through binding of glutamate to receptors located in the PSD and the subsequent opening of receptor-coupled ion channels to permit cation influx and postsynaptic depolarization (Fig. 2.3). More generally, glutamate receptors can be classified into two groups: metabotropic GluRs, which are coupled to G-proteins, and ionotropic GluRs. In vertebrates, ionotropic receptors are subdivided into three classes: NMDA (N-methyl-D-aspartate), AMPA ( $\alpha$ -amino-3-hydroxyl-5-methyl-4-isoxalone propionic acid) and kainate receptors (Dingledine, 1999). NMDA receptors have high permeability to  $\text{Ca}^{2+}$  ions, long channel burst time, and voltage dependence (Hille, 2001). These receptors are widely regarded as the main triggers for the induction of long-term potentiation (LTP) together with long-term depression (LTD) (Collingridge, 2004). Non-NMDA receptors form homo- or hetero-oligomers, most likely tetramers (Rosenmund, Stern-Bach et al. 1998), consisting of the subunits GluR1-4 (AMPA type) and GluR5-7 and/or KA1-2 (Kainate type) (Madden 2002). AMPA receptors express the synaptic response during LTP, and are important targets of modulation during synaptic plasticity (Bliss and Collingridge, 1993; Linden and Connor, 1995; Collingridge, 2004). AMPA receptors are likely hetero-oligomeric complexes (Rosenmund, 1998; Madden, 2002). The receptor subunits GluR1-4 are expressed in the mouse hippocampus (Seeburg, 1993; Dingledine, 1999). AMPA receptor subunit composition determines the function of these receptor complexes throughout synaptic plasticity. During LTP, GluR1/GluR2 receptors appear to be transported to the synapse (Shi, 2001), thereby converting previously silent sites into active

synapses in the activity dependent manner, which leads to an enhancement of transmission. GluR2/GluR3 receptor complexes, however, continuously substitute already synaptically localized GluR1/GluR2 receptors, and are thereby thought to preserve the plastic changes (Zhu, 2000). Kainate receptors can trigger NMDA-receptor-independent forms of LTP and are key modulators of network activity (Pinheiro and Mulle, 2006). Furthermore, the subunit-specific regulation of transport and synaptic presentation of receptor complexes are thought to be involved in interactions with PDZ domain-proteins (Shi, 2001).

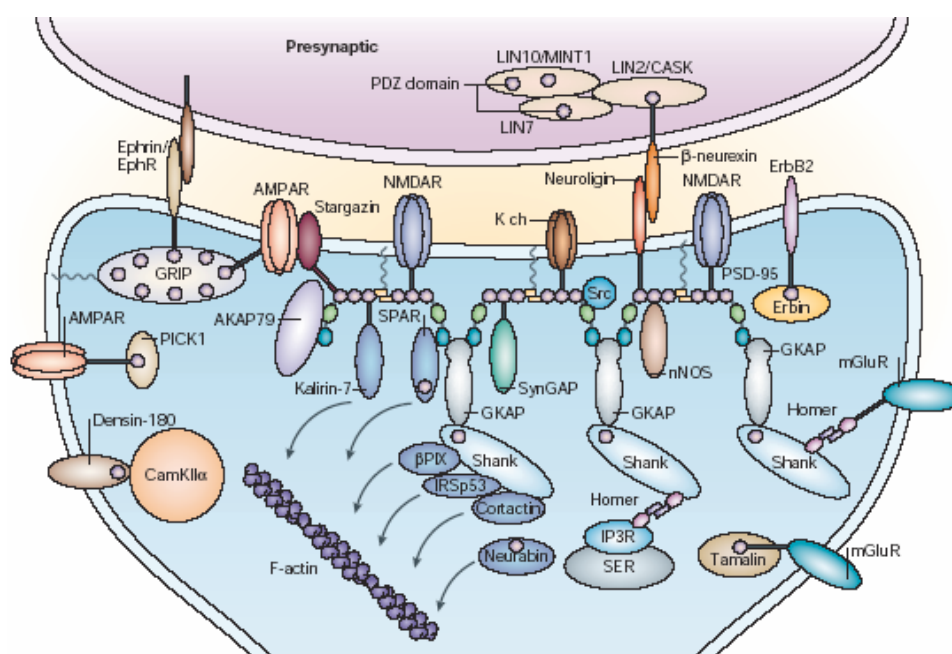


**Figure 2.3 Schematic diagram of the organization of the PSD at a mammalian excitatory synapse.** The main PDZ-containing proteins are shown on the postsynaptic density at the glutamatergic synapse. Purple circles and black lines, respectively, represent PDZ domains and the C-terminal cytoplasmic tails of membrane proteins. Green and blue ellipses in PSD-95 represent SH3 and GK domains, respectively. Crooked lines indicate palmitoylation of PSD-95 and GRIP. Overlap of proteins indicates specific protein–protein interactions. Binding and/or regulatory actions of proteins on the actin cytoskeleton are indicated by grey arrows. AKAP79, A-kinase anchor protein 79; AMPAR, AMPA ( $\alpha$ -amino-3-hydroxy-5-methyl-4-isoxazole propionic acid) receptor;  $\beta$ PIX,  $\beta$ PAK-interactive exchange factor; CaMKII $\alpha$ ,  $\alpha$ -subunit

of  $\text{Ca}^{2+}$ /calmodulin-dependent protein kinase II; GK, guanylate kinase-like domain; Eph, ephrin receptor; ErbB2, EGF-related peptide receptor; GKAP, guanylate kinase-associated protein; GRIP, glutamate-receptor-interacting protein; IP3R, IP3 receptor; IRSp53, insulin-receptor substrate p53; K chi, potassium channel; LIN7, lin7 homolog; LIN10, lin10 homolog; miler, metabotropic glutamate receptor; NMDAR, NMDA (N-methyl-D-aspartate) receptor; none, neuronal nitric oxide synthases; PICK1, protein interacting with C kinase 1; PSD-95, postsynaptic density protein 95; SER, smooth endoplasmic reticulum; SH3, Src homology 3 domain; Shank, SH3 and ankyrin repeat-containing protein; SPAR, spine-associated RapGAP; SynGAP, synaptic Ras GTPase-activating protein (Adopted from Kim and Shang, 2004).

The glutamate receptor subunits expressed at the *Drosophila* NMJ are related to mammalian non-NMDA type glutamate receptors. Five different glutamate receptor subunits, including GluRIIA, IIB, IIC, IID and IIE, have been identified so far (Schuster, Ultsch et al. 1991; Petersen, Fetter et al. 1997; Marrus, Portman et al. 2004; Featherstone, Rushton et al. 2005; Qin, Schwarz et al. 2005). The most likely tetrameric receptor complexes are composed of GluRIIC, GluRIID, GluRIIE and either GluRIIA or GluRIIB (Qin, Schwarz et al. 2005). *gluRIICnull*, *gluRIIDnull* and *gluRIIEnull* single mutants, as well as *gluRIIA&IIB* double mutants (*gluRIIAnullIIBnull*), are embryonic lethal due to the absence of all synaptic glutamate receptors (Petersen, Fetter et al. 1997; Featherstone and Broadie 2002; Marrus, Portman et al. 2004; Qin, Schwarz et al. 2005). GluRIIB complexes show an about 10-fold faster desensitization than GluRIIA complexes, however an unchanged single-channel amplitude (DiAntonio, Petersen et al. 1999). *gluRIIA* mutants shows a strongly decrease in quantal size (miniature evoked junctional current, mEJC) and a concomitant compensatory increase in quantal content (Petersen, Fetter et al. 1997; DiAntonio, Petersen et al. 1999) along with structural alterations in smaller presynaptic terminal area with increased density of T-bars at AZ (Reiff, Thiel et al. 2002).



## 2.4 Synaptic transport

In neurons, the transport of membranous organelles along axons is driven by molecular motors along microtubules (Burton and Paige, 1981). The axonal transport system includes cargo, motor proteins which originate force and drive cargo transport, and linker proteins which attach motor proteins to cargo or other cellular structures, and accessory molecules for initiating and regulating transport. In axon, long-distance transport is in a microtubule-dependent manner, which the microtubule is oriented with the fast-growing (plus) ends toward the synapse and the slow-growing (minus) ends toward the cell body (Fig. 2.4, for review, see Duncan, 2006). The motor proteins identified so far include the kinesin and dynein superfamilies, which drive axonal transport on microtubules (Miki, 2001). Kinesins, generally plus-end-directed motor proteins, transport cargoes, including synaptic vesicle precursors and membranous organelles anterogradely toward the synapse (for review, see Duncan, 2006). Imaging of most anterogradely transported axonal cargoes reveals that they move bidirectionally (Schroer, 1985; Shapira, 2003; Miller, 2005), suggesting that most cargoes are able to associate with both anterograde and retrograde motors. Kinesin heavy chains contains a highly conserved motor domain with ATPase and microtubule-binding regions, and a divergent tail domain binding with regulatory and/or accessory subunits kinesin light chain (Klc) for cargo-binding specificity and regulation (reviewed in Goldstein, 2001a and 2001b). Synaptic vesicle (SV) precursors transported by kinesin-3 heavy chain KIF1A (Okada, 1995) probably combined with the cargo adapter liprin- $\alpha$  (Shin, 2003; Miller, 2005), and Piccolo-Bassoon transport vesicles (PTVs) combined with the syntaxin1–syntabulin adapter complex to the heavy chain of conventional kinesin-1, KIF5B (Cai, 2007).

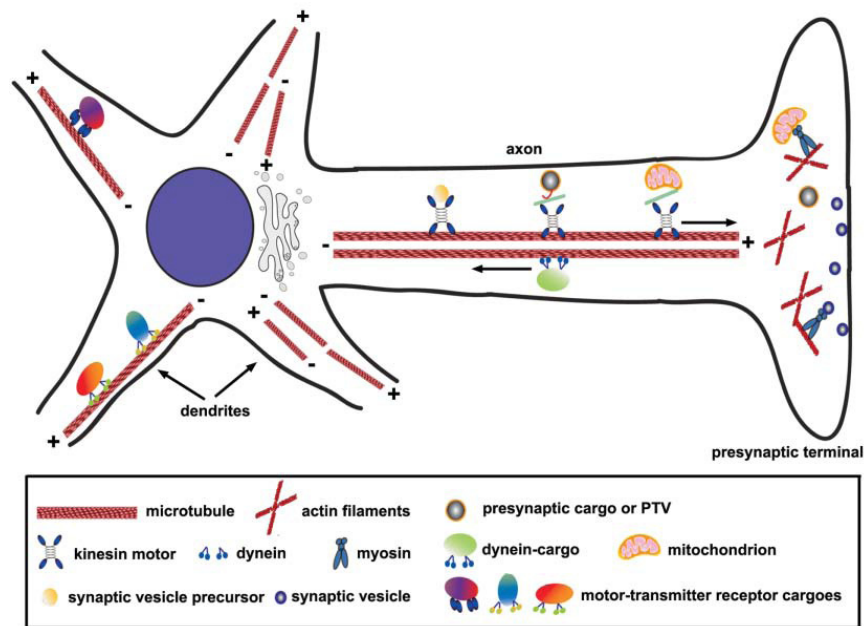


**Figure 2.4 The targeted transport of synaptic cargoes and organelles from the soma to synapses.** In axons, microtubules are uniformly organized with the plus (+) ends toward the synapse and the minus (–) ends toward the cell body. However, in the proximal region of dendrites there is mixed microtubule polarity, but in the distal dendrites there is uniform microtubule arrangement similar to that of the axons. The kinesin motor proteins move mostly toward the plus ends of microtubules, however, dynein are minus end directed. Therefore, the kinesin superfamily motors generally mediate anterograde axonal transport of cargoes, and dynein drives retrograde axonal transport in neurons (Adopted from Cai and Sheng, 2009).

The mammalian cytoplasmic dynein family comprises two dynein heavy chain (Dhc) motor subunits and various intermediate, light intermediate and light chain (DLC) subunits (reviewed in Pfister, 2006). In mammals, two DLC isoforms, DLC-1 and DLC-2, function as a cargo adapter (Puthalakath, 2001) linking cargoes to the dynein motor (Schnorrer, 2000; Navarro, 2004; Lee, 2006) to associate with the actin-dependent motor myosin V (Espindola, 2000). Dynein functioning in axonal retrograde transport is dependent on dynactin, which is proposed to link cytoplasmic dynein to its cargo and/or to increase dynein processivity through an association with microtubules (Waterman-Storer, 1997; LaMonte, 2002).

DLCs have additional motor-independent cellular functions (Jaffrey and Snyder, 1996; Vadlamudi, 2004).

## **2.5 Apoptotic death of neurons**

A plethora of neurons produced in the developing brain need be removed by physiological cell death also called programmed cell death (PCD) without interfering with the further development of remaining cells during embryonic and postnatal refinement of CNS. During development, two waves of neuronal cell death, including early elimination (EE) and PCD (Gilmore, 2000), serve two different purposes: to regulate the neuronal precursor pool size and to ensure the proper wiring of developing neuronal networks, respectively. Both processes, EE and PCD, is suggested to result partially from competition for a limited supply of neurotrophic factors, including nerve growth factor (NGF), the glial cell-derived neurotrophic factor (GDNF), and the neurotrophic cytokines (Blomgren, 2007).

Several molecules involved in neuronal development were found to regulate physiological neuronal death: Glial cells, as key regulators of neuronal development by dynamically influencing neural precursors divisions at early stages, also promotes neuronal cell death by engulfment at later stages (Freeman, 2006); the chemorepellent netrin-1 receptors, UNC5 proteins and the axonal guidance molecule semaphorin 3A mediate neuronal cell death (Williams, 2006); consistently, integrin and ephrin, members of the extracellular matrix component family ensuring proper cell adhesion and cell recognition, play a role in developmental apoptosis (Leu, 2004; Depaepe, 2005); Fas, a member of the TNF-alpha receptor family, also was found involved in the death of motoneurons (Raoul, 1999; Adachi M., 1995; Watanabe-Fukunaga, 1992).

### **2.5.1 Cell death intracellular effectors**

The number of molecules involved in cell death identified did increase dramatically over the last decade. Activation of the caspase-9/APAF-1 complex, which in turn activates caspase-3, is a central pathway for PCD (Fig. 2.5). Consistently, cell death of post-mitotic migratory neurons is directly linked to caspase-3 activation although apoptosis of proliferating cerebellar granule cells and young pre-migratory cells occurs in the absence of caspase-3 cleavage (Lossi, 2004). Caspase-2 controls an early checkpoint for apoptosis initiation in cortical neurons (Chauvier, 2005). Bcl-2 family, upstream of caspase activation, acts a critical intracellular checkpoint in the pathways of neuronal apoptosis during development (Danial, 2004). Bax/Bak transmits a neuronal death signal, which is a gateway to the intrinsic pathway executed at the mitochondrial level as a critical organelle for developmental apoptosis. The commitment for developing neurons toward survival or cell death would then depend on the ratio between anti-apoptotic (e.g. Bcl-2 and Bcl-XL) and pro-apoptotic (e.g. Bax) factors (Danial, 2004). Beside mitochondria, some endoplasmic reticulum and endosomal proteins also activate the apoptotic machinery during cell death of developmental neurons (Zekri, 2005; Tajiri, 2006).

The degradation of chromosomal DNA into nucleosomal units is a common and prominent biochemical hallmark of apoptotic cells (Wyllie, 1980). can be blocked by inhibiting caspase-3-like activity suggesting a strong linkage between caspase-3 activation and inter-nucleosomal DNA fragmentation in neurons (Yakovlev, 1997; Himi, 1998). Activated

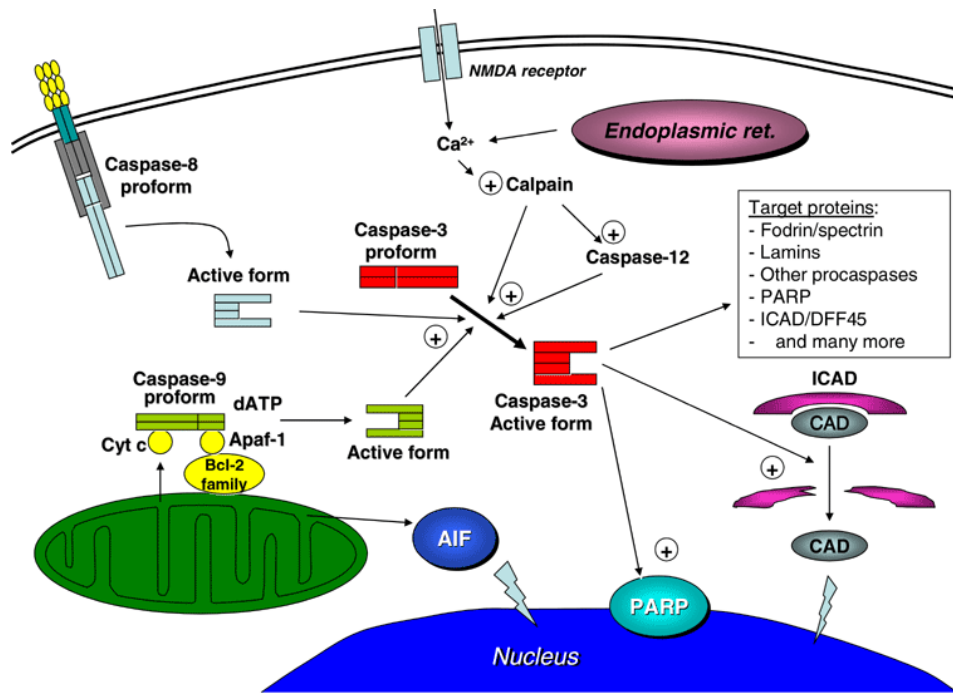


**Figure 2.5 Schematic representations of the three mechanisms converging on caspase-3.** Amongst caspases, caspase-3 is the critical one in the brain, particularly in the developing brain, which cleaves a number of target proteins, including ICAD/DFF45 and PARP, during cell death (Adopted from Blomgren, 2007).

caspase-3 will cleave a number of target proteins, including ICAD/DFF45 and poly adenosine 5-diphosphate–ribose polymerase (PARP), as indicated in the figure (Fig. 2.5). CAD (caspase-activated DNase; also known as DFF40, DNA fragmentation factor 40 kDa, and DRPE-4) is activated in selectively vulnerable neurons after transient cerebral ischemia and in cultured neurons under ischemia-related conditions. ICAD as an inhibitor of CAD exists in two isoforms produced by alternative splicing : the long form, ICAD-L (also known as DFF45, DNA fragmentation factor 45 kDa, DREP-1), and the short form, ICAD-S (also known as DFF35) (Enari, 1998). ICAD-L functions as a specific and indispensable chaperone for the synthesis of properly folded CAD *in vivo* (Enari, 1998) and (Sakahira, 1999), therefore ICAD-L strictly controls the activity and the synthesis of CAD. In dying cells, CAD is activated by dissociation with ICAD-L,

followed by the cleavage of the inhibitor into three fragments by caspases under various apoptotic stimuli (Sakahira, 1998).

## **2.6. Functional analysis of synaptic and neuronal proteins in *Drosophila melanogaster***

### **2.6.1 *Drosophila melanogaster* as a model organism for genetic analysis**

*Drosophila* as one of the oldest genetic model organisms offers several particular advantages for the study of cellular processes. Firstly, *Drosophila* has short generation time. The *Drosophila* life cycle is dependent on temperature, and approximately 10 days at 25°C (Fig. 2.6). Such animals raised at lower temperatures have longer life cycle. Secondly, the analysis of individual cells morphologically is available at all developmental stages. Thirdly, strong genetic tools have already established in *Drosophila melanogaster*. The use of P-element-based genetics has greatly simplified both targeted mutagenesis and ectopic expression of genes. The *UAS/Gal4* system allows spatio-temporal control over the expression of the gene of interest (Brand and Perrimon, 1993). Using the technique, a minimal cassette of the yeast transcription factor Gal4 is inserted in a genetic locus, where it is expressed by surrounding promoters. The second part of the expression system is a randomly inserted construct encoding the sequence to be expressed, fused downstream of the yeast upstream activating sequence (UAS) recognized by the Gal4 transcription factor, which thereby leads to the desired gene only being expressed in those tissues and at those time points where the

Gal4 cassette itself is expressed. Thus, using this system one can change expression pattern or the target gene to be expressed with relative ease, allowing to differentiate between pre- and postsynaptic effects.

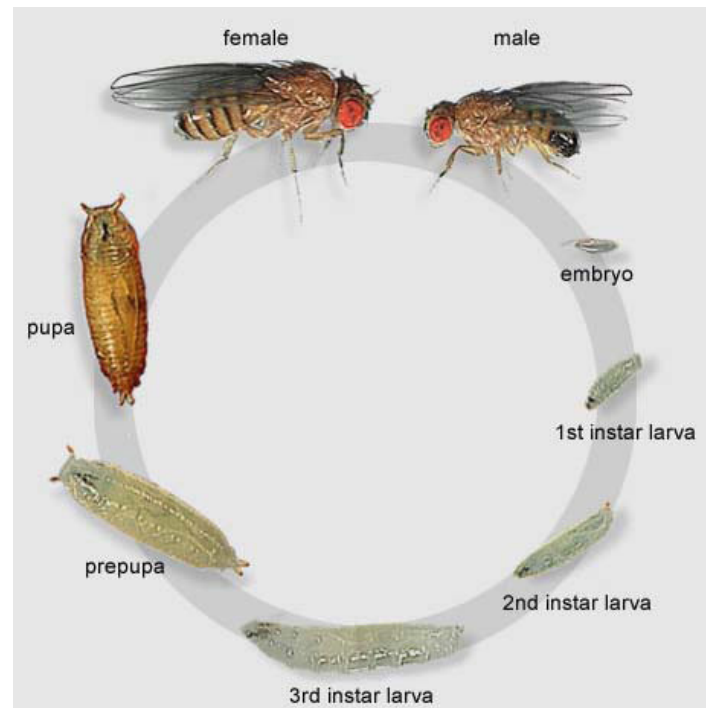


**Figure 2.6 Life cycle of *Drosophila melanogaster*.** The embryonic stage lasts roughly 24h and ends with the hatching of the larva. Larvae pass through three stages: 1st and 2<sup>nd</sup> instar larval stages last one day each; 3<sup>rd</sup> instar larval stage lasts two to three days followed by pupating. Metamorphosis takes four to five days and finishes with the hatching of the adult fly (adopted from Weigmann, 2003, flymove.uni-muenster.de).

### 2.6.2 The Neuromuscular junction of *Drosophila*

Using the *Drosophila* neuromuscular junction (NMJ) as a model system offers several advantages, such as its structural accessibility and amenability to powerful genetic, electrophysiological and microscopic techniques, for addressing fundamental mechanisms governing synapse formation, growth and neuronal circuits. In *Drosophila* late stage embryo and larva, body wall musculature shows a segmentally repeated pattern of 30 muscle cells (in each symmetric hemisegment, Fig. 2.7A) innervated by

about 45 motor axons (Goodman, 1986). Each of these muscles is easily identified by its distinct position and size, and is innervated by specific motoneurons. The NMJ morphology is highly stereotyped, the axons of motoneurons spread onto the muscle surface, forming a synaptic arbor composed of series of varicosities connected by thin axonal processes. These varicosities, or called synaptic boutons, are categorized by three classes (Rheuben, 1999): type I glutamatergic boutons, type II and type III boutons. All 30 body wall muscles are innervated by type I boutons, but some muscles are also innervated by type II and type III boutons, which contain octopamine or peptide neurotransmitters. The major classes of boutons (type I) contain clear vesicles and are glutamatergic, and at larval stage, they are surrounded by the characteristic subsynaptic reticulum (SSR), which originates from the muscle membrane at the junctional region (Atwood, 1993) (Fig. 2.7 B). Type I boutons can be subdivided into type I small (Is) and type I big (Ib) by size, the extent of the folding of SSR, and electrophysiological properties. The most commonly used model synapse is the synapse of the ISNb neuron on muscles 6 and 7 or muscle 4 (Fig. 2.7A-D), which contains both type Ib and type Is synapses, but no peptidergic type II synapses at this junction. Type Ib boutons contain small, clear synaptic vesicles (Atwood, 1993). The neuromuscular junction is organized into a series of boutons, which can be added and eliminated during development and plasticity. Each bouton contains several synapses identified as pairs of a postsynaptic density with corresponding specializations at the presynaptic sites (Fig. 2.7B-D, the active zone is marked by the expression of the nc82 epitope which recognizes BRP) and postsynaptic marker (GluRIID). This thesis will focus on type 1 boutons.



### 2.6.3 Organization and development of *Drosophila* NMJ synapses

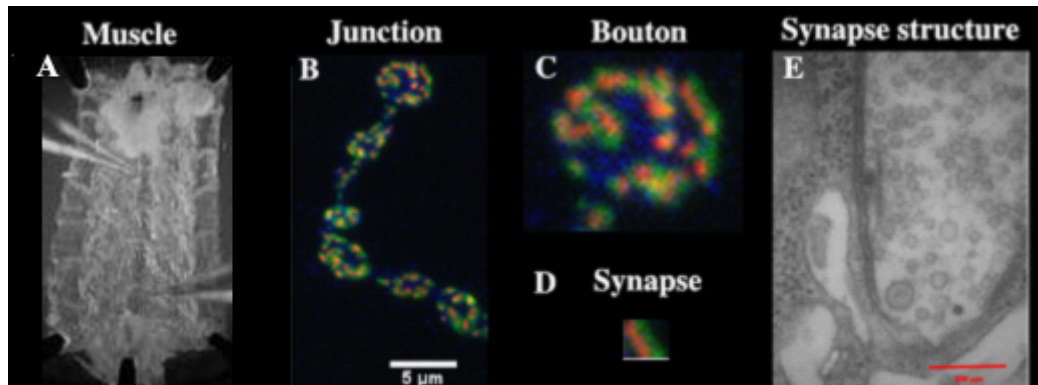


**Figure 2.7 Organization and development of *Drosophila* NMJ synapses.** Images of the ventral body-wall muscles and motor nerves from the dorsal aspect of the *Drosophila* larvae (A) and the neuromuscular junction at muscle 6/7 (B) as well as the enlargement of a single bouton (C) and a single synapse in  $w^{1118}$  (D). (B-D) The synapses visualized by nc82 (red, which recognizes Brp, active zone marker) and *Drosophila* glutamate receptor subunit GluRIID (green) (E) Ultrastructure of a synapse at the NMJ at muscle 6/7 in  $w^{1118}$ .

The NMJ in 3rd instar *Drosophila* larvae is composed of boutons, which each of them contains roughly 10-20 individual synapses as visualized by AZ marker nc82 (red) and postsynaptic marker *Drosophila* glutamate receptor subunit GluRIID (green, Fig. 2.7B-D). The same structure is shown using electron microscopy (Fig. 2.7E). The presynaptic bouton is filled with small, clear synaptic vesicles containing glutamate (Fig. 2.7E). Frequently an electron-dense matrix display different shapes, such as T-shaped at the *Drosophila* NMJ, and ribbons or pyramids in other organisms, Fig. 2.7E) (Zhai and Bellen, 2004). Active zones dock high density of synaptic vesicles and define the sites of transmitter release. Directly apposed to the active zone on the postsynaptic site is an electron-dense membrane specialization also called the postsynaptic density (PSD, Fig.

2.7E) where clusters glutamate receptors (GluRs), voltage-gated ion channels and various scaffolding molecules (Petersen, 1997; Sheng, 2001).

## 2.7 Objectives

### 2.7.1 DREP proteins

Interestingly, DREP-2 was identified as a putative Brp binding partner by co-IP experiments (Dr. Manuela Schmidt, unpublished data). So far, little is known about DREP-2. In this thesis, genetic analyses of DREP-2 and DREP-4 in *Drosophila melanogaster* were performed to provide insight into their roles *in vivo* and *in vitro*.

DREP proteins (DREP-1, DREP-2, DREP-3 and DREP-4) are members of the DFF (DNA fragmentation factor) family, including according to the high homology of sequence. DREP-1 and DREP-4 was investigated as an apoptosis regulator (Yokoyama, 2000; Mukae, 2000). DFF, involved in apoptosis, is composed of two subunits, DFF40 (caspase activated DNase, CAD and caspase-activated nuclease, also called DREP-4) and DFF45 (inhibitor of CAD, ICAD, also called DREP-1). DFF40 has a nuclease domain that can cleave naked and chromosomal DNA, whereas DFF45 is a regulatory subunit that suppresses the nuclease activity of DFF40. Immunoprecipitation and immunoblotting analysis of co-expressed tagged DREPs in human 293T cells have shown that DREP-1 and DREP-3 can interact with DREP-2 (Inohara and Nuñez, 1999). No nuclease activity was detected in DREP-1, DREP-2, or DREP-3 (and their complexes) in the absence or presence of human caspase-3, which has a substrate specificity similar to that of *Drosophila melanogaster* downstream caspases, suggesting that DREP-2 and DREP-3 are not nucleases, but they might regulate the activity of DREP-1.

## **2.7.2 GIT**

### **2.7.2.1 Membrane trafficking and remodeling of the actin cytoskeleton**

Membrane trafficking and remodeling of the actin cytoskeleton are critical activities contributing to cellular events that include cell growth, migration and tumor invasion. Cell migration is driven by the protrusive activity at the leading edge of the cell, where continuous remodeling of actin and adhesive contacts are required. Membrane internalized from the cell surface is recycled to the front of migrating cells for the extension of the cell border (Bretscher, 1996). Both, membrane internalization and the actin cytoskeleton are affected by ADP-ribosylation factor (ARF)-directed GTPase activating proteins (GAPs) (ARFGAPs) (D'Souza-Schorey, 1995; Peters, 1995; D'Souza-Schorey, 2006; Donaldson, 2003).

### **2.7.2.2 Actin cytoskeleton remodeling and vesicle recycling by ARF GAPs**

The actin structures include invadopodia, focal adhesions, peripheral membrane ruffles and circular dorsal ruffles (CDRs). Invadopodia, focal adhesions and podosomes attach the actin cytoskeleton to the extracellular matrix (ECM), which are sites of active endo- and exo-cytosis mediated by signal transduction. Peripheral membrane ruffles are actin-rich extensions from the cell edge, which are also sites of active endo- and exocytosis and signaling. ADP-ribosylation factor (ARF)-directed GTPase activating proteins (GAPs) (ARFGAPs) are involved in these processes. The function of ARF proteins is regulated by binding and hydrolyzing GTP. The ARF family of GTP-binding proteins belongs to a subfamily of the Ras superfamily. Six *Arf* genes in the mammalian genome are classified into three classes on the basis of amino acid sequence: class I includes

ARF1, ARF2 and ARF3; class II includes ARF4 and ARF5; and class III includes ARF6. ARF1 has been implicated in Golgi–endoplasmic reticulum (ER) retrograde transport, intra-Golgi transport, trafficking from the *trans* Golgi network (TGN), transport in the endocytic pathway and recruitment of paxillin to focal adhesions (FAs) (Roth, 1999). ARF1 regulates specifically the formation of vesicles within the Golgi compartment (Roth, 1999). ARF6 is involved in endocytosis, phagocytosis, receptor recycling and the formation of actin-rich protrusions and ruffles (D'Souza-Schorey, 2006; Donaldson, 2003). Furthermore, ARF6 regulates membrane traffic between the recycling endosomal compartment and the plasma membrane (D'Souza-Schorey, 1995; Peters, 1995). ARF6 appears to be functionally linked to Rac1, a Rho family GTPase involved in the formation of actin-rich ruffles and lamellipodia (Ridley, 1992). Rac1 and ARF6 colocalize at the plasma membrane and on recycling endosomes, and Rac1-stimulated ruffling is blocked by the GTP binding-defective N27-ARF6 mutant (Radhakrishna, 1999). The effect of ARF6 on Rac1-mediated lamellipodial formation depends partially on ARF6-mediated regulation of Rac1 trafficking to the plasma membrane. Interestingly, GIT proteins contain a GTPase-activating protein (GAP) domain for ADP-ribosylation factors (ARFs), implicated its potential role in the regulation of membrane trafficking and the actin cytoskeleton formation.

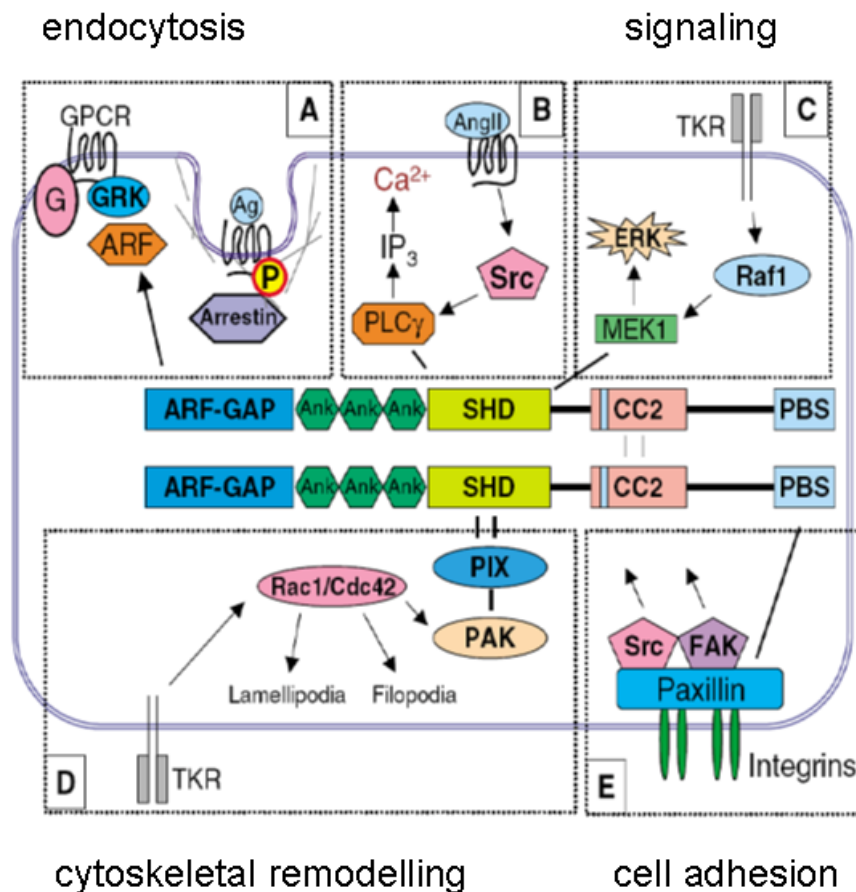


**Figure 2.8 Summary of GIT1 protein interactions and suggested functions.** Major signaling pathways include (A) GPCR endocytosis; (B) PLC activation and  $\text{Ca}^{2+}$  mobilization stimulated by angiotensin-II (AngII); (C) scaffolding MEK1 activation by tyrosine kinase receptor (TKR); (D) cytoskeletal regulation through p21-associated kinase (PAK) and GTPases family; and (E) association with paxillin involved in cell adhesion. G, heterotrimeric G proteins; GRK, GPCR kinase; GPCR, G-protein-coupled receptor; IP $_3$ , inositol (1, 4, 5)-trisphosphate; P, phosphorylation; TKR, tyrosine kinase receptor. (Adapted from Hoefen and Berk, 2006)

### 2.7.2.3 GIT proteins of ARFGAP family

The effect of the ARFGAPs on cytoskeletal structures is mediated by ARFs. According to the overall domain structure, the ARFGAPs were classified into two major types, ARFGAP1 and AZAP. ARFGAP1 type is divided into three subtypes – ARFGAP, SMAP and GIT. The mammalian GIT protein family contains GIT1/Cat-1/p95-APP1 and GIT2/Cat-

2/PKL/p95-APP2/KIAA0148. However, only one orthologue (CG16728) of GIT1 is identified in *Drosophila melanogaster*. Mammalian GIT proteins contain various domains, including the ARFGAP domain, ankyrin repeats, the Spa2 homology domain (SHD), the G-protein-coupled receptor kinase-binding domain (GRKBD) and the paxillin-binding subdomain (PBS). The GITs have been indicated to regulate both membrane traffic and forming of FAs. GITs colocalize with ARF6 in the cell periphery *in vivo*. Functional analyses suggested that GITs function together with ARF6 involved in G-protein coupled receptor internalization (Premont, 1998). Major signaling pathways of GIT1 include agonist (Ag)-receptor G-protein-coupled receptor (GPCR) endocytosis, angiotensin-II (AngII)-stimulated PLC  $\gamma$  activation,  $\text{Ca}^{2+}$  mobilization and scaffolding MEK1 activation in response to TRK (tyrosine kinase receptor) activation (Premont, 1998; Bagrodia, 1999; Di Cesare, 2000; Turner, 1999; Premont, 2000; Turner, 2001; Donaldson, 2000; Jackson, 2000). GIT1 is involved in cytoskeletal regulation mediated by PAK and Rho-family GTPases and also cell adhesion by focal complex assembly and disassembly (Premont, 1998). GIT proteins regulate endocytosis (Premont, 1998; Claing, 2000; Zhao, 2000) by interacting with the Rho-type guanine nucleotide exchange factor (GEF)  $\beta$ PIX, focal adhesion kinase (FAK), and the adhesion adaptor protein-paxillin to assembly focal adhesion complexes (Fig. 2.8) (Bagrodia, 1999; Turner, 1999). The GIT proteins form multimers and associate with the presynaptic cytomatrix protein Piccolo. Immunoprecipitation on detergent lysates of the crude synaptosomal fraction of adult rat brain with Piccolo antibodies could precipitate Piccolo and coprecipitated GIT1 and other proteins, which are known to associate with GIT1, including  $\beta$ PIX, FAK, Paxillin, Liprin- $\alpha$  and the Liprin- $\alpha$ -associated GRIP1 (Fig. 2.8) (Kim, 2003). However, neuronal functions of *Drosophila* GIT proteins are still unclear-how DGIT is involved in the regulation of vesicle recycling,

membrane trafficking, receptor trafficking and actin cytoskeleton remodeling. In this thesis, DGIT functions were analyzed at *Drosophila* NMJs.

### 2.7.3 DJM-1

Mental retardation (MR) defined by an intelligence quotient (IQ) below 70 affects about 1-3% of the human population (Curry *et al.*, 1997; Roeleveld *et al.*, 1997; Croen *et al.*, 2001). Mental retardation patients suffer from insufficient cognitive and adaptive disabilities. The causes of MR are extremely diverse including environmental factors and genetic factors. Environmental factors include environmental contaminants, radiation, infection, malnutrition, prenatal exposure of the fetus to toxic substances (e.g., alcohol, drugs), and illness of the mother during pregnancy etc. In addition, many problems during or after birth may induce brain damage and mental retardation, for example unusual stress during birth, especially premature birth and low birth weight.

By using cutting edge genomic technology, the Ropers group at Max-Planck Institute for Molecular Genetics in Berlin recently could link *djm-1*, to inborn forms of inherited MR in human beings. The principles by how this gene functions for human oligophrenies remain to be elucidated. *Djm-1* related disease has very high clinical score, and their direct orthologs (CG9951) exists in *Drosophila melanogaster*. In this thesis, efficient genetics of the fruit fly *Drosophila* were used to study functions of *djm-1* with the final goal to identify cellular and molecular scenarios causally involved in defective brain development of humans.

## **3. Materials and Methods**

### **3.1 Molecular biology**

#### **3.1.1 Materials**

The following plasmids were used for molecular cloning:

pBluescript® II KS + (pKS+; Stratagene, La Jolla, USA)

pSL1180 (Amersham Pharmacia Biotech, Buckinghamshire, England)

pSL fa1180fa (Horn and Wimmer 2000)

pUAST (Brand and Perrimon 1993)

pDEST17 (Carnegie Institution of Washington)

pTW (Carnegie Institution of Washington)

pTWG (Carnegie Institution of Washington)

pTGW (Carnegie Institution of Washington)

pTWM (Carnegie Institution of Washington)

pTStrawberryW (gateway destination vector created with the primer extension method, substituting the EGFP of the pTWG for mStrawberry, see (Shu, Shaner et al. 2006)

pTWStrawberry (gateway destination vector created with the primer extension method, substituting the EGFP of the pTWG for mStrawberry, see (Shu, Shaner et al. 2006)



pGADT7 IIB (Clontech laboratories, Inc)

pGBKT7 (Clontech laboratories, Inc)

pUbiP-EGFP-rfA (Carnegie Institution of Washington)

pUbiP-rfA-EGFP (Carnegie Institution of Washington)

pEF-BOS-*drep-4* (gift from Prof. Dr. Nagata lab, Japan. Please refer to Yokoyama, 2000 for the details)

All chemicals were, if not stated elsewhere, purchased from Roth (Karlsruhe, Germany), Sigma (St. Louis, USA) or Merck (Darmstadt, Germany). Agarose was obtained from Peqlab (Erlangen, Germany). Alkaline phosphatase, T4 DNA ligase, T4 polynucleotide kinase, Taq Polymerase and various restriction endonucleases were purchased from Roche (Mannheim, Germany). The restriction endonuclease *AscI* as well as Vent DNA-Polymerase were obtained from New England Biolabs (Beverly, USA). Elongase® enzyme mix used for overlap-extension PCRs was purchased from Invitrogen (Karlsruhe, Germany). All oligonucleotides were synthesized by MWG Biotech (Ebersberg, Germany). Unless stated elsewhere all molecular biology kits for RNA or DNA extraction and purification were obtained from Qiagen (Hilden, Germany). Chemically competent *E. coli* XL1 blue cells were produced in the lab with standard procedures. All PCRs were performed with the PCR System GeneAmp 9700 (Applied Biosystems, Foster City, USA).

### **3.1.2 Buffer solutions**

->HL-3

70mM NaCl, 5mM KCl, 20mM MgCl<sub>2</sub>, 10mM NaHCO<sub>3</sub>, 5mM trehalose, 115mM sucrose, 5mM HEPES, pH adjusted to 7.2

->PBS

8g NaCl, 0,2g KCl, 0.2g KH<sub>2</sub>PO<sub>4</sub>, 1.15g NaH<sub>2</sub>PO<sub>4</sub>·2H<sub>2</sub>O

->PBS/Tween

0,05% (w/v) Tween 20 in PBS

->SDS-electrophoresis buffer

25mM Tris/HCl, 3.5mM SDS, 192mM glycine pH 8.3

->SDS sample buffer

50mM TRIS/HCl pH 6.8, 2% SDS, 10% (v/v) glycerol, 0.1% bromophenol-blue, 2% β-mercaptoethanol

->Squishing buffer

10mM Tris/HCl pH 8.2, 1mM EDTA, 25mM NaCl, 200μg/ml proteinase K

->Transfer buffer

25mM Tris/HCl, 192mM glycine, 20% (v/v) methanol, pH 8.3

### **3.1.3 Construction of fluorophore tagged proteins**

The molecular cloning of transgenes was performed using standard molecular biology procedures (Sambrook and Gething 1989). All constructs were double stranded sequenced (MWG Biotech, Ebersberg, Germany). DNA sequences were verified with Sci-Ed Central (Scientific &

Educational Software, NC, USA). All constructions of fluorophore tagged proteins were based on the *Drosophila* Gateway® technology.

The *Drosophila* Gateway vector collection is a combination of 68 Gateway®-based vectors designed to express fluorophore-tagged proteins in *Drosophila* flies (Carnegie Institution of Washington). Its main tool consists of Invitrogen's Gateway® recombination cassette, which enables the recombination of an Open Reading Frame (ORF) of interest into any of the destination vectors using a simple but efficient recombinase reaction (Fig. 3.1). This reaction results in a fusion gene consisting of your ORF placed in frame with many different fluorescent proteins tags (GFP, CFP, Venus and mRFP, between others) and expressed by the UAS<sub>t</sub> promoter.

Gateway® technology uses lambda integrase to recombine the desired ORF, flanked by attL1 and attL2 recombination sites, with the attR1 and attR2 recombination sites of a destination vector (Fig. 3.1). The result is a highly efficient and reliable ‘swap’ of your ORF with the cassette containing the ccdB reporter gene in the destination vector. Successfully swapped vectors can be selected based on their resistance to ampicillin and cell lethality derived from the ccdB gene. Once the desired ORF is brought into an entry vector, it can be easily moved into several different destination vectors, suited with different fluorescent proteins either adding a fluorophore at the very N-Term or the very C-term of the cloned protein. Red regions represent the att recombination sites.

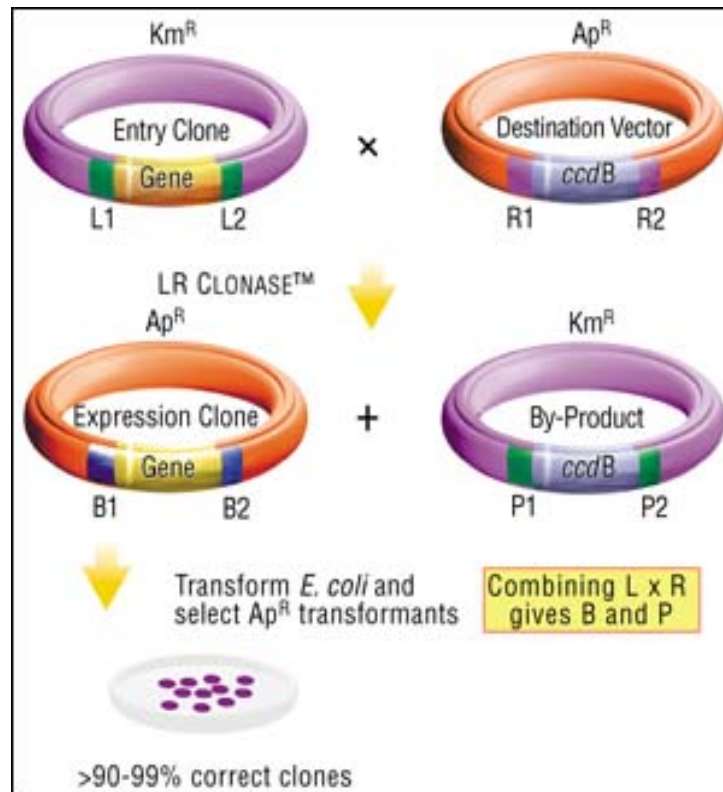


**Figure 3.1 LR reaction.** Recombination between an entry clone with attL and a destination vector with attR forms a new expression clone with attB and a byproduct with attP (Adopted from invitrogen's website).

### ->Construction of fluorophore tagged *Drosophila drep-2* full length CDS

Entry cloning:

Restriction digestion: *SpeI* / *XbaI*

Insert: *drep-2* full length CDS

Vector: pENTER

Template: LD32009 cDNA

Forward primer: 5' CTAGACTAGTGCCAGAGAGGAGTCTCGC 3'

Reverse primer: 5' CAGCTCTAGAGCAATTCTGTCCTCCTCATCCTC 3'

Furtherly, perform LR reaction using entry construct (pENTER-*drep-2*) and destination vectors: pTW, pTGW, pTWG, pTWstrawberry, pTStrawberryW.

**->Construction of fluorophore tagged *Drosophila drep-4* full length CDS:**

Entry cloning:

Restriction digestion: *NotI* / *Sall*

Insert: *drep-4* full length CDS

Vector: pENTR4

Template: PKS-*drep-4* cDNA

Forward primer: 5' GACCGTCGACATCAGCTACATTAGAGATGC 3'

Reverse primer: 5' CAGCGCGGCCGCGAAGTGGCTAGACTGTCCACCT3'

Furtherly, perform LR reaction using entry construct (pENTR4-DREP-4) and destination vectors: pTW, pTGW, pTWG.

**->Construction of fluorophore tagged *Drosophila digit* full length CDS:**

Entry cloning:

Restriction digestion: *NotI* / *SpeI*

Insert: DIGIT full length CDS

Entry vector: pENTER

Template: LD30319 cDNA

Forward primer: 5' GAGCACTAGTTGTTTCGCCAGCAGTATAATCG 3'

Reverse primer: 5' GAGCGCGGCCGCGATAGAACTGCAACACCAAAGTC 3'

Furtherly, perform LR reaction using entry construct (pENTER-DGIT) and destination vectors: pTW, pTGW, pTWG, pTWstrawberry, pTStrawberryW.

**->Construction of fluorophore tagged *Drosophila stnB* full length CDS:**

Entry cloning:

Restriction digestion: *NotI* / *BamHI*

Insert: *stnB* full length CDS (1-1262aa)

Entry vector: pENTR4

Template: RH38069 cDNA

(Primer pairs refer to Volker Haucke Lab, Institute of Chemistry & Biochemistry, Freie Universität Berlin)

Furtherly, perform LR reaction using entry construct (pENTER-*stnB*) and destination vectors: pTW, pTGW, pTWG, pTWM.

**->Construction of fluorophore tagged *Drosophila djm-1* full length CDS:**

Entry cloning:

Restriction digestion: *SalI* / *XhoI*

Insert: *djm-1* full length CDS

Entry vector: pENTR4

Template: GH12970 cDNA

Forward primer: 5' CTAGGTCGACATGGACGAAGTGGACAAG3'

Reverse primer: 5' CTAGCTCGAGTG ACTCCCTGCGTTCGTCTG 3'

Furtherly, perform LR reaction using entry construct (pENTR4-*djm-1*) and destination vectors: pTGW, pTWG, pTWM, pTVW.

### **3.1.4 *In situ* hybridization**

#### **I. Preparation of embryos**

1. Collect embryos every 3 hours for 24 hours and wash 3X with 0.02% Triton X (Tx) (15ml for up to 2ml embryos in a 50ml falcon tube).
2. Dechorionate 3 min in 50% bleach.
3. Wash 3X with 0.02% Tx.
4. Fill tube with equal parts heptane and 4% formaldehyde/PBS (filtered).
5. Incubate 25 min with frequent shaking.
6. Remove LOWER aqueous phase and replace with equal volume methanol.
7. Shake for 1 min allowing embryos to settle. Do not vortex.

8. Remove UPPER phase along with embryos and vitelline membranes and remaining at the interphase.
9. Rinse settled embryos 3X with methanol (embryos can be stored at -20°C)
10. Rehydrate in 3:1 (MeOH: 4% formaldehyde/PBS) for 2 min, then 1:3 (MeOH: 4% formaldehyde/PBS) for 5 min.
11. Fix 10 min. in 4% formaldehyde/PBS.
12. Rinse 6X with PBS + 0.1% Tween 20 (PBT).

## **II. Preparation of probe**

1. Perform restriction digestion of the vectors containing the sequences of interest. For preparing antisense RNA probes of LD32009 (*drep-2*) and GH12970 (*djm-1*) plasmids were cut with *Bam*HI and *Sma*I, respectively.
2. Run the digest on agarose gel and extract the DNA (elute the DNA in 10 µl of H<sub>2</sub>O)
3. Run 1 µl of DNA on a test gel.
4. *In-vitro* transcription:

Set the following reaction mixture:

DNA 9 µl

RNase free water 3 µl

10xTrancription buffer 2 µl

RNase inhibitor 2 µl



DIG-labelling mix 2  $\mu$ l

Sp6 RNA polymerase 2  $\mu$ l

Incubate at 37°C for 2 hours.

5. Then add 2  $\mu$ l RNase free DNase and incubate at 37°C for 15 minutes.

6. Extract the RNAs by using RNAeasy Kit

7. Fragmentation of RNA (RNA sample in RNase free water 25  $\mu$ l + 2xcarbonate buffer 25  $\mu$ l)

8. Divide the above mixture into two parts. Incubate 25  $\mu$ l at 60°C for 5 min and incubate the other 25  $\mu$ l at 60°C for 15 min.

9. Add RNase free water to the fragmented RNA sample to get a final volume of 100  $\mu$ l, add 10  $\mu$ l of NaAc buffer (PH 5.2) and 1 $\mu$ l of LPA, and 250  $\mu$ l of absolute ethanol. Mix and centrifuge for 5 min at full speed remove supernatant and wash the pellet with 75% ethanol.

10. Dissolve the RNAs sample with 25  $\mu$ l of probe resuspension buffer.

### **III. Hybridization of embryos (fillets)**

1. Wash the prepared embryos (fillets) in 1ml Pre-hybridization buffer (-DS)

Formamide 25 ml

20x SSC 10 ml

50x Denhardts 1 ml

tRNA 10 mg/ml 1.25 ml

ssDNA 10 mg/ml 1.25 ml (preheated for 10 min at 100°C, followed by chilling on ice)

Heparin 50 mg/ml 0.05 ml

20% Tween 0.25 ml

Water 6.20 ml

Combine 9 ml with 1 ml water to get the Pre-hybridization buffer (-DS)

2. Incubate the samples in 1 ml of Pre-hybridization buffer (-DS) for 1 hr at RT.

3. Add 1 µl of probe to 0.5 ml hybridization buffer (+DS) (9:1). Incubate overnight at 55°C.

4. 2x wash with 0.5 ml Wash buffer pre-warmed at 55°C.

Wash buffer:

Formamide 250 ml

20x SSC 50 ml

Water 200 ml

20% Tween-20 2.5 ml

5. 7x 0.5 ml warmed wash buffer 1 hr at 55°C.

6. Incubate in 0.5 ml warmed wash buffer overnight at 55°C.

7. 2x wash with PBTw at RT.

8. Incubate for 30 min in PBTw at RT.
9. Incubate in 0.5 ml PBTw + 5% NGS + Antikörper (1:2000) (anti-DIG-AP FAB-Frag.) for 2 hrs. at RT.
10. 2x wash with PBTw at RT.
11. 9x 10 min. PBTw at RT.
12. 2x wash with Alkaline Phosphatase Buffer + 0.1% Tween-20

**Alkaline Phosphatase Buffer:**

100 mM NaCl (= 20 ml 5M NaCl)

5 mM MgCl<sub>2</sub> (=5 ml MgCl<sub>2</sub>)

100 mM Tris/HCl pH 9.5 (= 100 ml 1M Tris + 875 ml water)

1/100 V 10% Tween-20

13. 5 min of incubation in AP buffer at RT.
14. Transfer the samples into 24 well plates, wash one time with 0.2 ml of BM Purple AP substrate, then add 0.2 ml of BM Purple AP substrate.
15. At proper stages, stop staining by 3 times of wash with PBTw and add 80% Glycerin/ H<sub>2</sub>O. Store the plate at 4 degrees.

III. Mounting and light microscopy

### **3.1.5 Production of DREP-2 antibody**

#### **3.1.5.1 Construction of His-tagged DREP-2 peptides**

##### **->Construction of His6 tagged DREP-2 N-terminal peptide**

### **Entry cloning:**

Restriction digestion: *SalI* / *XhoI*

Insert: 1-249 aa of DREP-2

Entry vector: pENTR4

Template: LD32009 cDNA

Forward primer: 5' GACCGTCGACGCCAGAGAGGAGTCTCGCGG3'

Reverse primer: 5'GACCCTCGAGTGGCCTACGGTGCTGTCGAAGG3'

### **->Construction of His6 tagged DREP-2 C-terminal peptide**

### **Entry cloning:**

Restriction digestion: *SalI* / *XhoI*

Insert: 252-483 aa of DREP-2

Entry vector: pENTR4

Template: LD30319 cDNA

Forward primer: 5' GACCGTCGACGTGGGTGTGGGAGCTGTCCA 3'

Reverse primer: 5' GACCCTCGAGTGAATTCTGTCCTCCTCATCCTC 3'

Furtherly, perform LR reaction using entry construct (pENTR4-DREP-2 N- or C- terminal peptide) and destination vectors, pDEST17.

### 3.1.5.2 Overexpression and isolation of DREP-2 fusion proteins

For the expression of recombinant proteins BL21(DE3) *E. coli* strains was used. To optimize the expression of fusion proteins pre-tests of expression were performed as follows: A single clone was grown in 50 ml LB medium in a 500 ml flask, shaking at 37°C, until reaching OD<sub>600</sub> 0.6. A 1ml sample of the culture was taken. Fusion protein expression was induced by the addition of Isopropyl β-D-1-thiogalactopyranoside (IPTG) to a final concentration of 1 mM. The culture was split in two, one half incubated at 25°C and the other at 37°C, and 1ml samples taken after 1 hour, 3 hours and the next morning after induction. These samples were pelleted and a) boiled in 200 µl Laemmli buffer for 5 minutes to extract the total protein or b) treated with 160 µl BugBuster (Novagen) plus Benzonase (Merck), then repelleted. The supernatant (soluble proteins) is separated from the pellet (insoluble) and analyzed on a Coomassiestained 10% PAA gel. These were then compared to obtain the best conditions for expression and solubility.

1-2 L cultures were grown at 37 degree and induced with IPTG at the final concentration of 1 mM (every 500 ml culture in a 2 L flask), and then followed by harvest the pellet. The pellet was resuspended with 80 ml 1X Equilibration Buffer (pH 7.0) for every 1L LB cultures. For the two His-tagged DREP-2 peptides, the standard protocol for TALON-resin purification (Clontech) was used in denaturing conditions. The supernatant was incubated with approx. 1ml of glutathione-agarose resin per 250 ml culture volume at 4°C overnight. The pelleted resin washed three times with ice cold 1X Equilibration Buffer (pH 7.0). Fusion peptides were then eluted in 1 ml fractions with 1X Imidazole Elution buffer (pH 7.0), and each fraction analyzed for protein content. All fusion peptides were then dialyzed into standard 1x PBS before being sent for injection into rabbits (SEQLAB Sequence Laboratories Göttingen GmbH).

• **1X Equilibration Buffer** (pH 7.0)

50 mM sodium phosphate

6 M guanidine-HCl

300 mM NaCl

• **1X Imidazole Elution Buffer** (pH 7.0)

45 mM sodium phosphate

5.4 M guanidine-HCl

270 mM NaCl

150 mM imidazole

### **3.1.5.3 Affinity purification of DREP-2 antibody**

The polyclonal DREP-2 antibody was produced by injecting a 6xHis-fused N-terminal (1-249 aa) and C-terminal fusion protein (252-483 aa) of DREP-2 into two different rabbits each (SEQLAB Sequence Laboratories Göttingen GmbH). In total six animals, 2 animals (Cat. No: 7185 and 7186) for N-term peptide; 2 (Cat. No: 7183 and 7184) for C-term peptide; 2 (Cat. No: 7187 and 7188) for N+C-term peptides, were injected. The serum was harvested from the injected rabbit after three-months. The antigen injection and serum harvest were performed 3 times, followed by affinity purification under denaturing conditions using the corresponding purified his tagged DREP-2 peptide as bait.

1. Denatured histidine-tagged DREP-2 peptides by 6 M Urea incubated with activated CnBr-Sepharose 4B at 4 °C overnight on the wheel.

2. The next day, the beads were washed and then Spun (600 rpm, 4 min, at 4 °C) three times with Buffer B (8 M Urea, 0.1 M NaH<sub>2</sub>PO<sub>4</sub>, pH 8.0) and one time 1 M Ethanolamine pH 8.0, followed by blocked by 1 M Ethanolamine at RT for 2 hours.

3. The further washing and spinning the beads in the following sequence for 3 times: 0.1 M Na-acetate, pH 4.0; 0.1M Borate, 0.5 M NaCl, pH 8.0. Then, the beads washed with PBS until pH reached to 7.4.
4. Spun the serum for 20 min at 4000 rpm to get rid of fat and cell bodies at 4 °C. The above beads incubated with the serum at 4 °C overnight on the wheel.
5. The next day, spun and washed the beads with PBS of 5 ml.
6. Put 750 µl elutionbuffer (10 ml 2M Glycin/HCL, pH2.2 plus 1 ml Dioxan) onto the beads and incubated for 5 min at RT, and then collected the flowthrough of 750 µl into 250 µl K<sub>2</sub>HPO<sub>4</sub> and mixed immediately to stabilize the pH (Repeated 9 times, but incubated the beads with elution buffer only for 2 min in between later).
7. Measured the OD<sub>280</sub> of the elutions. The reference was 250 µl K<sub>2</sub>HPO<sub>4</sub> +750 µl elution buffer. The pH of all elutions was checked. If there were some sour ones, added 300-500 µl K<sub>2</sub>HPO<sub>4</sub> until the pH is 7.4.
8. Washed the beads with PBS until the pH is 7.4 and stored the column at 4 °C with PBS containing 0.1% NaN<sub>3</sub>.

The three different polyclonal DREP-2 antibodies were purified from the serum of animal Cat. No 1785 (against N-term peptide), Cat. No 1783 (against C-term peptide) and Cat. No 1787 (against N+C-term peptides). The purified antibody against the N+C-term peptide of DREP-2 was used in this thesis.

## **3.2 *Drosophila melanogaster***

### **3.2.1 Fly culturing**

Fly strains are, if not otherwise stated, maintained at 25°C in plastic bottles (Greiner Bio-one, Kremsmünster, Austria) containing cultivation medium (195 g agar, 200 g soy flour, 360 g yeast, 1600 g corn flour, 440 g beet syrup, 1600 g malt, 30 g nipagine, 126 ml propionic acid, add 18 L H<sub>2</sub>O). Embryonic collections for intense care rearing were performed in plastic cylinders placed on apple agar plates (1 L apple juice, 100 g saccharose, 85 g agar, 40 ml nipagine (15%), add 3 L H<sub>2</sub>O). First instar larvae were collected from agar plates 24h AEL and transferred to small (5.5 cm diameter) Petri dishes containing a small amount of mashed cultivation medium. The Petri dishes, sealing with parafim® (American Nation Can Company) with small holes, were kept at 25°C, followed by checking Petri dish conditions every 12 h for optimal moisture and larval fitness.

### **3.2.2 Transgenesis**

*Drosophila* germ line transformation was performed with an Eppendorf InjectMan (Hamburg, Germany) as described previously (Rubin and Spradling 1982) using 300 ng/μl P-element DNA (pUAST with inserted transgene) and 100 ng/μl helper plasmid (pΔ2-3). Transgenic animals were established in the following wild type genetic backgrounds:  $w^l$  for *djm-1* and  $w^{1118}$  for *drep-2*, *drep-4*, *stnB* and *digit*.

### **3.2.3 The UAS/Gal4 system and drivers**

The UAS/Gal4 expression system is broadly used in *Drosophila* for the ectopic expression of transgenic insertions. The yeast transcription factor



Gal4, is not present and therefore presumably inactive in the fruit fly. The expression system utilizes the yeast Gal4 insertion and its associated upstream activating sequence (UAS) to which Gal4 binds in order to enable gene transcription (Fig. 3.2). Gal4 may be expressed in many different patterns and tissues by creating enhancer trap lines and placing it under control of specific endogenous promoters. Since UAS promoter sequences cannot be found in the fruit fly, the transcription of the transgenic insertion will only be activated in tissues in which Gal4 is expressed (Brand and Perrimon 1993).

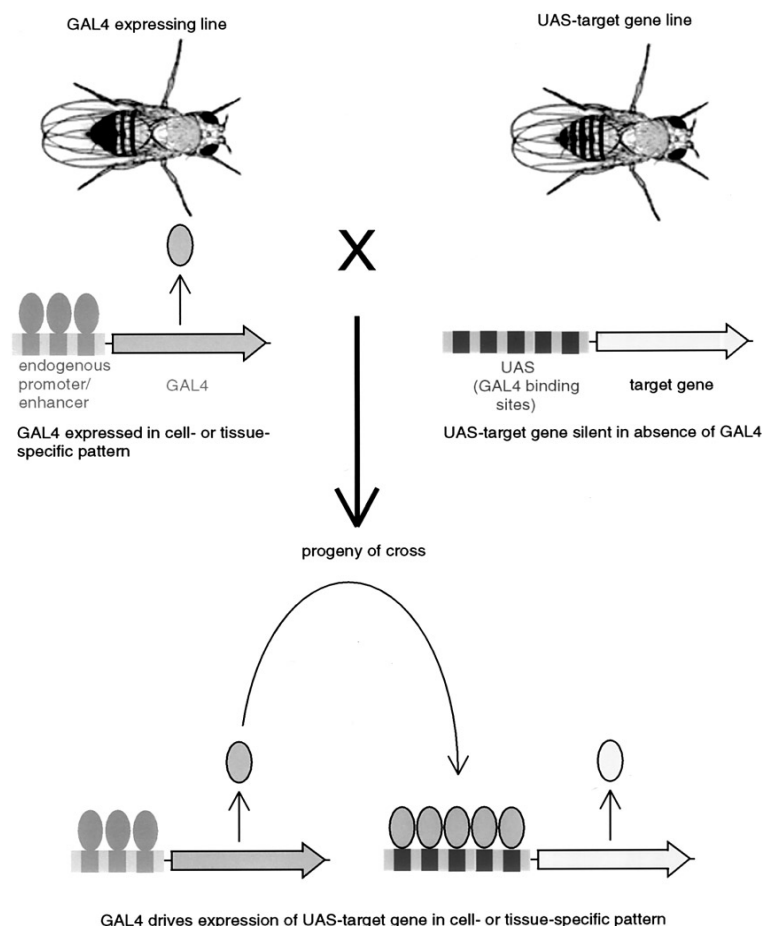


**Fig. 3.2 UAS/Gal4 system (Adopted from Brand and Perrimon 1993)**

In this project motoneuron/neuron or muscle specific driver lines (expressing Gal4 exclusively in motoneurons/neurons or in muscle) were used to overexpress fluorescently tagged proteins in order to visualize its synaptic localization in living animals and in fixed samples, in case no antibody were available for the specific protein. In this thesis, the following driver lines are used: Elav-Gal4, OK6-Gal4, D42-Gal4 and Mhc-Gal4.

### 3.2.4 FLP-FRT recombination deletion

Parks et al. described the use of FRT sites within XP, RB and WH for FLP-mediated recombination between two insertions, enabling a rapid method for generating molecularly defined deficiencies (Parks, 2004). These transposon insertions contain FRT sites of 199 bp either 5' (in XP and WH transposons) or 3' (in RB transposons) of the white<sup>+</sup> transgene (w<sup>+</sup>). In the presence of FLP recombinase, efficient trans-recombination between FRT elements results in a genomic deletion with a single residual element tagging the deletion site (Fig. 3.3 a, b, c). Progeny are screened for the presence of the residual element by PCR detection of a resulting hybrid element (e.g., XP, WH) using element-specific primers, or by detection of residual element ends using paired element-specific and genome-specific primers. Final confirmation of the deletion ends can be provided by PCR or sequencing with genome-specific primers. In general, PCR screening of five w<sup>-</sup> individual progeny from w<sup>-</sup> deletion generation crosses, or 50 progeny from w<sup>+</sup> deletion generation crosses, resulted in four confirmed deletions .

Based on FLP-FRT recombination, the following mutants were produced and used in this thesis: *drep-2<sup>ex13</sup>* (completely deleting its CDS using d00223 and e04659 transposon lines), *drep-2<sup>ex27</sup>* (partially deleting its CDS

using e02920 and e04659 transposon lines), and transposon line *drep-4* f02123, *digit*<sup>l0</sup> (deleting the partially *digit* and partially the 5' *StIP* locus using *digit*<sup>f03586</sup> and *digit*<sup>d02327</sup> transposon lines) and transposon line PBac CG16728f03586. For live imaging, *UAS-drep-2-mStraw*+/+, *D42-Gal4*+/+ was used.

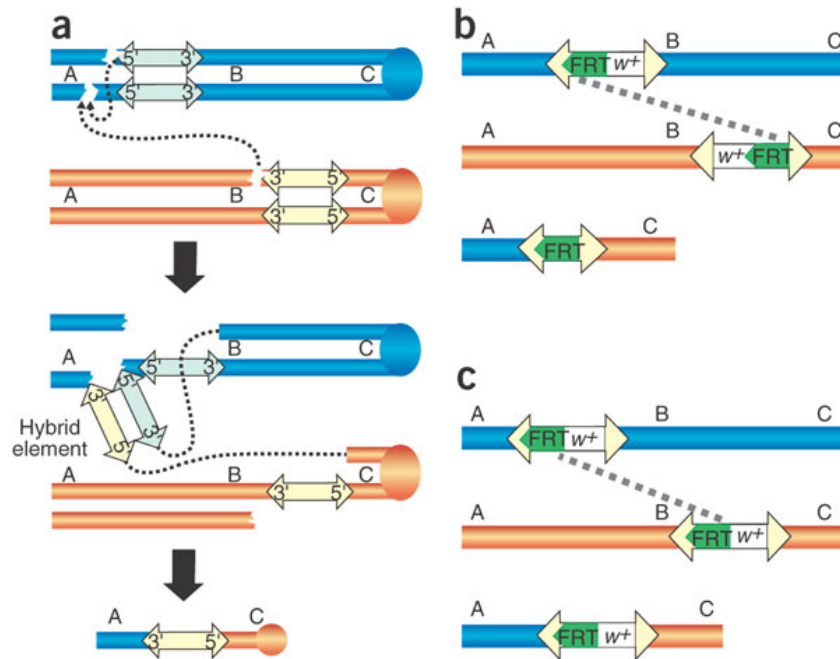


**Figure 3.3 Schematics for deficiency generation.** (a) The HEI strategy which was used at Bloomington. (b) and (c) w- and w+ deficiencies generation from Exelixis transposon insertions using FLP-FRT recombination, respectively. (Adopted from Parks, 2004)

### 3.2.5 P-element imprecise excision screen

In the *Drosophila* genome transposable elements called P-elements which can be mobilized via an enzyme termed transposase occur naturally. The transposase encoding sequence is situated between inverted terminal repeats in the P-element. Stable inserted P-elements lack the transposase encoding sequence but carry genetic markers showing for instance a certain eye or body color. These stable inserted P-elements can be

mobilized with a probability of 11-13% (Karess and Rubin, 1984) by crossing in a transposase expressing chromosome. The majority of the P-elements will jump out precisely removing just the P-element from its insertion site. However a minority of the P-elements removes a random part of the adjacent genomic regions when mobilized in a process termed imprecise excision. In a genetic screen animals carrying a P-element in the gene of interest are exposed to transposase and the next generation is screened for animals lacking the genetic P-element marker. *Djm-1* deletion mutants were generated by the use of a fly line carrying the P-element P{SUPor-P}KG04920 [BDGP Gene Disruption Project (Bellen, 2004)] located in downstream of 3' UTR of *djm-1* CG9951 on the 3<sup>rd</sup> chromosome. A fruit fly line carrying the  $\Delta 2-3$  Transposase on the 2nd chromosome was used to activate P-element mobilization. Adult male flies from lines in which P{SUPor-P}KG04920 might be mobilized were tested for imprecise and precise excision events via single fly genomic PCR (primer pairs: p-element primer together with genomic primer). For mapping imprecise excision furtherly, we used 5 genomic primer pairs of *djm-1* and 4 genomic primer pairs of *Impt*. Single flies genomic PCR was performed according to Gloor (Gloor, 1993).

### 3.3 Yeast two-hybrid

In principle all experiments were conducted according to the yeast two-hybrid protocols of Clontech using the strain AH109 with minor adjustments meeting the requirements of the interaction-domain mapping experiments. Co-transformation of the yeast strain AH109 with both prey and bait constructs (Clontech) was conducted using the following protocol: The yeast was plated on an YPDA (yeast, peptone, dextrose, and adenine) medium agar plate and cultured for two days at 30 °C. An appropriate

amount of YPDA medium was inoculated with a single clone and cultured at 30°C overnight while shaking at approximately 200 rpm. After dilution to OD600 0.2 (10 mL culture volume per transformation) the culture was grown until OD600 reached 0.6. The cells were pelleted, washed in 1xTE (Tris-EDTA)-medium at pH 8.0, repelleted and resuspended in TE/LiAc (100 µl per 10 ml culture volume; LiAc: Lithium acetate). 100 µL resuspended yeast were mixed with the transformation mix which was composed as follows, 500 ng of each of the two plasmids and 10 µl (= 100 µg) Herring Testes carrier DNA (Clontech). After adding 600 µl PEG (Polyethylene glycol)/LiAc, the mix was vortexed and left to incubate at 30°C for 30 minutes in a shaker. Then 70 µl DMSO (10 % final concentration) were added and the cells were heat shocked for 15 minutes at 42°C. After chilling on ice, the yeast was carefully sedimented, the pellet suspended in 100 µl 1xTE-medium pH 8.0, and the transformation plated on minimal SD (synthetic defined) /-Leu/-Trp medium plates, to ensure the presence of both plasmids. After growing for 2 - 3 days at least 10 clones each were analyzed on SD/ -Ade/ -His/ -Leu/ -Trp/ X-α-gal medium plates to select for positive interaction. If > 70% of the clones plated on SD/ -Ade/ -His/ -Leu/ -Trp/ X-α-gal medium plates grew, this was regarded as weak positive interaction (+), > 80% as Intermediate interaction (++) and > 90% and blue clones as strong interaction (+++). Negative controls consisted both of laminin as bait and the prey to be tested and the corresponding bait and the empty prey vector. In the positive control pGBKT7 p53 was cotransformed with pGADT7 containing the SV40 large T antigen.

### **3.4 Cell culture and CoIP**

**(Collaborated with Harald Depner)**

### 3.4.1 Cell culture

Adherent *Drosophila* S2R cells which were kindly provided by Benjamin Mentzel (MSZ, Würzburg) and Alf Herzig (MPI, Göttingen) were cultured at 25 °C in an ambient atmosphere in Schneider's *Drosophila* medium (Biowest) supplemented with 10% fetal calf serum (FCS) + 2 mM L-glutamine, 100 U/ml penicillin and 100 µg/mL Streptomycin (Gibco). Exchange of medium occurred every three to four days. To avoid outgrowth, cell cultures were split every 10 to 14 days. Cell (co-) transfection was conducted using the Effectene® Transfection reagent kit (Qiagen).

### 3.4.2 Cell lysis

Cell Lysis occurred for 45 min on ice with lysis buffer containing 25 mM Tris-HCl pH 7.5, 150 mM NaCl, 2 mM EDTA, 2 mM EGTA, 10% (v/v) Glycerol, 1% (v/v) NP-40 and Roche complete protease inhibitor. Total protein concentrations were determined by BCA protein assay (Pierce) using NanoDrop® ND-1000 or a customary Eppendorf BioPhotometer®. Thereby, a calibration straight line that was previously calculated and stored in a database for the respective assay conditions was used.

### 3.4.3 Immunoprecipitation

For each co-immunoprecipitation test, 350 µg total protein extract from whole-cell lysates was mixed with 30 µl Protein A agarose beads (Affi prep® Protein A support, Bio-Rad) precoupled with the respective antibody or the respective IgG control from mouse or rabbit. These were then incubated for at least one hour at room temperature with slow

agitation. Bound protein was washed four times for 10 minutes with lysis buffer and eluted by boiling in 50 µl Laemmli buffer.

### **3.4.4 Western blot**

IP elutes and whole-cell lysates were subjected to denaturing SDS–PAGE using Tris/HCl NuPAGE 4-12% gradient gels and then transferred to a nitrocellulose membrane (iBlot®, Invitrogen). Membranes were probed with primary antibody directed against the target sequence of the protein or the corresponding tag. Incubation occurred at 4 °C overnight with slow agitation. Detection was done with horseradish peroxidase (HRP)-conjugated secondary antibodies and enhanced chemi-luminescence (ECL, GE Healthcare) with an exposure time of 30 minutes using a Bio-Rad imaging system (Quantity One®). Molecular weight [kDa] of protein bands was assessed using Precision Plus Protein™ All Blue Standards (Bio-Rad).

## **3.5 NMJ Immunohistochemistry**

### **3.5.1 Material**

For all dissections hemolymph-like (HL-3) saline without  $\text{Ca}^{2+}$  (Stewart, Atwood et al. 1994) was used: NaCl 70 mM, KCl 5 mM,  $\text{MgCl}_2$  20 mM,  $\text{NaHCO}_3$  10 mM, trehalose 5 mM, sucrose 115 mM, HEPES 5 mM, pH adjusted to 7.2.

### **3.5.2 Larval body wall preparation**

3<sup>rd</sup> instar larvae were fixed on a rubber dissection pad with fine insect pins (0.1x10 mm, Thorns, Göttingen, Germany) and covered with a drop of ice

cold HL-3 solution. Then, the larvae were opened dorsally along the midline from the posterior to the anterior end with dissection spring scissors (FST, Vancouver, Canada). Subsequently, the epidermis was stretched and pinned down with two to three pins on each side and all internal organs including the central nervous system were removed carefully with fine forceps (FST, Vancouver, Canada).

### **3.5.3 Fixation and staining procedures**

The dissected samples were fixed either for 10' with 4% paraformaldehyde (PFA) in PBS (8 g NaCl, 2 g KCl, 2 g KH<sub>2</sub>PO<sub>4</sub>, 1.15 g Na<sub>2</sub>HPO<sub>4</sub> x 2H<sub>2</sub>O, add 1 L H<sub>2</sub>O, pH 7.4), followed by 30' blocking with PBT (PBS with 0.05% Triton TX100 for NMJ staining and PBS with 0.3% Triton TX100 for CNS staining) containing 5% normal goat serum (NGS). After the blocking, primary antibodies were added into PBT containing 5% NGS, and the dissections were incubated overnight at 4°C. The samples were rinsed for three times shortly on the next day and washed three times for 20' with PBT. Then, fluorescence-labeled secondary antibodies were applied for at least 3 h and at most for 12 h in PBT with 5% NGS at room temperature (RT). The dissections were washed after the appliance of the secondary antibodies and mounted on an object slide in VectaShield Mounting Medium for fluorescent samples (Vector Laboratories, Burlingame, USA).

**->Primary antibodies were used at the following concentrations:**

mouse anti-Brp nc82 (gift of E. Buchner, University of Würzburg, Würzburg, Germany), 1:200

mouse anti-CSP (gift of E. Buchner, University of Würzburg, Würzburg, Germany), 1:50



mouse anti-Futsch 1:50

mouse anti-FasII (1D4, DSHB), 1:40

rabbit anti-GluRIID (Qin and Schwarz, 2005), 1:500

rabbit anti-Brp N-term (Fouquet , submitted), 1:250

rabbit anti-DREP-2, 1:100

rabbit anti-DREP-4, 1:100

rabbit anti-DGIT, 1:250

rabbit anti-StnB, 1:500

mouse anti-GFP 3E6 (A-11120; Molecular Probes, Eugene, USA), 1:500

rabbit anti-GFP (A-11122; Molecular Probes, Eugene, USA), 1:500

goat anti-HRP Cy5 (Dianova, Hamburg, Germany), 1:200

**->Secondary antibodies were used at the following concentrations:**

goat anti-mouse Alexa488 (A-31560, Invitrogen, Karlsruhe, Germany)  
1:500

goat anti-rabbit Alexa488 (A-11034, Invitrogen, Karlsruhe, Germany),  
1:500

goat anti-mouse Cy3 (A-10521, Invitrogen, Karlsruhe, Germany), 1:500

goat anti-rabbit Cy3 (A-10520, Invitrogen, Karlsruhe, Germany), 1:500

goat anti-mouse Atto647N (50185, Sigma-Aldrich, St. Luis, USA), 1:200

goat anti-rabbit Atto647N (40839, Sigma-Aldrich, St. Luis, USA), 1:100

## **3.6 Image acquisition**

### **3.6.1 Procedures for fixed samples imaging**

Conventional confocal images were acquired with a 63x, 1.4 N.A. oil objective suited in a Leica TCS SP5 (Leica Microsystems, Mannheim, Germany). Images taken from fixed samples were exclusively from 3<sup>rd</sup> instar larval NMJs 6/7 (segments A2, A3). The fluorescence detection was set with the AOBS between 500-530 nm for Alexa 488, between 575-620 nm for Cy3, and 650-700 nm for Cy5. PMT gain was set between 800 and 1100 V for maximum sensibility thereby avoiding the bleaching of fluorescent proteins. Alexa 488 was excited using the 488 nm ArKr laser line, while Cy3 were excited with a 561 nm DPSS laser and Cy5 was excited using the 633 nm HeNe laser. The pinhole ranged between 0.5 to 1 airy units, depending on signal strength. Scanning speed was kept at 400 Hz and pixel size varied between 75 nm and 120 nm.

### **3.6.2 *In vivo* imaging**

(in collaboration with Till Andlauer)

*In vivo* imaging was performed on a Leica DMI6000 inverted microscope equipped with a Leica TCS SP5 AOBS scan head and a HCX PL Apo CS 63x 1.32 N.A. OIL objective. The following settings were applied:

->GFP:

Excitation: 488 nm (Ar/ArKr laser)

Detection: 500 – 540 nm, gain 1250 V

->mStrawberry:

Excitation: 561 nm (He/HeNe laser)

Detection: 575 – 620 nm, gain 1250 V

Format: 512 x 512 pixel

pixel size: 97.75 x 97.75 nm

pinhole: 1-2 airy units

All *in vivo* imaging experiments were done as recently presented (Andlauer and Sigrist, 2010). In short, early 3<sup>rd</sup> instar larvae were selected and mounted inside an airproof anaesthetization chamber between two 0.12 mm coverslips. The damaging of the larvae was avoided by placing them in a slit of a thin plastic film, which also held the larvae in place until anaesthetization. The thickness of the film and the size of the slit were adjusted according to the size of the larvae. Both coverslips were covered with Voltalef H 10S oil (Lehman & Voss, Hamburg, Germany) to enable optimal optical access to the ventral larval body wall muscles. Further, a metal ring was placed onto the upper coverslip to fix the animal position and to flatten the larvae as much as possible to improve optic accessibility. To anesthetize the larvae, a mixture of air and Suprane containing the anesthetic desflurane (Baxter, Unterschleißheim, Germany) was lead into the Desflurane to stop all internal movement, including gut peristaltic and heart beating, which is necessary for undisturbed high resolution imaging of the NMJ synapses. It has been demonstrated, that even several rounds of anaesthetization do not interfere with further growth and function of the synaptic system (Rasse, 2005; Fuger, 2007).

## **3.7 Image processing and analysis**

### **3.7.1 Software**

The image analysis itself was led through with ImageJ (NIH, Bethesda, USA). All calculations were performed with Microsoft Excel (Microsoft Corporation, Redmond, USA). Graphics and statistics were produced with Origin 8.0 (OriginLab). Confocal stacks were mainly processed with ImageJ software. Image transformation and compilation was done with Adobe Photoshop (Adobe Systems, San Jose, USA).

### **3.7. 2 Image quantifications**

All images comprising the synapse number quantification were acquired using the same microscope settings, control and mutant dissections were stained in the same vial.

To count the number of synapses per NMJ, first the original stack was scaled up two-fold. A Gaussian filter with a radius of two pixels was applied. The contrast of the maximum projection of that image stack was adjusted in such way, that the intensity maximum of the picture was set to 255 (min/max contrast function, ImageJ). Afterwards a threshold was set excluding all pixels with a value inferior to 51. The segmentation of single synapses was done by hand with the pencil tool and a line thickness of 2 pixels. The processed image was then transformed into a binary picture with all pixels with a value lower than 51 receiving the value “0” and all pixels with a value higher and equal to 51 were reassigned to a value of “255”. This binary mask was then projected onto the original unmodified image using the “min” operation from the ImageJ image calculator. The synapses of resulting image were counted with the help of the “analyze

particle” function with the threshold set to 1, thereby measuring the number, the size and the mean intensity for every synapse.

### **3.7.3 Statistical analysis**

The nonparametric Mann-Whitney rank sum test was used for statistical analysis of all linear independent data groups. The data are reported as mean  $\pm$  SEM, n indicates the sample number, and p denotes the significance: \*  $p < 0.05$ , \*\*  $p < 0.01$ , \*\*\* $p < 0.001$ . Linear and non-linear (Gaussian fit) regression was used to determine significant data correlation.

## **3.8 EM**

**(Collaborated with Carolin Wichmann)**

### **3.8.1 Image acquisition**

Dissected preparations were primary fixed in a mixture of 4% paraformaldehyde and 0.5% glutaraldehyde in 0.1M PBS (pH 7.2) for 10 min and fixed additionally 60 min with secondary fixative comprising of 2% glutaraldehyde in 0.1 M sodium cacodylate buffer (pH7.2), washed three times for 5min in sodium cacodylate buffer, and postfixed on ice for 1hr with 1% osmium tetroxide and 0.8% KFeCn in 0.1 M cacodylate buffer, followed by an 1hr washing step in sodium cacodylate buffer and three brief washing steps in distilled water. The samples were stained en bloc with 1% uranyl acetate in distilled water for 1hr on ice. After a brief wash with distilled water, the samples were dehydrated in increasing ethanol concentrations (30%, 50%, 70%, 95%, 100%), infiltrated in Epon resin (100% EtOH/Epon 1:1, 30 min and 90 min; 100% Epon, over night). Muscles 6/7 were cut out (5 animals for each genotype) and embedded in a

single block. Blocks were polymerized for 48hr at 85°C. The samples were trimmed, and series of 65nm ultrathin sections were cut with a diamond knife on a Leica Ultracut Ultramicrotome (UC6) and mounted on Formvar-coated grids. The sections were stained in uranyl acetate (4%) and lead citrate. Micrographs were taken with a  $1024 \times 1024$  CCD detector (Proscan CCD HSS 512/1024; Proscan Electronic Systems, Scheuring, Germany) in an EM 902A (Zeiss, Oberkochen, Germany), operated in bright field mode.

### **3.8.2 Statistics of the EM images**

Quantification of SVs density close to the bouton periphery: A square of  $0.4 \times 0.4 \mu\text{m}$  was placed in the bouton periphery, close to AZ, followed by counting the number of SVs and normalize to  $\text{SV}/\mu\text{m}^2$ . Quantification of clustered SVs: In order to count the number of SVs in a distance of 50-150 nm to the T-bar, a grid (in a radius of 150 nm) was placed around the T-bar and the number of SVs was counted in each shell. Quantification of the SV-density of whole bouton: All SVs per section per bouton were counted, followed by normalizing to  $\text{SV}/\mu\text{m}^2$ . Large sized vesicles: counted per section per bouton. The data are reported as mean  $\pm$  SEM, and unless otherwise noted n indicates the number of junctions examined and P designates the significance according to the Student's t-test. In the figures, significance is marked with asterisks:  $p < 0.05$  (\*),  $p < 0.01$  (\*\*),  $p < 0.005$  (\*\*\*), t-test.

## **3.9 Behavioral assays**

For negative geotaxis, flies with clipped wings were tested individually in an empty food vial in dark (Wagh, 2006). The height of the fly on the vial wall 30 s after tapping the fly to the bottom of the vial was recorded. For

the walking test, individual flies with clipped wings were placed in the center of a large size paper (80 x 120 cm) on which had been marked with a  $2 \times 2$  cm square grid. The number of grid line crossings within a period of 30 s was recorded.

## **4. Results part1: functional analysis of DREP-2, a novel synaptic protein of *Drosophila***

### **4.1 Identification of DREP-2 within Brp immunoprecipitates**

Manuela Schmidt in her PhD thesis (“characterization of synaptic protein complexes in *Drosophila melanogaster*”; Universität Göttingen 2006) performed co-immunoprecipitations using a monoclonal antibody (MAB Nc82) directed against Bruchpilot (Brp). MAB Nc82 efficiently precipitated Brp (see thesis of Manuela Schmidt). Amongst other proteins, DREP-2 was found to co-precipitate with Brp by mass spectrometry (MS) analysis (Fig. 4.1A).

To test whether DREP-2 and Brp can in principle form a complex, they were co-expressed in *Drosophila* S2R+ cells (DREP-2-EGFP and Brp D1-2-Myc co-transfected) and interaction tested by CoIP from *Drosophila* S2R+ cells (Fig. 4.1B). Brp D1-D2 (1-617 aa of Brp) or D2 (268-617 aa of Brp) could pull down DREP-2 GFP.

In order to elucidate whether DREP-2 might directly interact with Brp or DLC-2, overlapping constructs of those proteins were used as bait or prey in a yeast-two-hybrid (Y2H) assay. The autotrophic yeast strain was cotransfected with a single pair of bait and prey vectors to be tested. Y2H analysis shows that robust interaction “in both directions” (concerning bait and prey relation) of DREP-2 C-terminal and Brp D2 domain, and also that



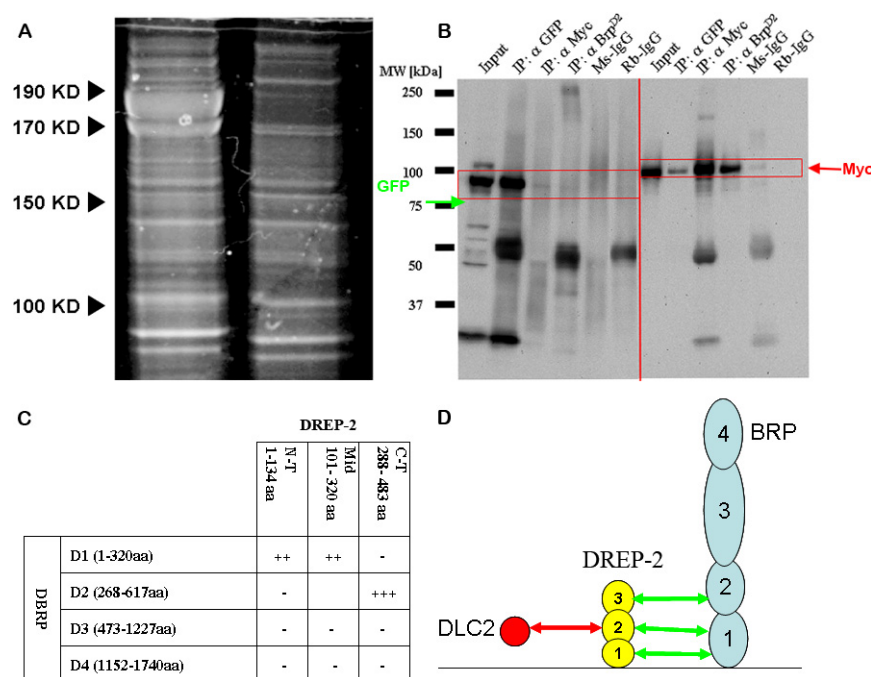


**Figure 4.1 DREP-2 could interact with Brp.** (A) SDS-PAGE of an anti-MAB nc82-IP and the corresponding control eluted with SDS sample buffer (see thesis of Manuela Schmidt, unpublished data). Manuela Schmidt found that DREP-2 could co-precipitate with Brp by MS/MS analysis. (B) Immunoblots of co-immunoprecipitation obtained from GFP-DREP-2 (full length) and Brp D1-D2-myc (aa1152-1740) co-transfected *Drosophila* Schneider S2R cells. Anti-Myc, -EGFP, -nc82 and control IPs are shown. (This result was obtained in collaboration with Harald Depner) (C) DREP-2 could interact physically with Brp D1-D2 domains in the Yeast-two-hybrid (Y2H). Robust interaction of DREP-2 C-terminal and Brp D2 domain was found by Y2H analysis. Y2H also showed that the N-terminal and middle of DREP-2 interacted with Brp D2 domain (when DREP-2 was used as bait). (D) Interaction summary of DLC-2, Brp and DREP-2 detected by Y2H.

the N-terminal and middle of DREP-2 interacted with Brp D2 domain “in one direction” (when using DREP-2 as bait) suggesting that DREP-2 could also interact physically with Brp D1-D2 domains (Fig. 4.1C-D) in the Y2H analysis. In summary, these results open the possibility that DREP-2 biochemically interacts with Brp. Thus, reagents for further *in vivo* analysis were generated.

According to the yeast-2-hybrid interaction data from BioGRID (<http://www.thebiogrid.org/searchresults.php?id=61791>), Dynein light chain 2 (DLC-2) might be an interaction partner of DREP-2. In fact, also in Y2H analysis of our lab, DLC-2 interacted physically with the middle domain of DREP-2 (Fig. 4.1C-D). This result is visualized in Fig. 4.1D.

## 4.2 DREP-2 - structural considerations

DREP-2 contains one CIDE-N (cell death-inducing DFF45-like effector N terminus) domain, which is a member of the novel family of apoptosis-inducing factors that share homology with the N-terminal region of DFF, a DNA fragmentation factor (Fig. 4.2). Beside DREP-2 (CG1975), the *Drosophila melanogaster* genome encodes three additional DFF-related proteins, namely DREP-1 (CG8357), DREP-3 (CG8364) and DREP-4 (CG9414) (Fig. 4.2), based on their homology with mammalian DFF and CIDE proteins. DFF is composed of two subunits, DFF40 (caspase activated DNase, CAD and caspase-activated nuclease) and DFF45 (inhibitor of CAD, ICAD). DFF40 has a nuclease domain that can cleave naked and chromosomal DNA, whereas DFF45 is a regulatory subunit that suppresses the nuclease activity of DFF40. DREP-1 (DFF45-related protein-1) is highly conserved during evolution. DREP-4 was investigated as an apoptosis effector recently. The CIDE-N peptide sequence of the DFF40 (CAD) nuclease as well as in CIDE proteins in general acts as a regulatory domain (Fig. 4.2). Similarly, the activity of DREP-2, DREP-3 and DREP-4 might be regulated by their corresponding CIDE-N domains. FlyAtlas provides the most comprehensive view of expression in multiple tissues of *Drosophila melanogaster* (Canton S strain) from equal numbers of male and female 7-day old flies or 3<sup>rd</sup> instar larvae by quantitative analysis using real time PCR for different tissues (Chintapalli, 2007; [www.flyatlas.org](http://www.flyatlas.org)). The mRNA of *drep-2* enriches in adult brain

(enrichment, 20.7), adult ventral ganglion (enrichment, 11.6) and larval CNS (enrichment, 12.02), respectively (Table 1). Similarly, the mRNA of *drep-3* also enriches in adult brain (enrichment, 31), adult ventral ganglion (VG, enrichment, 17.2) and larvae CNS (enrichment, 11.37), respectively. The mRNA enrichment of *drep-1* in adult brain, adult ventral ganglion, adult ovary and larval CNS is 2.8, 1.3 and 1.21, but that of *drep-4* in adult brain, adult ventral ganglion and larval CNS is 2.9, 2.9 and 1.39, respectively. In summary, it seems that the mRNA of *drep-2* and *drep-3* is enriched in brain and ventral ganglion of adult flies and larvae CNS rather than *drep-1* and *drep-4*.

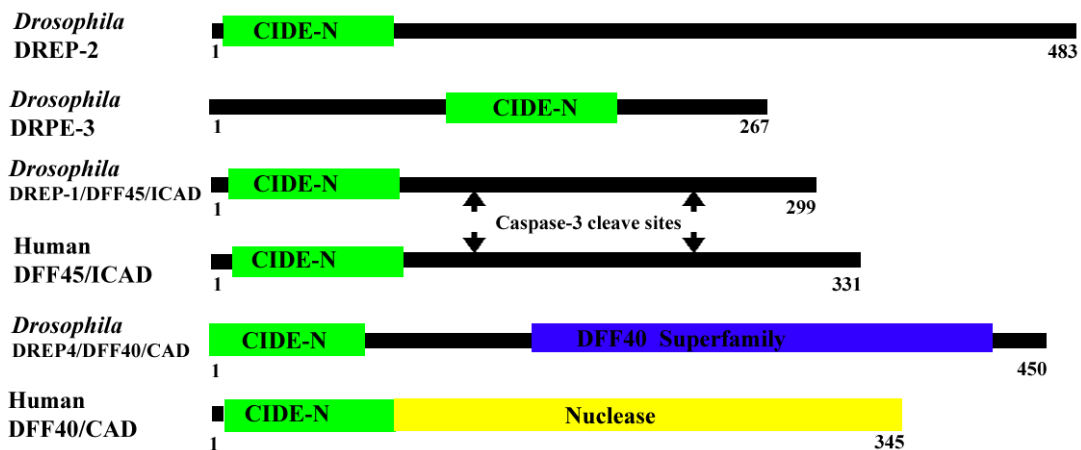


**Figure 4.2 Schematic structures of DREP and DFF proteins.** *Drosophila* DREP proteins share homology with mammalian DFF proteins. All proteins display a conserved CIDE-N (green bar) domain. DREP-4 has another DFF40 [caspase activated DNase (CAD) or caspase-activated nuclease] domain. DREP-1 and DREP-4 are the *Drosophila* homologues of DFF45 and DFF40, respectively. DFF45 has two sites that are cleaved by caspase-3 and conserved in DREP-1 (arrows), whereas DFF40 contains a nuclease domain (blue bar).

	<i>drep-1</i>	<i>drep-2</i>	<i>drep-3</i>	<i>drep-4</i>
<b>Adult brain</b>	2.8	20.7	31	2.9
<b>Adult VG</b>	1.3	11.6	17.2	2.9
<b>Larval CNS</b>	1.21	12.02	11.37	1.39

**Table 1 *drep* mRNA enrichment in adult flies and larvae as detected by RT-PCR from flyatlas database** (www.flyatlas.org; Chintapalli, 2007). Tissues were dissected out from equal numbers of male and female 7-day old Canton S wild-type flies and pooled to make at least 1500 ng mRNA, then amplified and hybridized using the Affymetrix standard protocol. The numbers in the table represent the enrichment in the corresponding tissue, which was normalized to that of whole flies. These data are taken from the FlyAtlas database (www.flyatlas.org; Chintapalli, 2007).

### 4.3 *drep-2* is specifically expressed in the nervous system

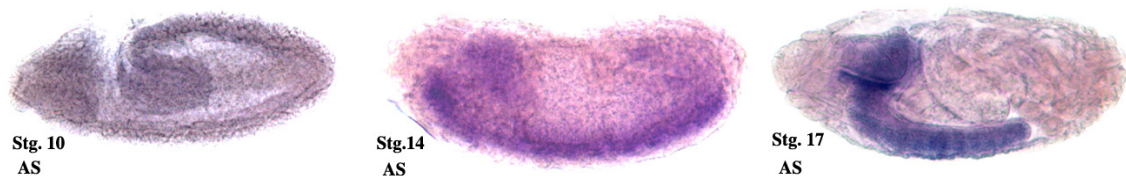


**Figure 4.3 *In situ* hybridization of *drep-2* in *Drosophila* embryos.** Specific staining was obtained when an antisense probe of *drep-2* cDNA was used. Sense probes did not produce any label in the experiment. *Drosophila drep-2* was specifically expressed in the CNS and ventral chord from stage 14 throughout embryogenesis.

*In situ* hybridizations were of *Drosophila* embryos to investigate the spatio-temporal expression pattern of *drep-2* were performed. A strong, specific label of *drep-2* was detected in the central nervous system (CNS) from stage 14 on (Fig. 4.3). The onset of *drep-2* mRNA expression thereby corresponded to the onset of neuronal differentiation and axon outgrowth (Broadie and Bate, 1993). Thus, the spatio-temporal expression profile of

the *drep-2* mRNA expression is consistent with the assumption that it is specifically expressed in postmitotic neurons.

## 4.4 Generating tools for analysis of *drep-2*:

### Mutants and antibodies

#### 4.4.1 Generation of a *drep-2* deletion mutant

We intended to subject *drep-2* for genetic analysis. However, a priori no mutant for this locus was available. Thus, a transposon based strategy for producing a precise deletion of the locus was entailed. According to Parks et al (Parks, 2004), activation of heat shock–driven FLP recombinase (*hs-FLP*) at 37 degree results in the precise recombination deletion between two FRT-bearing transposon insertions in *trans*. Candidate chromosomes then have to be confirmed by genomic PCR. Deletions get established in isogenized background (Fig. 4.4.1). Based on FLP-FRT recombination between *drep-2*<sup>d00223</sup> and *drep-2*<sup>e04659</sup> or between *drep-2*<sup>e02920</sup> and *drep-2*<sup>e04659</sup> transposon lines, mutant *drep-2*<sup>ex13</sup> (in red dash) and *drep-2*<sup>ex27</sup> (in green dash), which deletes its CDS (CDS, coding DNA sequence) completely and partially, respectively, was produced (Fig. 4.4.2A).

*Df4966*, which ordered from Bloomington stock center (No. 4966), was used in *trans* as “large”, non-locus-specific deficiency, which also eliminates *drep-2*. *Drep-2*<sup>ex13/Df4966</sup> was used in this thesis as a “*drep-2* mutant” (Fig. 4.4.2A). Deletions were confirmed by genomic PCR using *drep-2* genomic primer pairs (Fo: GCTGCTTGAGTATGGGTGCA; Re: GGAGACATCCTCTCAAAGC; Product size: 487 bp). This way, *drep-*

$2^{ex13}$  and  $drep-2^{ex27}$ , deletion of genomic sequence as indicated in Fig. 4.4.2B could be validated.

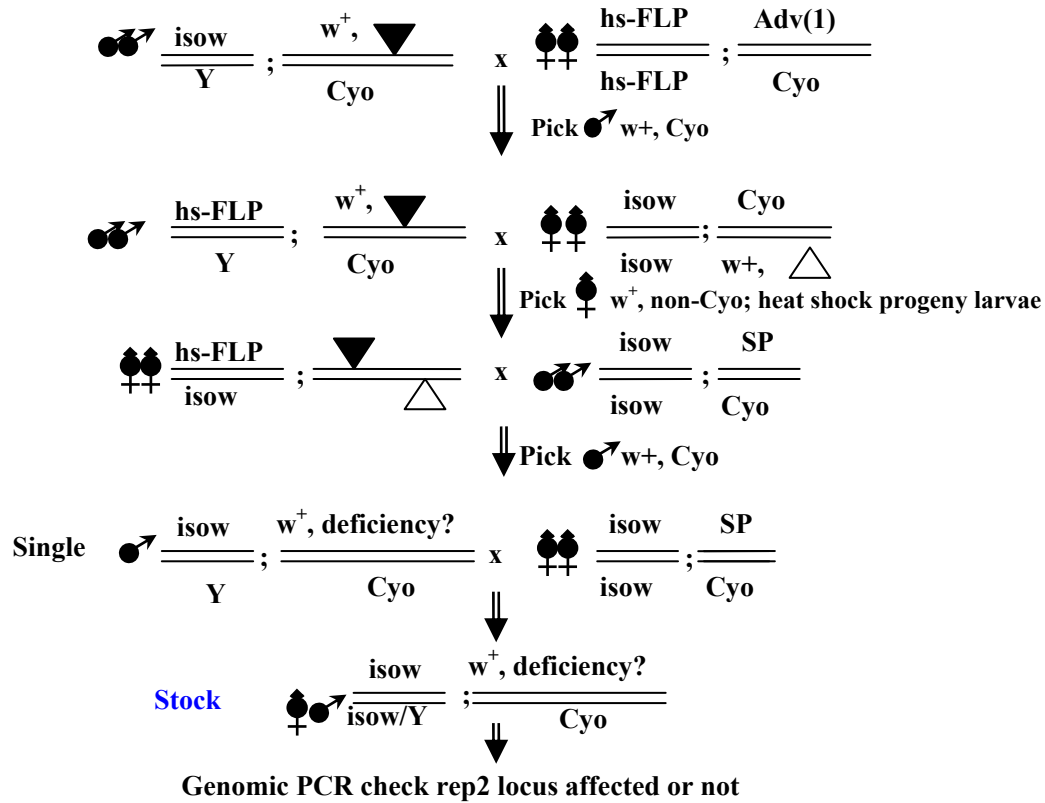


**Figure 4.4.1 Genetic scheme used for FLP-FRT-based *drep-2* deletions.** Crosses place two piggyBac (PBac) FRT-bearing transposon insertions in *trans* in the presence of heat shock-driven FLP recombinase (*hs-FLP*) at 37 °C. Activation of FLP recombinase results in the generation of deletions that can be detected by genomic PCR. Deletions are established in isogenized stocks with balancers (Cyo). *drep-2<sup>ex13</sup>* (in red dash) or *drep-2<sup>ex27</sup>* (in green dash) were produced based on FLP-FRT recombination between *drep-2<sup>d00223</sup>* and *drep-2<sup>e04659</sup>* or between *drep-2<sup>e02920</sup>* and *drep-2<sup>e04659</sup>* transposon lines. *iso*, isogenized chromosome; Y, Y chromosome; Adv (1) and Sp are the dominant markers. ▼ and Δ represents the FRT-bearing transposon element 1 and 2, respectively.

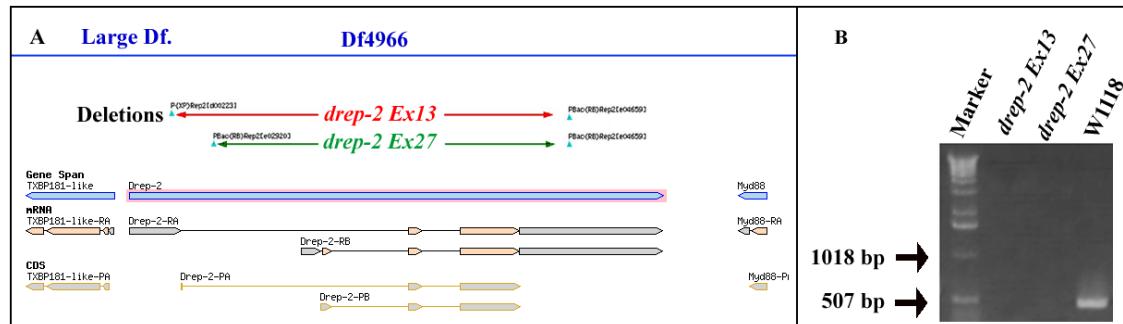


**Figure 4.4.2 *Drosophila drep-2* mutantgenesis** (A) Schematic overview of *drep-2* mutantgenesis. Based on FLP-FRT recombination between *drep-2*<sup>d00223</sup> and *drep-2*<sup>e04659</sup> or between *drep-2*<sup>e02920</sup> and *drep-2*<sup>e04659</sup> transposon lines, mutant *drep-2*<sup>ex13</sup> (in red dash) and *drep-2*<sup>ex27</sup> (in green dash), which delete its coding region completely and partially, respectively, were recovered. A large deficiency of *drep-2* used is *Df4966* ordered from Bloomington (No.4966) here, *drep-2*<sup>ex13/Df4966</sup> as gene-specific mutant was used in this thesis. (B) Chromosomal deletions were confirmed by genomic PCR. As expected, both mutants, *drep-2*<sup>ex13</sup> and *drep-2*<sup>ex27</sup>, lack the amplification products with a genomic primer pairs for the *drep-2* locus (Product size: 487 bp). In contrast, controls (*w*<sup>1118</sup>) allowed amplification.

## 4.4.2 Generating a polyclonal anti-DREP-2 antibody and transgenic flies of full length DREP-2

To visualize DREP-2 in western and immuno-stainings, polyclonal DREP-2 antibodies were produced. To this end, 6xHis-fused DREP-2 N-terminal (DREP-2-PA: 2-250 aa) and 6xHis-fused DREP-2 C-terminal fusion proteins (DREP-2-PA: 250-482 aa) were recombinately expressed in E-coli, purified using TALON-resin (Clontech), and finally injected into different rabbits. In total six animals were immunized and injected by SEQLAB Sequence Laboratories Göttingen GmbH: 2 animals (Cat. No. #7185 and

7186) for N-term peptide; 2 (#7183 and 7184) for C-term peptide; 2 (#7187 and 7188) for N+C-term peptides. The serum was harvested from the injected rabbit after three months. The antigen injection and serum harvest were performed for 3 times, followed by affinity purification under denatured conditions using the corresponding purified GST fused DREP-2 peptide as bait.

Three different polyclonal DREP-2 antibodies were purified from the serum against DREP-2 N-term (DREP-2-PA: 2-250 aa) and C-term (DREP-2-PA: 250-482 aa) fusion protein, respectively, as well as against a mixture of N- and C-term fusion proteins (N+C). The purified antibody against the N+C-term (DREP-2-PA: 2-250 aa and 250-482 aa) fusion proteins of DREP-2 gave a good staining signal, and was predominantly used in this thesis.

The CG1975 locus (II. Chromosome) encodes the DREP-2 proteins. The *Drosophila drep-2* cDNAs have two transcripts of 5.2 (DREP-2-RA) and 4.8 kb (DREP-2-RB) in length and encode two putative proteins (DREP-2) of 482 aa (DREP-2-PA) and 549 aa (DREP-2-PB) in length. The polyclonal DREP-2 antibody recognizes bands of molecular weight of about 60 and 68 kDa on immunoblots of wild type adult flies head lysate [shift the predicted sizes of for the two DREP-2 isoforms (52 and 58 kDa)], whereas *drep-2<sup>ex13</sup>* (Fig. 4.4.3A) as well as *drep-2<sup>ex27</sup>* (data not shown) did not show the bands. Thus, these results imply that the polyclonal DREP-2 antibody produced against a DREP-2 fusions proteins specifically recognizes the two isoforms on western blot, and also that both *drep-2<sup>ex13</sup>* (Fig. 4.4.3A) and *drep-2<sup>ex27</sup>* are null alleles of *drep-2*.

The specificity of the DREP-2 antibody was investigated in the CNS and at the NMJ by immunofluorescence. The DREP-2 antibody against its N+C-



terminal peptides (N-term, 1-249 aa;C-term, 252-483 aa) stained the brains of *w<sup>1118</sup>* 3<sup>rd</sup> instar larvae (Fig. 4.4.3B). However, *drep-2<sup>ex13/Df4966</sup>* (Fig. 4.4.3C) or *drep-2<sup>ex27/Df4966</sup>* (data not shown) animal were without staining. Thus, based on the absence of neuropil staining in the null mutants, the DREP-2 antibody in larvae seems specific.

These results also suggest that the DREP-2 antibody has specific staining in the larval CNS, and that the endogenous DREP-2 proteins exist in the larval CNS. However, the purified DREP-2 antibody against N+C-term peptides (data not shown) labeled not only NMJs of 3<sup>rd</sup> instar larvae in *w<sup>1118</sup>* (Fig. 4.4.3D), but also in *drep-2<sup>ex13</sup>*, which does not show an obvious different staining pattern in control and the null mutant (data not shown). This residual label of the DREP-2 antibody at NMJs of the null mutant (*drep-2<sup>ex13</sup>*) indicates that this particular antibody displays a cross reactivity.

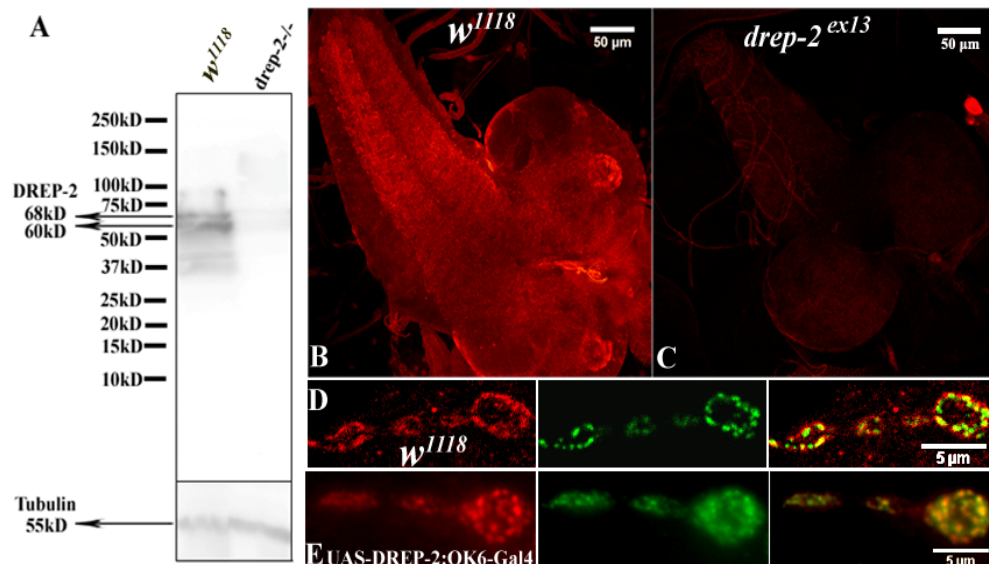


**Figure 4.4.3 DREP-2 antibody staining in immunoblot and immunofluorescence.** The DREP-2 antibody against its N+C-terminal peptides was used at 1:1000 and 1:100 dilutions for immunoblot and immunofluorescence, respectively. (A) Western blot of

DREP-2 in adult head extracts. The lysate from 20 adult fly heads of *drep-2<sup>ex13</sup>* or *w<sup>1118</sup>* was subjected to 10% SDS-PAGE, followed by immunoblot by the rabbit DREP-2 (1:1000) antibody against its N+C-terminal peptides and by the mouse tubulin (1:3000) to check the specificity of DREP-2 antibody. The polyclonal anti-DREP-2 antibody recognized two bands at the molecular weight of 60 and 68 kDa on immunoblots [shift the predicted sizes of for the two DREP-2 isoforms (52 and 58 kDa)] of wild type adult flies head lysate. But, the *drep-2* mutant lost any label at the both bands. (B) DREP-2 antibody neuropil staining in the CNS of 3<sup>rd</sup> instar larvae in *w<sup>1118</sup>*, but not in *drep-2<sup>ex13</sup>* (C). (D) DREP-2 antibody (in red) partially colabels with Brp (staining with nc82, in green) at NMJ of 3<sup>rd</sup> instar larvae not only in *w<sup>1118</sup>* but also in *drep-2<sup>ex13</sup>* (data not shown). (E) DREP-2 antibody (in red) labels the GFP fusion DREP-2 (UAS-GFP-DREP-2-PA, in green) driven by OK6-Gal4 (motor neuron specific) at NMJs of 3<sup>rd</sup> instar larvae.

What does the cross reactivity from? One possibility is that the cross reactivity comes from the interactor of DREP-2, for example other DREP proteins including DREP-3, -1 and -4. All DREP proteins have a conserved domain, CIDE-N, and might form a complex through the CIDE-N domain. Transgenic lines of UAS-GFP-DREP-2-PA were established. To investigate whether the transgene allows DREP-2 (over)expression, antibodies at 3<sup>rd</sup> instar larvae NMJ of OK6-Gal4/+; UAS-GFP-DREP-2-PA/+ was performed (Fig. 4.4.3E). The DREP-2 antibody co-labeled with GFP staining at the synaptic sites of 3<sup>rd</sup> instar larvae NMJs (Fig. 4.4.3E), suggesting that the transgenic UAS-GFP-DREP-2-PA could be driven at the NMJ by the motor neuron driver OK6-Gal4.

## **4.5 DREP-2 and DREP-4 localize at synapses of the fly CNS**

### **4.5.1 DREP-2 is a neuropil specific protein**

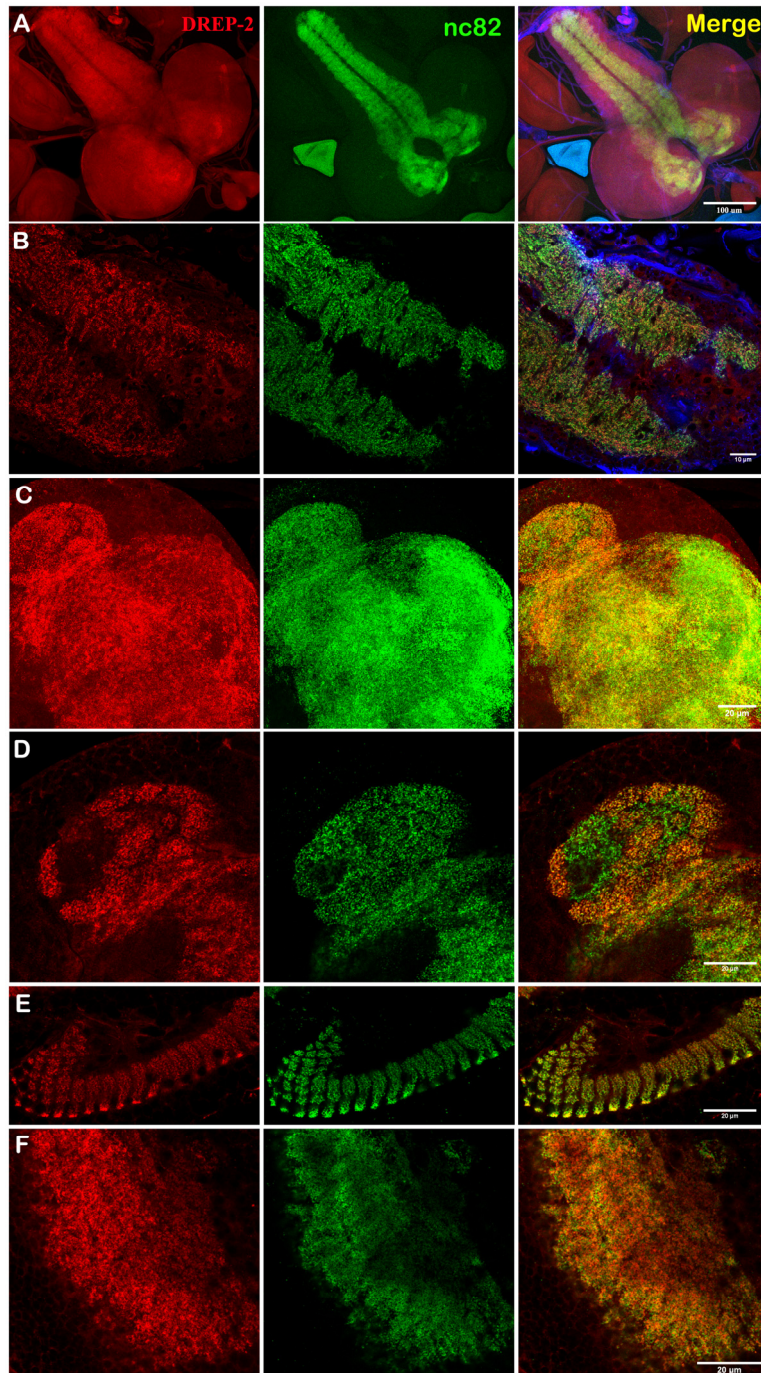


**Figure 4. 5.1 DREP-2 shows neuropil expression in the CNS of 3<sup>rd</sup> instar larvae.** Endogenous DREP-2 (red) and Brp protein (green) are recognized by the DREP-2 and BRP antibody in the CNS, y (A), including the ventral ganglion (B), the calyx of mushroom body (MB; C-D), as well as lamina (E) and lobular (F) of the optic system. Rectangle indicates MB. Scale bar, 20  $\mu$ m except for Fig. 4.5.1A (100 $\mu$ m) and Fig. 4.5.1B (10 $\mu$ m). (Collaborated with Till Andlauer)

To determine where DREP-2 localizes in subcellular regions of the larval CNS, triple-label immunofluorescence staining by DREP-2, nc82 (label BRP, as presynaptic active zone marker) and HRP (presynaptic membrane marker) antibodies at 3<sup>rd</sup> instar larvae brains was performed (Fig. 4.5.1). Endogenous DREP-2 protein (red) is present in the CNS (Fig. 4.5.1A), including the ventral ganglion (Fig. 4.5.1B), Calyx of mushroom body (MB, Fig. 4.5.1C-D), lamina (Fig. 4.5.1E) and lobula in optic lobe (Fig. 4.5.1F), which the staining is gone in the larval CNS of mutants, suggesting it is specific.

The expression of Brp is not only restricted to the glutamatergic type I boutons of the NMJ, but also Brp is present in active zones of presumably all synapses. Consistently, synapses that contain high levels of either choline acetyltransferase or GABA/glutamic acid decarboxylase do not show reduced Brp staining, and Brp staining is found at both glutamatergic and non-glutamatergic synapses (Wagh, 2006). Brp is required for normal synaptic transmission at histaminergic synapses (Wagh, 2006; Kittel, 2006). As shown in Fig. 4.5.1, DREP-2 presents and is very closed to Brp locally in some neuron types. It suggests that DREP-2 might be a synaptic protein playing important roles. Whether DREP-2 is a presynaptic or postsynaptic protein need be further investigated by ultrastructural analysis using Immuno-Electron Microscopy (IEM).

## **4.5.2 Synaptic localization of DREP-4 in the fly CNS**

Genes with homology to DFF/CIDEs were found in *Drosophila melanogaster*, including *drep-1*, *drep-3* and *drep-4*. DREP-1 and DREP-3

can interact with DREP-2 by immunoprecipitation and immunoblotting analysis (Inohara, 1999). It is likely that DREP-2 operates in conjunction with its family members, (Inohara N, 1998; Inohara and Nunez, 1999). To determine whether and if where the family member DREP-4 localizes at synaptic sites in CNS, a DREP-4 polyclonal antibody (Yokoyama, 2000) was used for immuno-fluorescence stainings at 3<sup>rd</sup> instar larvae (Fig. 4.5.2A-E). The DREP-4 polyclonal antibody labeled axons (Fig. 4.5.2A,

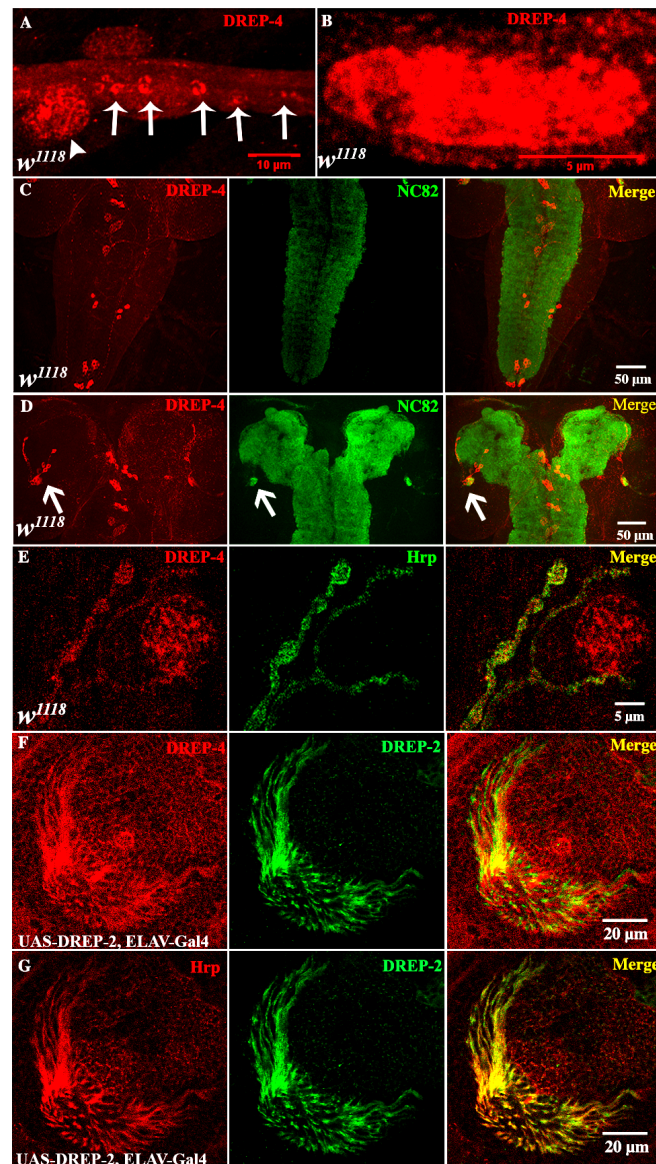


**Figure 4.5.2 DREP-4 staining in CNS.** DREP-4 polyclonal antibody could label not only in axon (A, arrows), nuclei (A, arrow heads) and mitochondria (B) of axon, also in cell body of ventral ganglion (C) and brain (D) as well as at boutons (E) of control *w<sup>1118</sup>*



*Drosophila* 3<sup>rd</sup> instar larvae. (F) DREP-4 and DREP-2 polyclonal antibody could label the optic lobe of *Drosophila* 3<sup>rd</sup> instar larvae in *UAS-DREP-2-GFP/+; Elav-Gal4/+* animals, however the two staining signals of DREP-2 and DREP-4 are very locally close each other, but do not colocalize. (G) DREP-2 polyclonal antibody and HRP antibody could partially co-label at the synaptic site of the optic lobe in *Drosophila* 3<sup>rd</sup> instar larvae of *UAS-DREP-2-GFP/+; Elav-Gal4/+*. Scale bar is indicated in the images.

arrows), muscle nuclei (Fig. 4.5.2A, arrow heads) and mitochondria (Fig. 4.5.2B) of axons, also cell bodies of the ventral ganglion (Fig. 4.5.2C) and brain (Fig. 4.5.2D) as well as at boutons (Fig. 4.5.2E) of *Drosophila* control *w<sup>1118</sup>* 3<sup>rd</sup> instar larvae. DREP-2 and DREP-4 do not colocalize in axon, mitochondria, muscle nuclei and cell body of the ventral ganglion of control *w<sup>1118</sup>* (data not shown). The staining signals of DREP-4 are restricted to a certain group of neurons of control *w<sup>1118</sup>* 3<sup>rd</sup> instar *Drosophila* larvae brain (Fig. 4.5.2D, arrows), but the identity of these neurons I have not worked out yet. DREP-4 polyclonal antibody could also label boutons (Fig. 4.5.2E) of control *w<sup>1118</sup>* *Drosophila* 3<sup>rd</sup> instar larvae similar with HRP, but not perfectly colocalize with HRP staining. The DREP-4 and DREP-2 polyclonal antibodies could label the optic lobe of *Drosophila* 3<sup>rd</sup> instar larvae in *UAS-DREP-2-GFP/+; Elav-Gal4/+* strain. However, the two staining signals of DREP-2 and DREP-4 are very locally close each other at synaptic sites, but not colocalize (Fig. 4.5.2F). These results indicate that DREP-4 might be expressed at synaptic sites of CNS, and might interact with DREP-2 or Brp playing roles in synapses.

## 4.6 *Drosophila drep-2* mutants potentially show a NMJ morphological phenotype

Homozygous *drep-2*<sup>ex13</sup> (Fig. 4.4.2A, in red dash), *drep-2*<sup>ex27</sup> (Fig. 4.4.2A, in green dash) and *drep-2*<sup>ex13/Df4966</sup> as well as *drep-2*<sup>ex27/Df4966</sup> adult flies are viable. Homozygous *drep-2*<sup>ex27</sup> is sterile in female, which might be due to a secondary mutation on this chromosome, as homozygous *drep-2*<sup>ex13</sup> is fertile. Thus, *drep-2*<sup>ex13/Df4966</sup> and *drep-2*<sup>ex27/Df4966</sup> were used in this thesis as *drep-2* mutant constellations (Fig. 4.4.2A). Negative geotaxis and walking abilities in these *drep-2* null mutant constellations were investigated. Both mutant constellations did not display defects in negative geotaxis or walking ability (Fig. 4.6A-B).

NMJs of 3<sup>rd</sup> instar *drep-2* mutant larvae were analyzed to investigate whether the *drep-2* mutant has any abnormal phenotype in the level and distribution of Brp by immunostainings with DREP-2, Brp and HRP antibodies. The *drep-2* mutant, *drep-2*<sup>ex13/Df4966</sup> (Fig. 4.6E, arrow heads) resulted in the formation of smaller mal-developed boutons, or satellite boutons, surrounding the large synaptic boutons, which is not observed so frequently in control *w*<sup>1118</sup> (Fig. 4.6D). Recently, it was suggested that these smaller satellite boutons are largely functional, but are often detected in mutants with endocytic defects (Koh, 2004; Marie, 2004; Ester, 2003; Dickman, 2006). By re-expression of *Drosophila* full length DREP-2-PA in *drep-2* mutants, the satellite boutons patterns could be restored to control level (Fig. 4.6G). Statistics of satellite boutons number in the *drep-2* mutant was done. Satellite boutons in the *drep-2* mutant are 6 times (2.0±1.3) higher than for control *w*<sup>1118</sup> (0.4±0.5), which could be rescued partially by re-expression (0.7±0.8) of full length DREP-2-PA in the *drep-2* mutant background (Fig. 4.6C). These results show that *drep-2*

deficiency induces the satellites boutons and mislocalization, DREP-2 might play roles for proper morphological development of the NMJ.

Occasionally, mislocalization between Brp and GluRIID was observed as well (Fig. 4.6F, arrows). Future analysis will have to show whether the mislocalization is specific dueing to the depletion of *drep-2*.

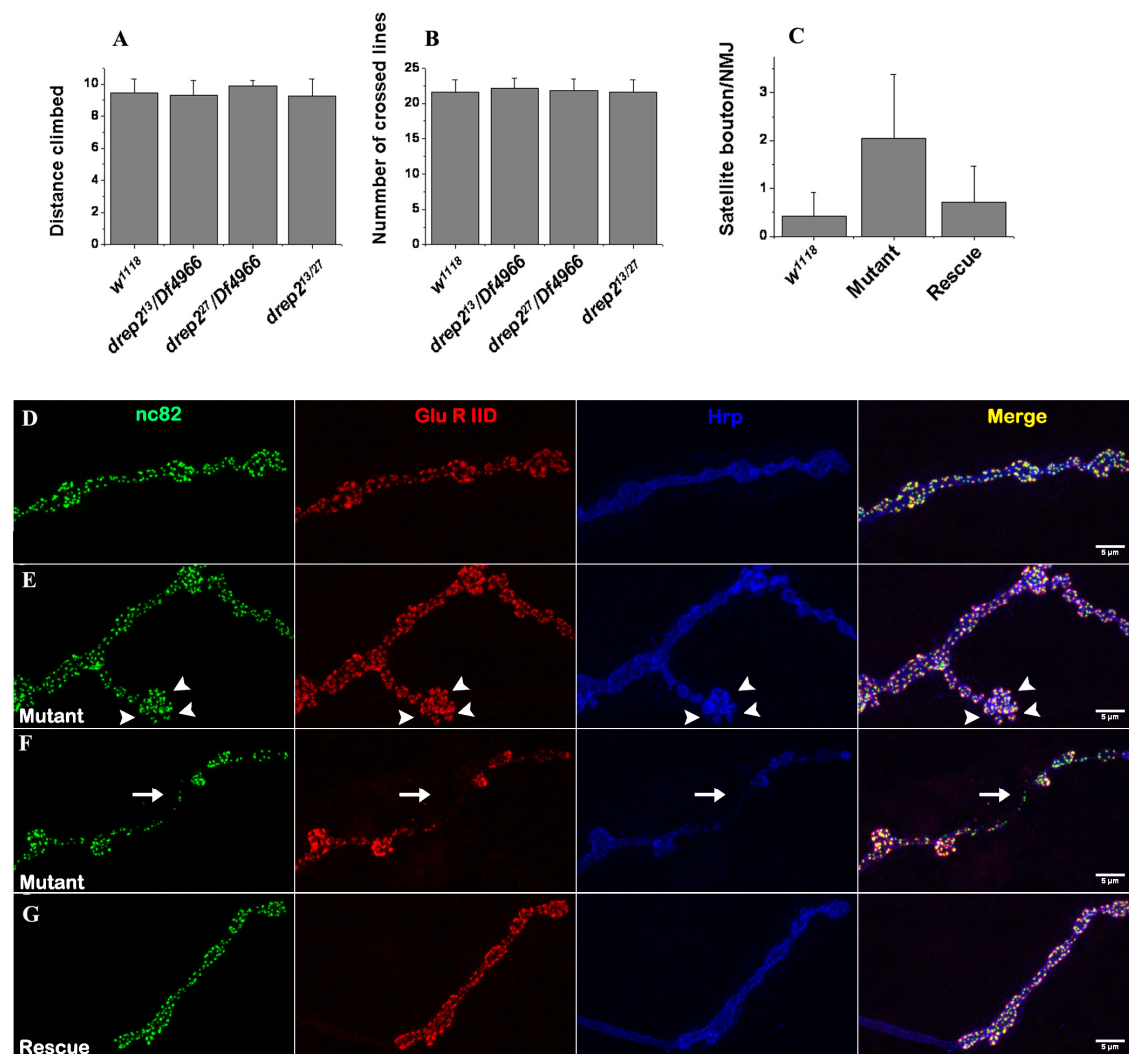


**Figure 4.6** Potentially a NMJ morphological phenotype in 3<sup>rd</sup> instar *drep-2* mutant larvae. Locomotion tests including negative geotaxis (A) and walking ability (B) were investigated the in control *w<sup>1118</sup>*, the mutant *drep2<sup>13</sup>/Df4966* and rescue *Elav/Y; drep2<sup>13</sup>/Df4966; UAS-DREP-2/+* adult flies after clipping the wings. Negative geotaxis



ability was quantified by the mean distance climbed vertically in an empty food vial within a period of 30 s (A) (n = 15). Spontaneous walking on a horizontal surface of such flies was tested as reflected by the number of lines of a 2 × 2 cm grid crossed within a 30 s period (B)(n = 15). Data are mean ± SD. (C) Statistics of satellite boutons number in the *drep-2* mutant. Satellite boutons were counted from segment A2 to A4 in muscle 4. The *drep-2* mutant has about 2 satellite boutons every NMJ in muscle 4, but *w<sup>1118</sup>* only has 0.4. Re-expression of *Drosophila* full length DREP-2-PA in a *drep-2* mutant background partially rescues the satellite boutons patterns. N, number of neuromuscular junction in muscle 4 (n=24). Data are mean ± SD. Compared with control *w<sup>1118</sup>* (D), the *drep-2* null mutant, *drep-2<sup>ex13/Df4966</sup>* shows the morphological phenotypes, including satellite boutons (E, arrow heads) and mislocalization between Brp and GluRIID (F, arrows) in 3<sup>rd</sup> instar larvae. Re-expression of *Drosophila* full length *UAS-DREP-2-PA* driven by *Elav-Gal4* in the *drep-2* mutant, restores the satellite boutons pattern to control level (G).

## 4.7 Bidirectional axonal transport of DREP-2-containing complexes

As DREP-2 and DLC-2 interacted by Y2H, the possibility arrived that DREP-2 might be part of actively moving complexes. Thus, a strawberry fused DREP-2 (UAS-strawberry-full length DREP-2-RA) line was generated and used to detect whether *drep-2* could transport or traffic in axons *in vivo*. Early third-instar larvae were imaged at 0.35 second intervals at 25 °C. *In vivo* imaging in fact showed that DREP-2-containing complexes moved in not only anterograde (Fig. 4.7, arrow heads) but also retrograde (Fig. 4.7, arrows) directions in the axon of *Drosophila* 3<sup>rd</sup> instar larvae. Potentially thus, DREP-2 might interact with dDLC-2 during cargo transport.

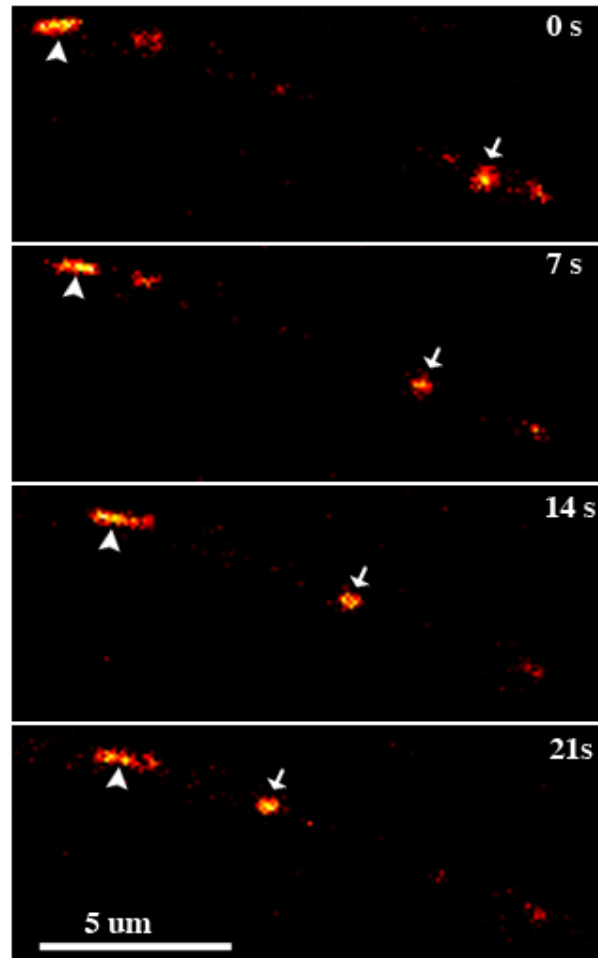


**Figure 4.7 Strawberry tagged DREP-2 molecules show bidirectional axonal transports in *Drosophila* 3<sup>rd</sup> instar larvae.** Confocal *in vivo* imaging (at 25 °C) of third-instar larvae expressing UAS-strawberry-DREP-2 (red) driven by OK6-Gal4 could transport in the anterograde (arrow heads) and retrograde directions. Scale bar, 5 μm. (in collaboration with Till Andlauer)

**4.8 *drep-2* mutant might show an accumulation of floating electron dense structure and large size vesicles by EM**

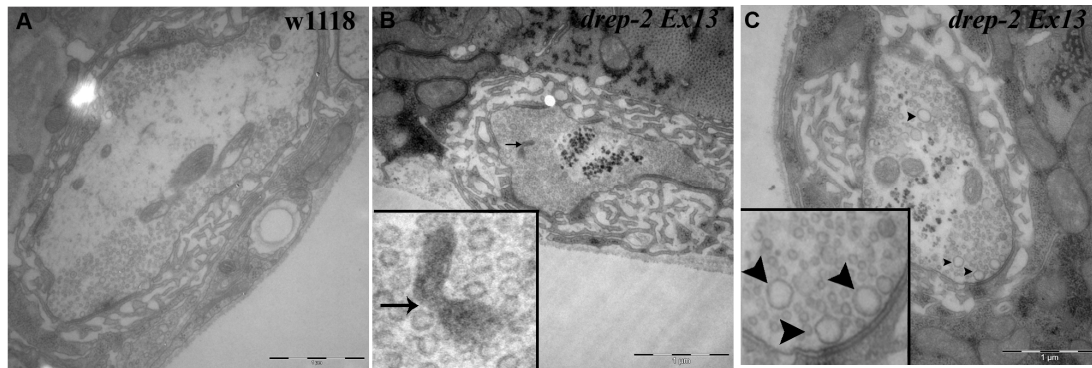


**Figure 4.8 An accumulation of large size vesicles and floating electron dense structure in *digit* mutant by EM.** Electron micrographs show the overall synaptic ultrastructure at boutons of 3<sup>rd</sup> instars neuromuscular junctions in *w<sup>1118</sup>* (A) and *drep-2 Ex13/Df4966* (B and C). In the mutant larvae, the accumulation in the floating electron dense structure (B, arrows) and large size vesicles (C, arrow heads) was observed at some boutons. The inset in B or C is the corresponding enlargement. Scale bar, 1  $\mu$ m. (The EM experiment conducted by Carolin Wichmann)

To further investigate the function of DREP-2, some images of the synaptic ultrastructures were of *drep-2<sup>ex13/Df4966</sup>* (Fig. 4.8B and Fig. 4.8C) NMJs were taken (Fig. 4.8A).

Regular ultrastructures, including normal synaptic vesicles comprising the most prominent membrane structure and normal active zones where synaptic vesicles clustered around active zone T-bars, were observed in the wild-type boutons (Fig. 4.8A) as well as in the *drep-2* mutant (4.8B and 4.8C). However, at least based on the images which could be taken, *drep-2* mutant NMJs also exhibited an accumulation of floating electron dense structures (Fig. 4.8B, arrows). These EM results might indicate that the elimination of *drep-2* might induce an ultrastructure morphological phenotype in synaptic terminal of NMJ, suggesting that *drep-2* might play important roles in presynapse. However, clearly further EM-based

quantifications are necessary to consolidate potential ultrastructural phenotypes of *drep-2* mutants.

## 4.9 Discussion

### 4.9.1 DREP-2 interacts with Brp

*In situ* hybridization experiment shows that a strong specific label of *drep-2* was detected in the central nervous system (CNS) from stage 14 on in *Drosophila* embryos (Fig. 4.3), which is similar to the spatio-temporal expression profile of *brp* (Wagh, 2006). Secondly, the polyclonal DREP-2 antibody recognizes specific bands at the molecular weight of 60 and 68 kDa [shift the predicted sizes of for the two DREP-2 isoforms (52 and 58 kDa)] on immunoblots of adult flies head lysate. Moreover, a strong specific staining was observed in the neuropil of CNS of *Drosophila* 3<sup>rd</sup> instar larvae (Fig. 4.4.3B) as well. These results suggest that the endogenous DREP-2 proteins exist in fly heads and are involved in neuronal function. While due to the specific neuropil staining it appears very likely that DREP-2 is a synaptic protein, future analysis is needed to address whether it is a pre- or postsynaptic protein.

Furthermore, endogenous DREP-2 and Brp both label neuropil in the fly CNS (Fig. 4.5.1A), including in ventral ganglion (Fig. 4.5.1B), calyx of MB (Fig. 4.5.1C-D), lamina (Fig. 4.5.1E) and lobula (Fig. 4.5.1F). DREP-2 was found to co-precipitate with Brp by Co-IP (Fig. 4.1A). In addition, DREP-2 and Brp could interact and form a complex physically by co-IP from *Drosophila* S2R+ cells co-transected by DREP-2-EGFP and Brp D1-2-Myc (Fig. 4.1B). Consistent with the above results, DREP-2 could also interact physically with Brp D1-D2 domains (Fig. 4.1C-D). These results open the possibility that DREP-2 might biochemically interact with Brp.

However, as biochemical analysis might be contain larger synaptic complexes even containing joined aggregates of pre- and postsynaptic matter (“Synaptosomes”), that DREP-2 was co-purified as a postsynaptic protein even remains a possibility. Nonetheless, by providing null mutants and antibodies, this thesis laid ground for a thorough analysis of this novel synaptic protein in *Drosophila*.

#### **4.9.2 Is DREP-2 involved in trafficking or anchoring of target proteins to the membrane?**

The transport of membranous organelles along axons in neurons relies on molecular motors to propel organelles along microtubules (Burton and Paige, 1981). Most of transported axonal cargoes are able to associate with both anterograde and retrograde motors, and move bidirectionally (Schroer et al., 1985; Shapira et al., 2003; Miller et al., 2005). Anterograde transport is driven by the kinesin family of molecular motors (Hirokawa and Takemura, 2005). Two classes of vesicular cargoes were studied in the context of presynaptic assembly in neurons: synaptic vesicle (SV) precursors transported by the kinesin-3 heavy chain KIF1A (Okada et al., 1995) probably linked via the cargo adapter liprin- $\alpha$  (Shin et al., 2003; Miller et al., 2005); and Piccolo-Bassoon transport vesicles (PTVs) linked via the syntaxin1–syntabulin adapter complex to the kinesin-1 heavy chain KIF5B (Cai et al., 2007). Axonal retrograde transport depends mainly on the cytoplasmic dynein motor complex (Vale, 2003). Dynein light chain 2 (DLC-2) are integral components of, or are associated with, many distinct cellular systems including cytoplasmic dynein (King, 1996; Tanner, 2008), myosin V (Espindola, 2000), neuronal nitric oxide synthase (Jaffrey and Snyder, 1996), flagellar radial spokes (Yang, 2001), the Bim proapoptotic factor (Puthalakath, 1999), Rabies virus P protein (Raux, 2000; Poisson,

2001), *Drosophila* swallow (Schnorrer, 2000). In *Drosophila*, complete lack of LC8 (*ddlc-1*) function is embryonic lethal due to the induction of apoptosis, whereas partial loss-of-function alleles show pleiotropic defects in bristle and wing development, female sterility, and altered neuronal development (Dick, 1996; Phillis, 1996). However, mechanisms organizing the transport of active zone precursor complexes *in vivo* remain hardly understood.

*In vivo* imaging showed strawberry tagged DREP-2 molecules could actively transport in the anterograde (Fig. 4.7, arrow heads) and retrograde (Fig. 4.7, arrows) directions in the axons of *Drosophila* 3<sup>rd</sup> instar larvae. The bidirectional axonal transport of DREP-2 is similar to dynein-dependent transport. In addition, DREP-2 was found to interact with dDLC-2 and Brp by Y2H assay (Fig. 4.1C-D). These indicate that DREP-2 might interact with dDLC-2 and could be involved in cargo transport to synapses.

In the first experiments, mutant of *drep-2*, *drep-2<sup>ex13/Df4966</sup>* (Fig. 4.6B, arrow heads) provoked more satellite boutons (~5 times more) compared with control larvae (Fig. 4.6A). In some boutons, the mutants also might show mislocalization between Brp and GluRIID (Fig. 4.6C, arrows), leading to spots of nc82 staining without adjacent GluRIID. Re-expression of *Drosophila* full length DREP-2-PA in the *drep-2* mutants, restores the satellite boutons patterns to control levels (Fig. 4.6D and 4.6E). These results start to suggest that the *drep-2* deficiency induces the satellites boutons and mislocalization, strongly supporting the proposal that DREP-2 might be involved in regulation and maintenance of synapses. Furthermore, the *drep-2* mutant also exhibits an accumulation of floating electron dense structure by EM (Fig. 4.8B, arrows). What are these electron dense structures? Where do they origin from? One possibility is that they could

be the electron dense body or pre-T bar structure, which they could not be transported to proper spots of active zone assembly due to a lack of DREP-2. Thus, DREP-2 might interact with Brp or DLC transporting or anchoring the electron dense body into the presynaptic membrane. To further address these aspects, immuno-EM by DREP-2 antibody need to be done to investigate whether the floating electron dense structures belong to electron dense body or pre-T bar structure in the future.

Alternatively, the electron dense structures could be membrane recycling intermediates, and they origin from membrane blebbing, cytosolic fragmentation or degradation of membrane. Overexpression of CIDE proteins induced not only nuclear condensation and DNA fragmentation, but also membrane blebbing and cytosolic fragmentation (Inohara, 1998). The *drep-2* mutant also shows increases of large size (>50nm) vesicles at some boutons of 3<sup>rd</sup> instars neuromuscular junctions (Fig. 4.8C, arrow heads). Large size vesicles belong to membranous recycling intermediates structures, which were also detected in endocytic mutants *stoned*, *synaptotagmin* and *dynamin* (Fergestad, 1999; Loewen, 2006; Sever, 2000 and Cooney, 2002). Further quantifications of large size vesicles are necessary to be investigated in order to figure out whether and how much the large size vesicle is increased in the *drep-2* mutant compared with control.

### **4.9.3 DREP family and apoptosis**

DREP denotes DFF-related proteins, including DREP-1, DREP-2, DREP-3 and DREP-4 (Fig. 4.2). DREP-4 and DREP-1, respectively, are homologous to human CAD/DFF40 and ICAD/ DFF45. *Drosophila* CAD/ DFF40, DREP-4, has a nuclease domain that can cleave naked and chromosomal DNA, whereas *Drosophila* CAD/ DFF40, DREP-1, is a

regulatory subunit that suppresses the nuclease activity of DFF40 (Yokoyama, 2000; Mukae, 2000). So far, DREP-2 and DREP-3 are still proteins of unknown function. The CIDE-N peptide sequence (CIDE domain) of the DFF40 (CAD) nuclease and CIDE proteins acts as a regulatory domain (Fig. 4.2). Similarly, the activity of DREP-2, DREP-3 and DREP-4 might be regulated by their corresponding CIDE-N domains. Once activated, a set of caspases cleave various protein substrates at specific caspase-recognition site(s), which eventually leads to the characteristic morphological changes of apoptotic cells, such as cell shrinkage, blebbing of plasma membranes, and chromatin condensation (Wyllie, 1980). DREP-1 and DREP-3 can interact with DREP-2 by immunoprecipitation and immunoblotting analysis (Inohara, 1999). DREP-1, DREP-2, or DREP-3 (and their complexes) have no nuclease activity in the absence or presence of human caspase-3. It suggests that DREP-2 and DREP-3 are not nucleases, but they might regulate the activity of DREP-1. Interestingly, DREP-2, as a potential Brp binding partner, was identified by the co-IP experiments (done by Manuela Schmidt, not published data). *Drosophila* Brp is homologous to the human ELKS/CAST/ERC family. Very interestingly, Jeanette et al. found that ELKS might be an essential regulatory subunit of the IKK (IkB kinase) complex (Jeanette, 2004). ELKS likely functions by recruiting IkB to the IKK complex and thus serves a regulatory function for IKK activation. The nuclear factor- $\kappa$ B (NF- $\kappa$ B) family of transcription factors is conserved in *Drosophila melanogaster*, and plays a seminal role in inflammation, apoptosis, development, and cancer. The physiological role of NF- $\kappa$ B's ability to protect cells from apoptosis was also examined in cells lacking ELKS. HeLa cells transduced with LV-siELKS displayed an increased sensitivity to apoptosis induced by TNF- $\alpha$ . Blebbing nuclei, poly (adenosine 5-diphosphate-ribose) polymerase (PARP) cleavage, and pro-Caspase3



cleavage, indicative of apoptosis, were increased in HeLa cells transduced with LV-siELKS, compared with cells transduced with LV-siGFP. Thus, in cells lacking ELKS, the failure to activate NF- $\kappa$  B results in a lack of the survival gene expression necessary to protect the cells from apoptosis induced by TNF- $\alpha$  (tumor necrosis factor- $\alpha$ ). DREP-4 and DREP-1 were found to be involved in neuronal apoptosis (Yokoyama, 2000; Mukae, 2000).

So far, I have no any evidence that cell death is changed in *drep2* mutants. DREP proteins might still be caspase substrates in *Drosophila*, but caspase activation might also play a role in synaptic plasticity. In fact, Caspase-3 and Dynein light chain1 in vertebrates has been linked to synaptic plasticity (Bateup, 2010; Batlevi, 2010; Kudryashova, 2009; Kozyrev, 2007). Caspase-3 is enriched in postsynaptic densities and increased in Alzheimer's disease (Louneva, 2008). One possibility is that DREP-2 is involved in synaptic plasticity and apoptosis to protect from synaptic dysfunction and insult. The increase of satellite boutons in NMJ of the *drep-2* null mutant might result from the apoptosis of synaptic terminus and blebbing of plasma membranes. Does *Drosophila* DREP-2 interact with DREP-1, DREP-2, DREP-4 and also probably Brp and form a complex involved in neuronal apoptosis? Whether DREP-2 plays in synaptic transport or neuronal apoptosis need further more investigation *in vivo*.

## **5 Results part2: analyzing synaptic functions of *Drosophila* GIT**

Two endocytic mechanisms, which have been suggested, likely coexist in some nerve terminals (von Gersdorff and Matthews, 1994; Kuromi and Kidokoro, 1998). Endocytosis takes place at sites distinct from active zones, which is mediated by clathrin, and often involves endosomal intermediates (Heuser and Reese, 1973), or at/near active zones (Ceccarelli et al., 1973).

Proteins of the GIT family are very highly conserved across the animal kingdom. In vertebrates two GIT proteins are expressed: GIT1 and GIT2. Human GIT1 and GIT2 share 65% sequence identity and 85% similarity (Hoefen and Berk, 2006). A major difference between these proteins is that, whereas GIT1 is expressed as one major dominant form, GIT2 is extensively alternatively spliced in a tissue-specific manner. Only one orthologue (CG16728) of GIT1 is present in *Drosophila melanogaster*.

CG16728, which is located on the second chromosome, is predicted as encoding a GIT protein homologous to mammalian GIT1 in *Drosophila melanogaster*. Putative DGIT encodes 731 amino acids. The *dgut* locus is predicted to encode 4 conserved domains, including the N-terminal ARF GTPase-activating protein (ARFGAP) domain, the ankyrin (ANK) repeats, the Spa2-homology domain (SHD), and the paxillin-binding subdomain (PBS) (Fig. 5.1A). Identities in the corresponding domain between DGIT and human GIT1 are 55% in ARFGAP, 53% in ANK, 57% in SHD and 34% in PBS, respectively.

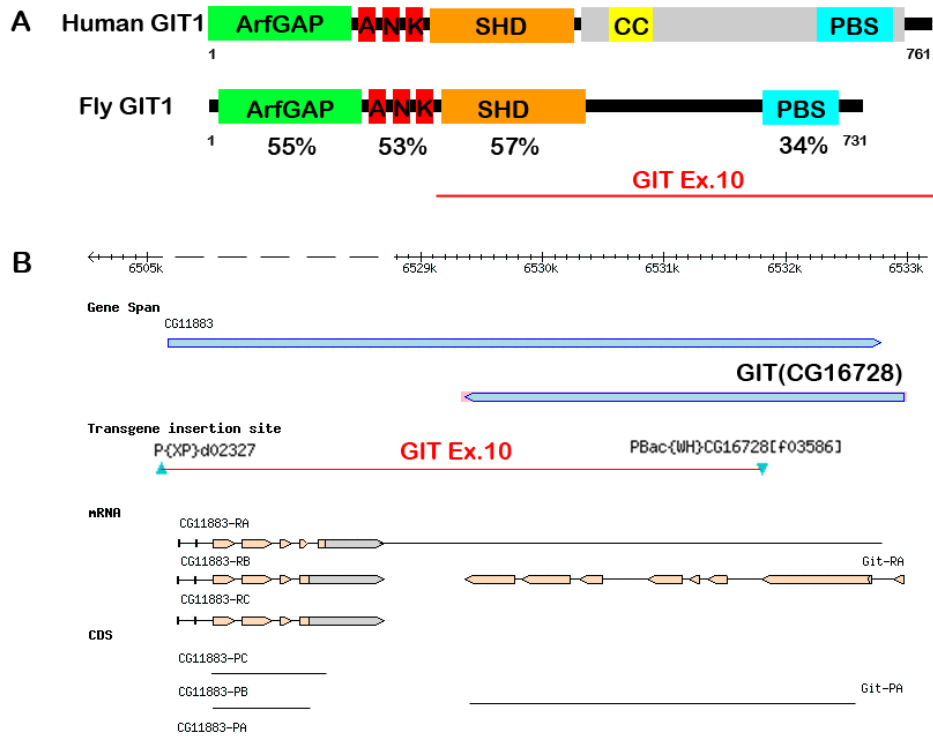


**Figure 5.1 Schematic overview of GIT protein structure (A) and *digit* mutantgenesis (B).** Scheme showing human GIT (HGIT) and *Drosophila* GIT (DGIT) protein domains. Identities between DGIT and human GIT1 in domains are indicated: ARFGAP domain (55%); ANK, ankyrin repeats (53%); SHD, Spa2 homology domain (57%); PBS, paxillin-binding subdomain (34%). GRKBD (G-protein-coupled receptor kinase-binding domain) and coiled coil (CC), respectively, represents a domain. Mutant *digit*<sup>10</sup> (in red dash) deletes SHD and PBS domains completely, but keeps ARFGAP and ANK domains. (B) Schematic overview of *digit* mutantgenesis. Mutant *digit*<sup>10</sup> (in red dash), which deletes SHD and PBS domains completely, was produced based on FLP-FRT recombination between *digit*<sup>f03586</sup> (PBac{WH}*digit*<sup>f03586</sup>) and *CG11883*<sup>d02327</sup> transposon lines.

## 5.1 Mutational analysis of *Drosophila* GIT

A deletion mutant for GIT (*dg<sup>it</sup><sup>10</sup>*, Fig. 5.1B, in red dash) was produced based on FLP-FRT recombination (Theodosiou, 1998) between the *dg<sup>it</sup><sup>f03586</sup>* and *dg<sup>it</sup><sup>d02327</sup>* insertion lines. The deletion which was recovered (*dg<sup>it</sup><sup>10</sup>*, in red dash) deletes the SHD and PBS domains completely, but leaves the sequences encoding ARF GAP and ANK domains. *dg<sup>it</sup><sup>21C</sup>* and *dg<sup>it</sup><sup>51C</sup>* were produced by the Yang Lab (Bahri, 2009) and are proven null alleles of *dg<sup>it</sup>* because they lost specific label in muscle attachment of embryo compared to control by immunofluorescence (Bahri, 2009). Homozygous *dg<sup>it</sup><sup>10</sup>* and *dg<sup>it</sup><sup>51C</sup>* are embryonic lethals. This is most likely due to secondary mutations on these chromosomes, as *dg<sup>it</sup><sup>10</sup>* when put over “large deficiency” Df596 (*dg<sup>it</sup><sup>10/Df596</sup>*) and *dg<sup>it</sup><sup>21C</sup>* are only larval lethals with a few adult escapers (~20% of expected number of animals, Table 2). The piggyBac (Van Deerlin, Sleiman et al.) line, *dg<sup>it</sup><sup>f03586</sup>*, was produced by the Berkeley *Drosophila* Genome Project (BDGP), and is a PiggyBac transposon insertion line of *dg<sup>it</sup>* gene. Homozygous *dg<sup>it</sup><sup>f03586</sup>* (~67%) and *dg<sup>it</sup><sup>f03586/10</sup>* (~61%) are also larval lethal with higher viability compared with null alleles, *dg<sup>it</sup><sup>10/Df596</sup>* and *dg<sup>it</sup><sup>21C</sup>*, strongly suggesting that *dg<sup>it</sup><sup>f03586</sup>* and *dg<sup>it</sup><sup>f03586/10</sup>* might be hypomorphs of *dg<sup>it</sup>*. Thus, we used *dg<sup>it</sup><sup>10/Df596</sup>* as well as *dg<sup>it</sup><sup>10/f03586</sup>* as *dg<sup>it</sup>* mutant constellations in this thesis. Additionally, *dg<sup>it</sup><sup>21C</sup>* also was used in some experiments here. Lethality of *dg<sup>it</sup><sup>f03586/10</sup>* was rescued to different extents by the expression of *dg<sup>it</sup>* in muscles by *Mhc-Gal4*, in neurons by pan-neuronal *Elav-Gal4* and *OK6-Gal4* or ubiquitously by actin-Gal4 using the *UAS-Gal4* system (Table 2), indicating that *dg<sup>it</sup>* is required for the normal development of different tissues, particularly the nervous system.

Genotype	Adult viabilities (%)	Numbers scored
<i>dgIt</i> <sup>10</sup>	0	765
<i>dgIt</i> <sup>51C</sup>	0	712
<i>dgIt</i> <sup>21C</sup>	21	568
<i>dgIt</i> <sup>10/Df596</sup>	20	621
<i>dgIt</i> <sup>f03586</sup>	67	483
<i>dgIt</i> <sup>10/f03586</sup>	61	528
<i>OK6-Gal4, dgIt</i> <sup>10/f03586</sup> ; <i>UAS-DGIT</i> /+	72	451
<i>Elav-Gal4/+; dgIt</i> <sup>10/f03586</sup> ; <i>UAS-DGIT</i> /+	86	461
<i>dgIt</i> <sup>10/f03586</sup> ; <i>UAS- DGIT/Mhc-Gal4</i>	71	539

**Table 5.1 Rescue of *dgIt* mutant lethality by tissue-specific expression of *dgIt*.** The number animals hatching of *dgIt* null alleles is shown as a percentage of viable adult flies compared to the expected viabilities, which number of animals expected from Mendelian ratios. *Drosophila dgIt* is expressed in muscles driven by Mhc-Gal4, in neurons by Elav-Gal4 and OK6-Gal4 or ubiquitously by Actin-Gal4 in the *dgIt* mutant background to examine its lethality rescue ability. For each tissue-specific Gal4 line, the percentage of rescued *dgIt*<sup>10/f03586</sup> lethality is given.

## 5.2 Expression of *Drosophila* GIT

Quantitative analysis using real time PCR for different tissues ([www.flyAtlas.org](http://www.flyAtlas.org), Chintapalli, 2007) showed that *dgIt* mRNA is a generally expressed transcript with a slight enrichment in the nervous system (larvae CNS enrichment, 1.3; see Table 3). However, its expression pattern in the nervous system has not been documented so far. The *Drosophila dgIt* cDNA is ~2.4 kb (Fig. 5.2A) in length and it encodes a putative protein (DGIT) of 731aa. In collaboration with the lab of Volker

Haucke (FU Berlin), we got access to a polyclonal anti-DGIT antibody against DGIT C-terminal aa590-731 (named Bob). This antibody recognizes a band of the predicted molecular weight of 80 kDa on immunoblots of wild type adult head lysates. In contrast, in *digit* mutant, *digit*<sup>10/Df596</sup>, no band was observed (Fig. 5.2A). Thus, DGIT seems expressed in fly heads, opening the possibility that the protein might be involved in synaptic functions.

<i>Tissue</i>	<i>mRNA Signal</i>	<i>Present Call</i>	<i>Enrichment</i>	<i>Affy Call</i>
Adult brain	57 ± 2	4 of 4	0.4	Down
Adult head	102 ± 6	4 of 4	0.7	Down
Adult eye	85 ± 3	4 of 4	0.6	Down
Adult thoracicoabdominal ganglion	66 ± 2	4 of 4	0.5	Down
Adult ovary	407 ± 16	4 of 4	2.8	Up
Adult testis	63 ± 2	4 of 4	0.4	Down
Larval CNS	186 ± 5	4 of 4	1.3	Up
Larval salivary gland	140 ± 3	0 of 4	0.97	None
Larval midgut	143 ± 4	4 of 4	0.99	None
Larval tubule	144 ± 4	4 of 4	1	None
Larval hindgut	134 ± 3	4 of 4	0.93	None
Larval fat body	86 ± 4	4 of 4	0.6	Down

**Table 5.2. The *digit* mRNA enrichment in different tissues of adult flies and larvae detected by RT-PCR.** Tissues were dissected out from equal numbers of male and female 7-day old Canton S wild-type flies and pooled to make at least 1500 ng mRNA, then amplified and hybridized using the Affymetrix standard protocol. The data refer to the FlyAtlas database ([www.flyatlas.org](http://www.flyatlas.org); Chintapalli, 2007), but not my results.

To investigate this possibility, we turned to analysis of *larval* neuromuscular junctions (NMJ). First we expressed a GFP-DGIT fusion in motoneurons by OK6-Gal4. GFP-DGIT in fact localized to synaptic

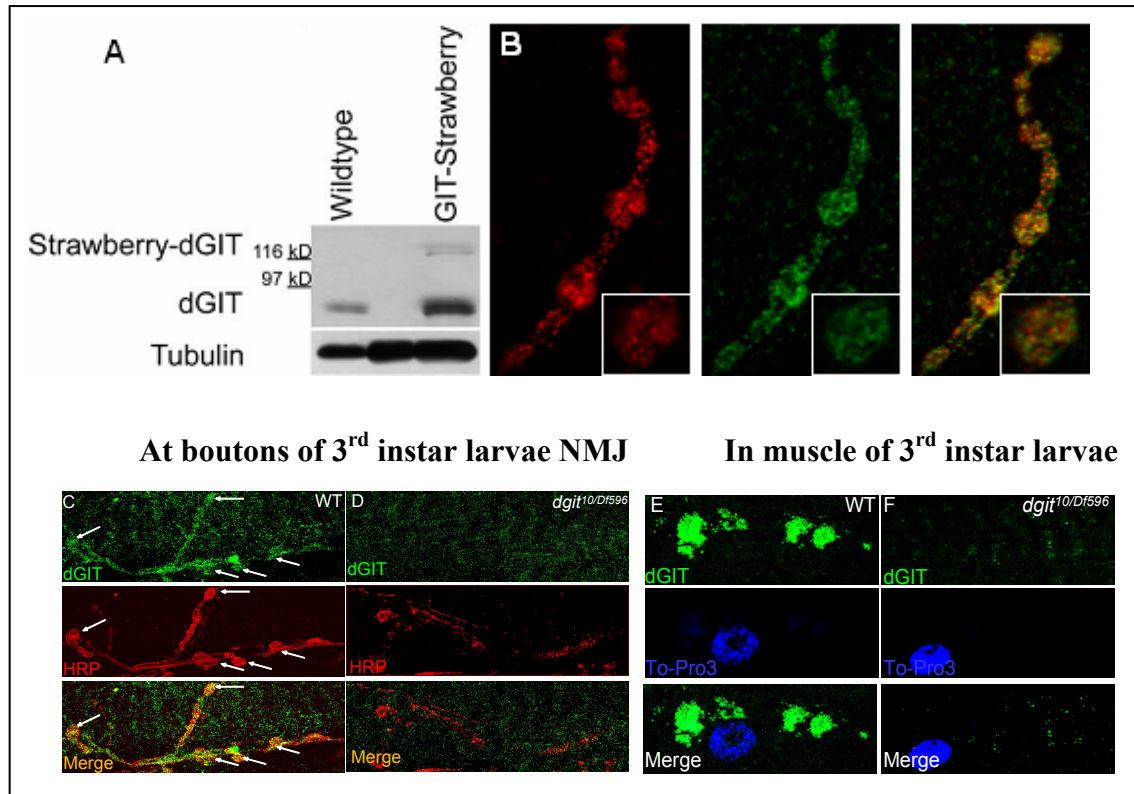


**Figure 5.2 *DGIT* is expressed at boutons of L3 NMJ.** (A) *dggit*<sup>10/Df596</sup> is a null mutant of *dggit*. The lysate from 20 adult fly heads was subjected to 10% SDS-PAGE, followed by immunoblot by the rabbit DGIT (1:200) and mouse tubulin (1:3000) antibody to check the antibody specificity of DGIT. The polyclonal anti-DGIT antibody recognizes the band at the predicted molecular weight of 80 kDa on immunoblots of wild type adult flies head lysate. The *dggit* mutant (*dggit*<sup>10/Df596</sup>), however, shows not such band. Df, deficiency. The genotype of Df596: Df(2R)stan2, b<sup>1</sup> pr<sup>1</sup> P{neoFRT}42D/CyO. (B) *Drosophila* GIT peptide (in red) antibody recognizes the GFP-tagged DGIT (in green) driven by OK6-Gal4 at *Drosophila* 3<sup>rd</sup> instar larvae NMJ.

boutons with anti-DGIT (in green, the presynaptic membrane marker anti-horseradish peroxidase (anti-HRP, in red) and nuclear marker To-Pro3 (in blue) showed that endogenous DGIT is also highly expressed in muscle (Fig. 5.2C) and diffusely expressed (Fig. 5.2E) at boutons of 3<sup>rd</sup> instar *Drosophila* NMJ. No such specific staining was observed in *dggit*<sup>ex10/Df596</sup> (Fig. 5.2D and 5.2F) and *dggit*<sup>21C</sup> (Data not shown), however, suggesting

that both *dgīt*<sup>10 /Df596</sup> and *dgīt*<sup>21C</sup> are null alleles or at least very strong alleles. The allele *dgīt*<sup>10 /f03586</sup> showed reduced intensity of DGIT antibody staining compared with control *w*<sup>1118</sup>, suggesting that *dgīt*<sup>10 /f03586</sup> is a hypomorph of *dgīt*.

## 5.3 DGIT associates with StnB

*Drosophila* Stoned B (StnB) protein has also been shown to interact with synaptic vesicles via synaptogamin-I and DAP-160 regulating synaptic vesicle recycling by recruiting dynamin to a pre-fission complex (Kelly and Phillips, 2005). Haucke group in Free University Berlin, our colaboratory lab, found that GIT1 is an interaction partner of Stoning 2 by large scale co-immunoprecipitation from rat brain, and that human GIT1, StnB and human Stonin2 form a complex in cell transfection assays, and that fly GIT1 could co-precipitate with human Stonin2. ArfGAP and ANK of human GIT1 could pull down with human Stonin2 from total protein lysates of COS 7 cells co-transfected with interested constructs, suggesting ArfGAP and ANK domains of human GIT1 are the binding activity domains with StnB, but not SHD domain. GIT1 colocalizes with Stonin 2 in hippocampal neurons at synaptic vesicle clusters. Mislocalization of the sytl1-binding deficient in *stonin2* mutant can be rescued by overexpressed GIT1. These data which they found suggest that GIT1 interacts with StnB physically.

To determine whether DGIT and StnB form a complex in fly brain, co-immunoprecipitation experiments were executed (Fig. 5.3A) with fly heads extracts (Homogenize fly head using 2 ul 2% SDS for each, then smash the heads with pipette. Keep the sample at 36 degree for 30 min, and then



centrifuging by 13000 rpm at 4 degree for 15 min. Finally, harvest the supernatant and store it at -80 degree until use). Immunoprecipitation on detergent lysates of crude synaptosomal fraction of adult fly heads with StnB antibodies precipitated StnB and coprecipitated DGIT. DGIT and StnB could be co-immunoprecipitated from fly head extract (Fig. 5.3A). This result indicates that DGIT associates with StnB physically.

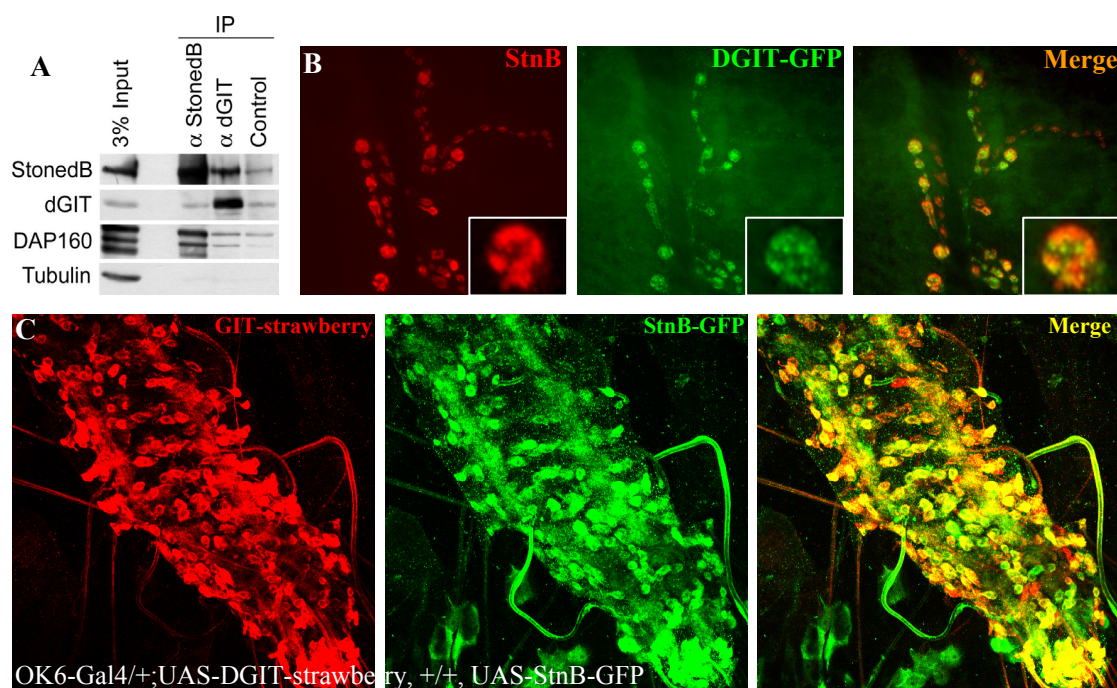


**Figure 5.3 *Drosophila* GIT interacts with StnB *in vivo*.** (A) DGIT and StnB could be co-immunoprecipitated from adult fly head extracts. (B) Overexpressed DGIT-GFP co-localizes with endogenous StnB at synaptic boutons of 3<sup>rd</sup> instar larvae (L3) *Drosophila melanogaster* NMJs. GFP fusion DGIT and endogenous StnB, respectively, is recognized by mouse anti-GFP (in green) and rabbit anti-StnB (in red). (C) Co-localization of overexpressed DGIT (in red) and StnB (in green) driven by OK6-Gal4 at ventral ganglion of *Drosophila*. L3. Double staining was applied to the ventral ganglion of 3<sup>rd</sup> instar larvae (L3) (Genotype: OK6-Gal4/+; UAS-DGIT-strawberry, +/+, UAS-StnB-GFP) with mouse anti-GFP antibody (1:500) and rabbit anti-Dsred (1:500) antibody.

To determine whether GFP or strawberry tagged DGIT and StnB colocalize in subcellular regions of neurons, double-label immunofluorescence stainings at 3<sup>rd</sup> instar larval NMJs (Fig. 5.3B) and in ventral ganglion were performed (Fig. 5.3C). Overexpressed DGIT (Fig. 5.3B, in green) driven by OK6-Gal4 partially co-localized with endogenous StnB (Fig. 5.3B, in red) at synaptic boutons of *w<sup>1118</sup>* 3<sup>rd</sup> instar larvae. Overexpressed DGIT (Fig. 5.3C, in red) partially co-localized with overexpressed StnB (Fig. 5.3C, in green) in ventral ganglion of *w<sup>1118</sup>* 3<sup>rd</sup> instar larvae. These results are consistent with the biochemical data that StnB interacts with DGIT. In the following, we turned to the larval NMJ to investigate synaptic organization of *digit* mutants in comparison to controls.

## **5.4 Active zones and postsynaptic densities of *digit* mutant NMJs**

First, we addressed the organization of presynaptic active zones by staining the presynaptic cytomatrix active zone (CAZ) marker Bruchpilot and glutamate receptor subunit GluRIID. Occasionally, *digit* mutant showed “mislocalizations” (arrow heads) between Brp and GluRIID. Here, Brp spots lacked postsynaptic glutamate receptor GluRIID (Fig. 5.4B). In the same number of controls, such kinds of mislocalizations were rarely observed (Fig. 5.4A). By re-expression of *Drosophila* GIT (Fig. 5.4C) or human GIT (Fig. 5.4D) driven using Elav-Gal4 in *digit* mutant background, this mislocalization defect could be restored to normal. In order to investigate whether StnB could compensate or rescue the mislocalization defect due to the deprivation of DGIT, re-expression of *Drosophila* StnB (Fig. 5.4E) driven using Elav-Gal4 in *digit* mutant background, however, this mislocalization defect could not be restored to normal. These preliminary results open the chance that DGIT might be involved in

synaptic assembly processes responsible to properly deposit pre- relative to postsynaptic proteins. Clearly, however, additional experiments will be needed to consolidate these results.

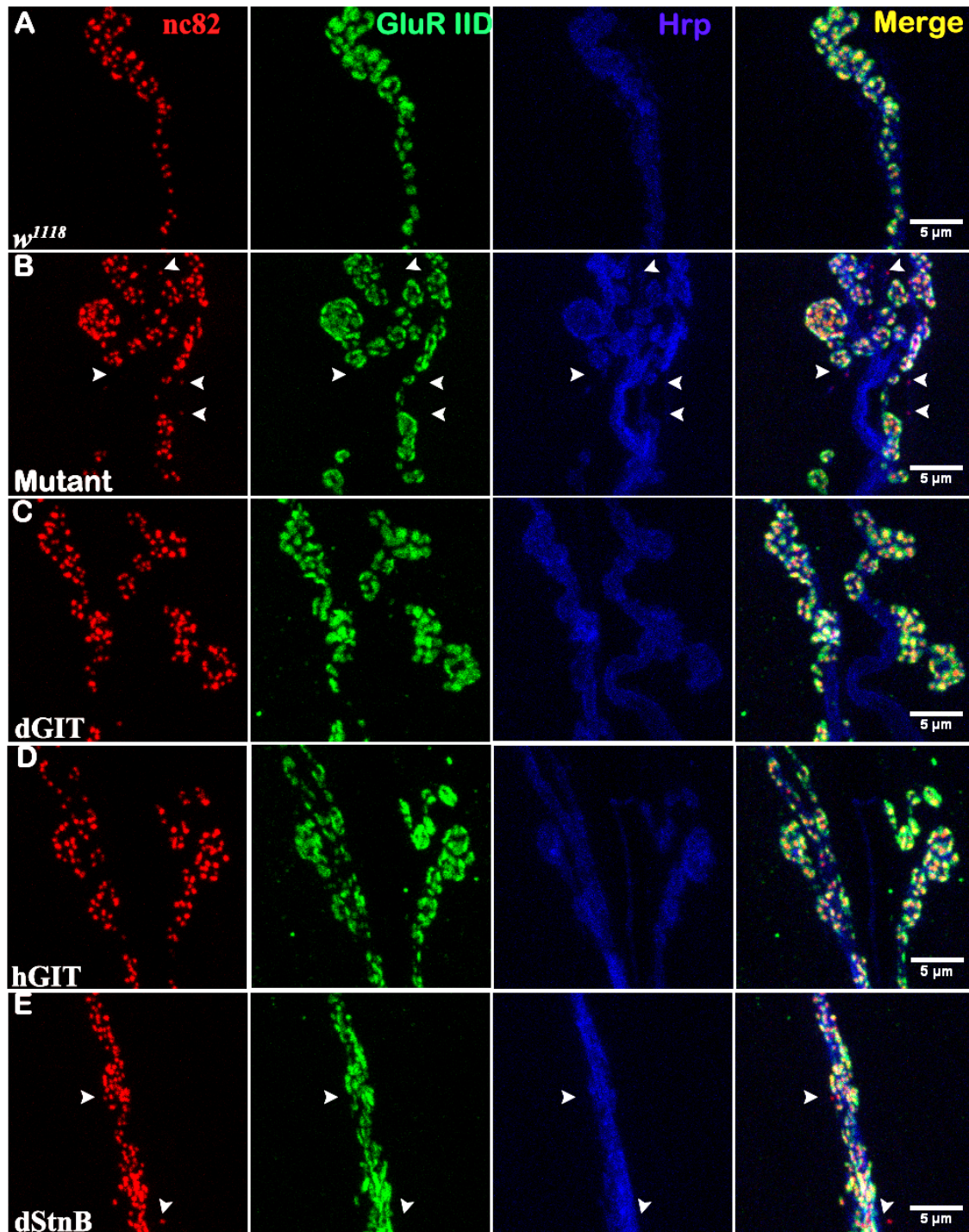


**Figure 5.4 Loss of glutamate receptor at glutamatergic boutons of *digit* mutants.** Compared with control *w<sup>1118</sup>* (A), the *digit* mutant, *digit<sup>10/f03586</sup>*, shows the

mislocalization (arrow heads) between presynaptic marker Brp and postsynaptic marker GluRIID (B). *w<sup>1118</sup>*, as control does not show this kind of mislocalization usually. Re-expression of DGIT (C) or human GIT (D) in *digit* mutant, the mislocalization morphological defect could be restored to normal, but not overexpression of *Drosophila* StnB (E).

## 5.5 Reduction in StnB level at *digit* mutant NMJs

As we found that DGIT associates with StnB (Fig. 5.3A), we asked whether *digit* mutants would suffer from changes in level and distribution of StnB or other synaptic vesicle-associated protein. To this end, NMJ immuno-stainings with StnB and CSP antibody (Zinsmaier, 1994; Umbach, 1994) were performed at 3<sup>rd</sup> instar larval NMJs. In fact, levels of StnB were found to be severely reduced at *digit<sup>10/f03586</sup>* mutant NMJs compared with controls (Fig. 5.5, in green). Question was whether this effect was restricted to StnB, or whether a more generalized deficit in the amount of synaptic vesicle proteins could be observed here. In fact, we found no obvious changes in the levels of CSP (Fig. 5.5, in red) and HRP (Fig. 5.5, in blue) were observed in the *digit* mutant compared with control *w<sup>1118</sup>*. Re-expression of *Drosophila* GIT (Fig. 5.5C), by driven by Elav-Gal4 in the *digit* mutant, StnB level could be restored to control level. Quantifications of stainings intensities showed StnB to be severely reduced at *digit<sup>10/f03586</sup>* mutant NMJs compared to controls (Fig. 5.5D).

Meanwhile bouton (Fig. 5.5E) and branch numbers (Fig. 5.5F) were only slightly reduced in *digit* mutants. These results show that *digit* deficiency affects the level of endocytosis-associated protein StnB. Thus, as StnB before has been shown to be important for synaptic vesicle endocytosis and synaptic vesicle recycling, DGIT might play a role for endocytosis.



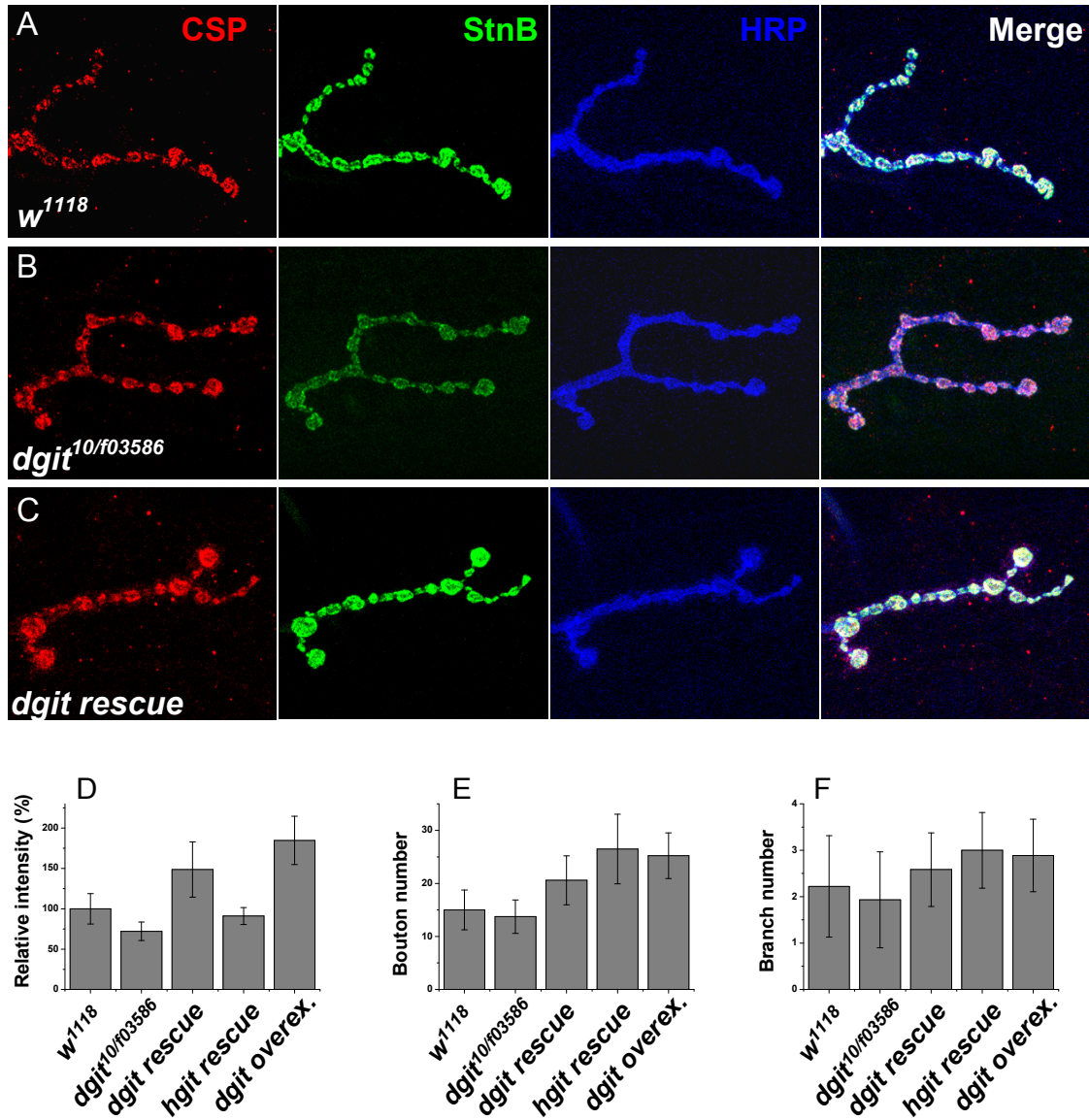


**Figure 5.5 Reduction in StnB level at *dglt* mutant NMJs.** Compared with control *w<sup>1118</sup>* (A), StnB level appeared to be severely decreased at *dglt* mutant *dglt<sup>10/f03586</sup>* NMJs (B, in green). Same time, no apparent changed in the levels of CSP (in red) and HRP (in blue) were observed in the *dglt* mutant compared with control *w<sup>1118</sup>*. By re-expression of DGIT (C) using by Elav-Gal4 in *dglt* mutant, StnB level could be restored to control level. (D–F) Quantification of intensity of StnB staining (D), bouton number (E), and branch number (F) at L3 NMJs from muscle 4 segment 2-3 ( $n=16$ ). Quantification of StnB staining level was found to be severely reduced at *dglt<sup>10/f03586</sup>* mutant NMJs compared with control *w<sup>1118</sup>*. Bouton (E) and branch number (F) are only slightly reduced at *dglt<sup>10/f03586</sup>* mutant NMJs.

## 5.6 Abnormal ultrastructure of *digit* mutant NMJs

(Data achieved in collaboration with Carolin Wichmann)

Based on the obvious light microscopic phenotypes concerning the distribution of synaptic proteins, we wondered whether the ultrastructure of neuromuscular synapses, particularly SV membranes, was affected in *digit* mutants as well. Thus, we examined serial cross-sections of both control and *digit* mutant boutons at muscles 6 and 7 of third instar larvae by transmission electron microscopy.

The architecture of NMJ active zones is exquisitely designed to facilitate the regulated tethering, docking, and fusing of the synaptic vesicles with the plasma membrane at larval neuromuscular junctions by electron microscopy. We found that at *digit* mutant synapses, per se active zones with T-bars formed, and SVs (synaptic vesicles) both within the bouton cytoplasm as well as clustered around the T-bars (Fig. 5.6A-B). Regular synaptic vesicles comprise the most prominent membrane structure in the wild-type bouton, and clusters of these vesicles are observed clustered around active zone T-bars. Moreover, a rather slight reduction in clustered synaptic vesicles in a distance of 50-150 nm to the T-bar were observed in the *digit* mutants but still remained in the rescue situations when compared with controls (Fig. 5.6B). Overall, these phenotypes suggest that deprivation of *digit* interferes with effective recycling of synaptic vesicles.

However, in fact an obvious increase in large size (70–300 nm) vesicles (Fig. 5.6 A-C, arrow heads) was obvious at EM micrographs of *digit* mutants. Large vesicles are a sign for deficits in SV endocytic cycling (Fergestad, 1999; Loewen, 2006; Sever, 2000 and Cooney, 2002). Moreover, an accumulation of atypical tubular structure and likely

endosome intermediates structures (Fig. 5.6A and 5.6C, small arrows), and unusual ruffling of the presynaptic membrane (Fig. 5.6C, middle, small arrow). Occasionally, floating electron dense structure (Figure 5.6 C, large arrow) associated with a tight cluster of vesicles in middle of bouton, but not attached to active zones could be observed in *dgīt* mutants as well. The two *dgīt* mutants, apart from synaptic vesicles, show a typical accumulation of membrane recycling intermediates including large size vesicles (Fig. 5.6A-C, arrow heads) and endosome intermediates structures (Fig. 5.6A and 5.6C, small arrows), which are also detected in other endocytic stoned mutants, synaptotagmin mutant and dynamin mutants (Fergestad, 1999; Loewen, 2006; Sever, 2000 and Cooney, 2002). The increase in large size vesicles (Fig. 5.6A and 5.6C, arrow heads) could be rescued by re-expression of full length DGIT driven by Elav-Gal4 in the *dgīt* mutant background, but not by StnB (Fig. 5.6C). Accumulation in tubular structure (Fig. 5.6A and 5.6C, small arrows) and an unusual ruffling of the presynaptic membrane (Fig. 5.6C, middle, small arrow) was observed in *dgīt* mutants, which could be rescued by reexpression *dgīt* in its mutant background, suggesting that *dgīt* might be involved in presynaptic membrane retrieval and recycling. Quantification of large sized vesicles per bouton in *w<sup>1118</sup>* is about 1.8 ( $\pm 0.3$ ), but those in *dgīt<sup>10/Df596</sup>* and *dgīt<sup>10/f03586</sup>* is about 3.2 ( $\pm 0.4$ ) and 3.8 ( $\pm 0.7$ ), respectively (Fig. 5.6D). The increase in large size vesicles per bouton could be restored partially by re-expression of DGIT ( $2 \pm 0.5$ ) in the *dgīt* mutant background, but not by StnB ( $6.5 \pm 1.2$ ). These EM results strongly support the above suggestion that DGIT is involved in the regulation of vesicle size, endocytosis and recycling of synaptic vesicles.

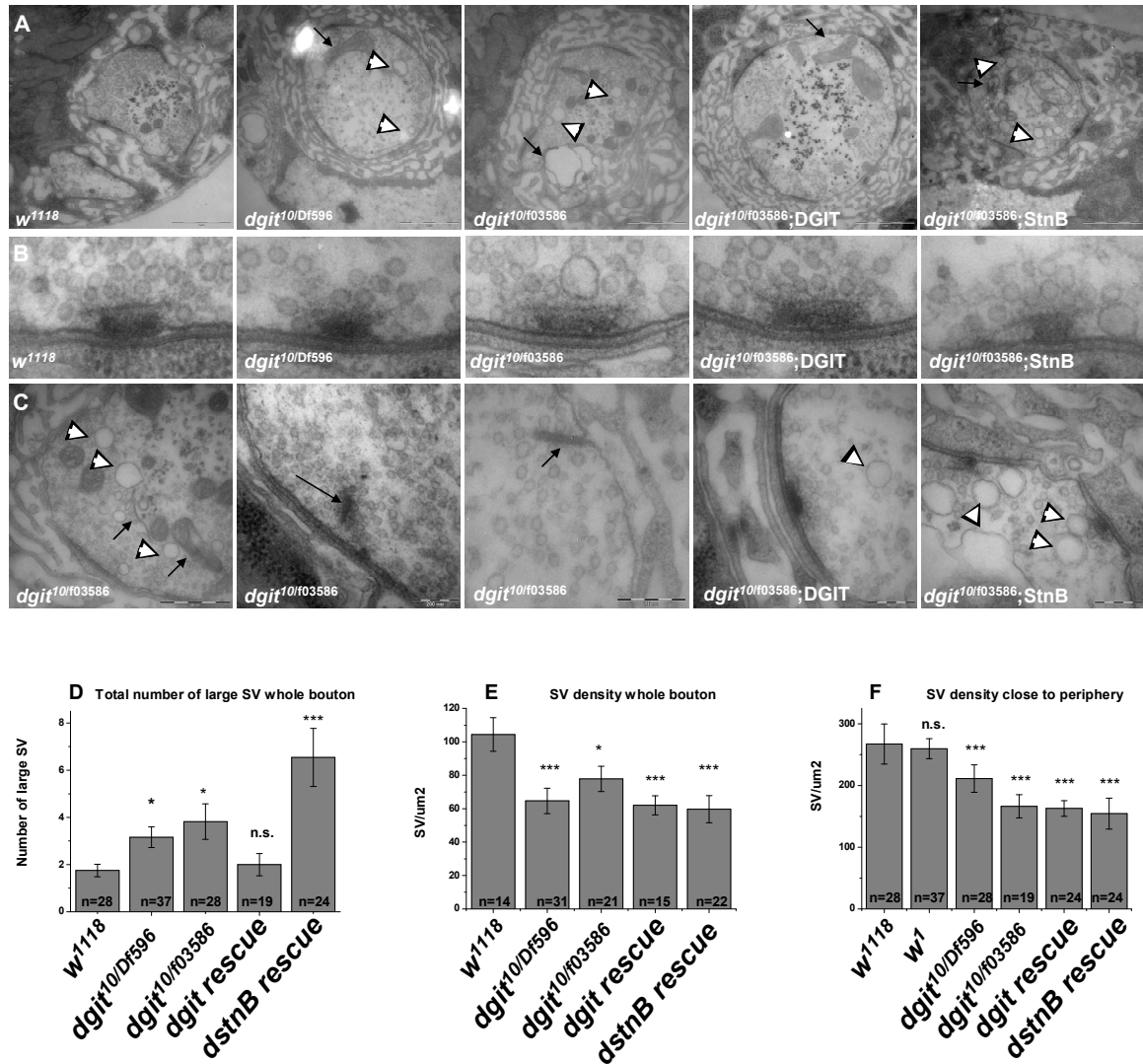


**Figure 5.6 A depletion of synaptic vesicles and accumulation of large size vesicles and membrane recycling intermediates in *dglt* mutant by EM.** (A) Electron micrographs show the overall synaptic ultrastructure at boutons of 3<sup>rd</sup> instars NMJs in control *w<sup>1118</sup>*, the *dglt* mutants (*dglt<sup>10/Df596</sup>* or *dglt<sup>10/f03586</sup>*), DGIT rescue (*Elav-Gal4/+; dglt<sup>10/f03586</sup>;UAS-DGIT/+*) and StnB rescue (*Elav-Gal4/+; dglt<sup>10/f03586</sup>;UAS-StnB/+*). By EM, *dglt* mutants show accumulation of large size vesicles (arrowheads) and tubular structures (small arrows), endosomal intermediate structures (Fig. 5.6A, middle, small arrows). Accumulation of large size vesicles could be rescued by overexpression of DGIT driven by *Elav-Gal4*. But, overexpression of StnB in *dglt<sup>10/f03586</sup>* background could not rescue and even induce much more accumulation of large SV compared with the *dglt* mutant. (B) Periphery active zone ultrastructure at boutons of 3<sup>rd</sup> instars NMJs in control *w<sup>1118</sup>*, the *dglt* mutants (*dglt<sup>10/Df596</sup>* or *dglt<sup>10/f03586</sup>*), DGIT rescue (*Elav-Gal4/+; dglt<sup>10/f03586</sup>;UAS-DGIT/+*) and StnB rescue (*Elav-Gal4/+; dglt<sup>10/f03586</sup>;UAS-StnB/+*). By EM, *dglt* mutants show accumulation of large size vesicles (arrowheads) and tubular structures (small arrows), endosomal intermediate structures (Fig. 5.6A, middle, small arrows). Accumulation of large size vesicles could be rescued by overexpression of DGIT driven by *Elav-Gal4*. But, overexpression of StnB in *dglt<sup>10/f03586</sup>* background could not rescue and even induce much more accumulation of large SV compared with the *dglt* mutant.



*dgat*<sup>10/f03586</sup>; *UAS-DGIT*/+) and StnB rescue (*Elav-Gal4*/+; *dgat*<sup>10/f03586</sup>; *UAS-StnB*/+). Regular synaptic vesicles comprise the most prominent membrane structure in the wild-type bouton, and clusters of these vesicles are observed clustered around active zone T-bars. Slightly reduction in clustered synaptic vesicles in a distance of 50-150 nm to the T-bar and were observed in the *dgat* mutants and also in the rescue situations compared with control. (C) Enlargement of abnormal NMJs ultrastructure in the mutants, DGIT or StnB rescue situation. In *dgat*<sup>10/f03586</sup> larvae, the accumulation in large size vesicles (arrow heads), tubular structure (small arrows), floating dense material (Fig. 5.6C, large arrow), ruffling of the presynaptic membrane (Fig. 5.6C, middle, small arrow) was observed at boutons. The increase in large size vesicles could be rescued to normal level by overexpression of full length DGIT driven by *Elav-Gal4* in the *dgat* mutant background. But, overexpression of full length StnB in the *dgat* mutant background induces the much more large size vesicles compared with the *dgat* mutant, but not decreased. Scale bar, 1  $\mu$ m. (D) Quantification of large sized vesicles per bouton. Large sized vesicles per bouton increase in the *dgat* mutants, which could be restored partially by overexpression of DGIT and HGIT, but not by StnB. Mutant1 and mutant 2 respectively, represents *dgat*<sup>10/Df596</sup> and *dgat*<sup>10/f03586</sup>. (E) Quantification of SV density per bouton (SV/ $\mu$ m<sup>2</sup>). A square of 0.4 x 0.4  $\mu$ m was placed on whole bouton, followed by counting the number of SVs and normalize to SV/ $\mu$ m<sup>2</sup>. (F) Quantification of SV density close to periphery. A square of 0.4 x 0.4  $\mu$ m was placed in the bouton periphery, close to AZ, followed by counting the number of SVs and normalize to SV/ $\mu$ m<sup>2</sup>. The data are reported as mean  $\pm$  SEM., and unless otherwise noted n indicates the number of junctions examined and P designates the significance according to the Student's test. In the figures, significance is marked with asterisks: p< 0,05 (\*), p<0,01 (\*\*), p<0,005 (\*\*\*), comparing to control *w*<sup>1118</sup>, t-test. N.s., not significant (data achieved in collaboration with Carolin Wichmann)

To quantify alterations in vesicle populations near neurotransmitter release sites, we counted the number of vesicles within a distance of 0-150 nm to the T-bar (clustered vesicles) at neuromuscular junctions of third instars larvae (Fig. 5.6E). The density of clustered vesicles in the controls, *w*<sup>1118</sup> and *w*<sup>l</sup>, is about 267( $\pm$ 33) and 260( $\pm$ 16) SV/ $\mu$ m<sup>2</sup>, respectively. The density of clustered vesicles in *dgat*<sup>10/Df596</sup> or *dgat*<sup>10/f03586</sup> is about 211( $\pm$ 22) and

166(±19) SV/μm<sup>2</sup>, respectively. The depletion of clustered vesicles could not be restored by the recruitment of DGIT (162±13 SV/μm<sup>2</sup>) and StnB (155±25 SV/μm<sup>2</sup>) in the *dgat* mutant background. To quantify alterations in the synaptic vesicle density of whole bouton, we counted the total number of vesicles at neuromuscular junctions of third instars larvae, followed by normalizing to SV/μm<sup>2</sup> (Fig. 5.6F). The SV density of whole bouton in the controls, *w<sup>1118</sup>*, is about 104(±10) SV/μm<sup>2</sup>, but that in *dgat<sup>10/Df596</sup>* or *dgat<sup>10/f03586</sup>* is about 64(±8) and 78(±7) SV/μm<sup>2</sup>, respectively. The depletion of clustered vesicles could not be restored by the recruitment of DGIT (63±6 SV/μm<sup>2</sup>) and StnB (60±8 SV/μm<sup>2</sup>) in the *dgat* mutant background. But, depletion of synaptic vesicles could not be rescued by recruitment of full length DGIT in the *dgat* mutant background, suggesting that accurate DGIT level in synapse is very vital for maintaining its normal function and overexpression of DGIT could induce the dysfunction of synaptic vesicles recycling.

Collectively, loss of DGIT provokes the accumulation of large size vesicles throughout the entire nerve terminal. These large size vesicles are much less frequent in control groups. Notably, overexpression of StnB in *dgat* mutant background did further boost the formation of these large sized vesicles, suggesting that StnB probably is upstream of DGIT and interact with DGIT involving in endocytosis and SV recycling.

## **5.7 Nervous system mediated locomotion-deficits in *dgat* mutants**

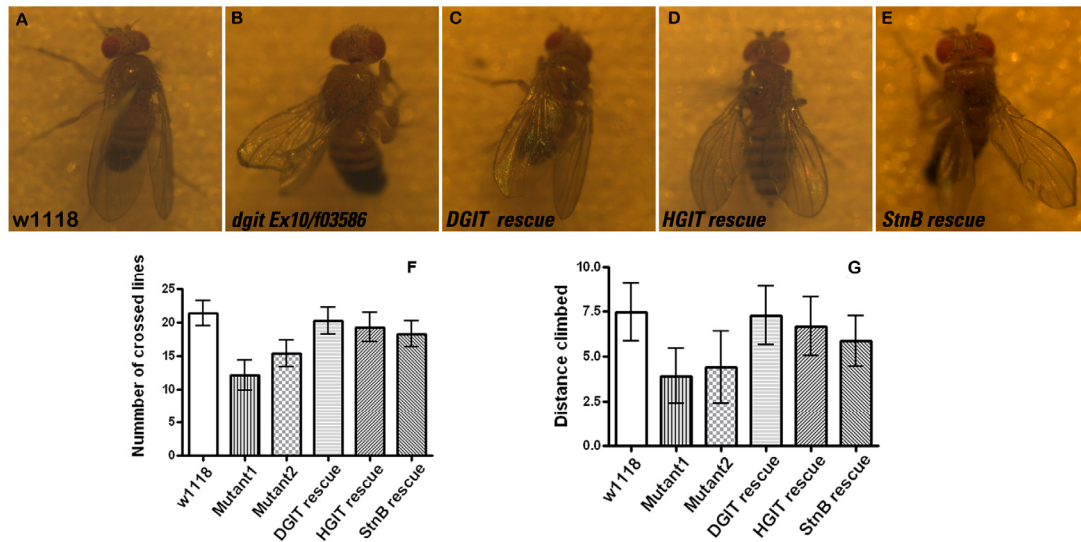


**Figure 5.7 Walking and geotaxis ability in *digit* mutants.** (A) Adult fly wings of *w*<sup>1118</sup> are flat and smooth. But, adult fly wings of *digit* mutants, *digit*<sup>10/f03586</sup> (B) and *digit*<sup>10/Df596</sup> (data not shown), cannot properly expand, which could be restored by recruitment of DGIT (C) and HGIT (D) driven by *Elav-Gal4*, but not by recruitment of *StnB* (E). Locomotion tests including walking ability (F) and negative geotaxis (G) were investigated in control *w*<sup>1118</sup>, the *digit* mutants and rescue adult flies after clipping the wings. Locomotion activity was reduced in both mutants (Fig. 5.7F-G). Spontaneous walking on a horizontal surface of such flies is reduced as reflected by the number of lines of a 2 × 2 cm grid crossed within a 30 s period (F). The mutants show a marked decrease in negative geotaxis ability as quantified by the mean distance climbed vertically in an empty food vial within a period of 30 s (G) (n = 15). Mutant1: *digit*<sup>10/Df596</sup>. Mutant 2: *digit*<sup>10/f03586</sup>. The genotype of DGIT rescue: *Elav-Gal4/Y; digit*<sup>10/f03586</sup>; *UAS-DGIT/+*. HGIT rescue: *Elav-Gal4/Y; digit*<sup>10/f03586</sup>; *UAS-HGIT/+*. *StnB* rescue: *Elav-Gal4/Y; digit*<sup>10/f03586</sup>; *UAS-StnB/+*. Data are mean ± SD

Adult fly wings of *digit* mutant cannot properly expand and are unsmooth and Cy-like (Fig. 5.7B) when compared to controls (Fig. 5.7A). The wing phenotype could be rescued to wild type like completely and partially (Fig. 5.7C-E), respectively, by re-expression of DGIT and HGIT driven by *Elav-Gal4*. In contrast, expression of *StnB* did not allow rescue

Already qualitatively, flies mutant for *digit* appear clearly affected in locomotion. To quantify this impression, we applied locomotion tests on the *digit* mutant adult flies. Locomotion activity was reduced in both *digit* mutants (Fig. 5.7F-G). The *w<sup>1118</sup>* control flies crossed 21( $\pm$ 1.5) lines within 30 s when walking on a horizontal surface with a 2  $\times$  2 cm square grid. In contrast, *digit<sup>10/Df596</sup>* and *digit<sup>10/f03586</sup>* animals only crossed 12 ( $\pm$ 2.2) and 18 ( $\pm$  1.4) lines, respectively (Fig. 5.7F). Notably, deficient walking ability in *digit* mutant could be rescued by expression of DGIT (21 $\pm$ 2.1 lines) or HGIT (19 $\pm$ 2.2 lines) driven by *Elav-Gal4*, but not by *StnB* expression (18 $\pm$ 1.2 lines). When control flies were tapped to the bottom of a cylindrical vial they immediately started climbing up the walls (negative geotaxis). Within 30 s, *w<sup>1118</sup>* animals climbed 7.5 ( $\pm$  1.6) cm, whereas *digit<sup>10/Df596</sup>* and *digit<sup>10/f03586</sup>* flies only climbed 3.9 ( $\pm$  1.4) and 4.4 ( $\pm$  2.0) cm (Fig. 5.7G). Deficient ability of negative geotaxis (Fig. 5.7G) in *digit* mutants could be partially rescued by re-expression of DGIT (7.3  $\pm$  1.6 cm) or HGIT (6.7  $\pm$  1.6 cm), but not by *StnB* (5.1  $\pm$  1.4 cm). It suggests that deprivation of DGIT induces a dysfunction of synaptic vesicles (SVs) endocytosis, vesicle recycling and transmission, and thereby impairs the locomotive abilities of adult flies.

## 5.8 Discussion

### 5.8.1 Synaptic vesicle recycling and endocytosis

Endogenous DGIT expression is observed at boutons of 3<sup>rd</sup> instar *Drosophila* NMJ (Fig. 5.2C). DGIT and endocytic protein *StnB* could be co-immunoprecipitated from adult fly head extracts (Fig. 5.3A). Additionally, overexpressed DGIT-GFP co-localizes *StnB* in motor neurons soma of ventral ganglion (Fig. 5.3C) and at boutons of 3<sup>rd</sup> instar

*Drosophila* NMJs (Fig. 5.3B). These results suggest that DGIT interacts with StnB and is probably involved in vesicle endocytosis together with StnB. By immunofluorescence, StnB levels decreased in *dgut* mutant *dgut*<sup>10/f03586</sup> (Fig. 5.5B, in green) as well as in *dgut*<sup>10/Df596</sup> (data not shown) compared with control *w*<sup>1118</sup> (Fig. 5.5B, in green). Re-expression of *Drosophila* GIT (Fig. 5.5C, in green and Fig. 5.5D) and human GIT (Fig. 5.5D) in *dgut* mutant, StnB level could be restored. These results show that DGIT deficiency affects specifically the level of endocytosis-associated molecule StnB. It suggests that DGIT interacts with StnB involved in endocytosis and recycling of synaptic vesicles. Electron microscopy reveals aberrant large size vesicles, and an accumulation of endocytic large size membranous recycling intermediates structures at boutons of 3<sup>rd</sup> instar *Drosophila* NMJ in both mutants, which could be rescued by recruitment of full length DGIT or HGIT in the *dgut* mutant background, but not by StnB (Fig. 5.6). Large size membranous recycling intermediates structures including large size vesicles and endosome intermediates structures (also called “cisternae”), which were also detected in other endocytic stoned mutants, synaptotagmin mutant and dynamin mutants (Fergestad, 1999; Loewen, 2006; Sever., 2000 and Cooney, 2002), and are hallmarks for all endocytotic mutants. Large size membranous recycling intermediates structures indicates a defect in the bulk uptake or degradative pathway, and are proposed to be involved in endocytosis and synaptic vesicle recycling (Loewen, 2006; Koenig, 1993; Wucherpennig, 2003). These results strongly support the above suggestion that DGIT is involved in the regulation of vesicle size, endocytosis and recycling of synaptic vesicles.

## **5.8.2 Receptor internalization and membrane trafficking**

GIT1 is enriched in pre- and postsynaptic densities (Kim, 2003; Zhang, 2003), and inhibiting formation of GIT-PIX oligomers in cultured hippocampal neurons decreases the number of synapses formed along dendrites (Zhang, 2003). Recent evidence suggests that GIT1 could be involved in the altered membrane trafficking that contributes to Huntington's disease. GIT1 associates with the pathogenic huntingtin protein mutant (Goehler, 2004). ARF6 is a central mediator in membrane trafficking between the cell surface and endosomes. ARF6 mutants constitutively bound to either GDP or GTP inhibit receptor internalization and resensitization in a similar manner to overexpression of GITs (Claing, 2001). Removal of ARF-GAP activity abolishes the effect of overexpressed GITs on receptor internalization (Premont, 1998). It is unclear how ARF-GAP activity regulates trafficking of agonist-bound receptors from the cell surface to recycling endosomes, then back to the cell surface. Some synapses at 3<sup>rd</sup> instar NMJ in the *dgut* mutants only appear Brp and HRP, but not postsynaptic receptor GluRIID in glutamatergic synapses (arrow head, Fig. 5.4B), which is not seen in *w<sup>1118</sup>* normally. Like ARF6, DGIT might be involved in the regulation of neurotransmitter release, trafficking and internalization of receptor. Unusually among ARF-GAPs, the DGIT proteins also act on ARF6 (Uchida, 2001). Moreover, their ARF-GAP activity is stimulated by phosphatidylinositol (3,4,5)-trisphosphate [PtdIns(3,4,5)P3] but not by phosphatidylinositol 5-phosphate, phosphatidylinositol (4,5)-bisphosphate [PtdIns(4,5)P2] or diacylglycerol (DAG) (Vitale, 2000). Taken together, GIT proteins might therefore be recruited to the plasma membrane and activated in response to signaling events, regulating signal-mediated membrane trafficking through ARF6. However, this hypothesis has to be addressed by future analysis.

## **6. Results part3: functional analysis of *djm-1*:**

Mental retardation (MR) is a common form of cognitive impairment affecting between 1 and 3% of the population of industrialized countries (Roeleveld, 1997; Aicardi, 1998). In central Europe, about 8% of health-care expenditure is spent on this disease. Causes of MR include genetic conditions, disorders that occur as a fetus develops during pregnancy and problems during or after birth. Some cases of mental retardation have multiple causes. There is no cure for MR so far. MR occurs significantly more often in males than in females. There is ample evidence to support the idea that this male bias is largely due to the involvement of X-linked genes that play a role in brain differentiation and function (Ropers, 2006). As deduced from the absolute and relative frequency of MR in males and females, approximately 2 males per 1000 carry a gene defect leading to X-linked mental retardation (XLMR).

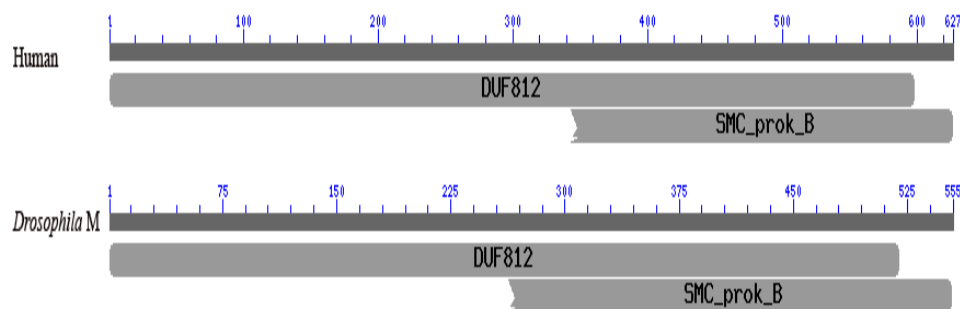


**Figure 6.1 Schematic overview of protein structures of DJM-1.**

By using cutting edge genomics technology, the group of Hilger Ropers (Max Planck Institute Human Molecular Genetics, Berlin) has recently found candidate mutations in the *djm-1* gene of XLMR patients. 4 missense mutations of *djm-1* were found in 200 not related MR patients,

but not observed in 200 controls. Thus, DJM-1 was proposed as a candidate gene for being MR-associated.

However, given the current knowledge, DJM-1 is a protein of completely unknown function. A direct orthologue of DJM-1 (CG9951) exists in *Drosophila melanogaster*, overall exhibiting ~30% identity and ~62% similarity at the amino acid level with the human homolog, indicating that DJM-1 function has been tightly conserved throughout evolution. The *djm-1* gene is on 2<sup>nd</sup> chromosome, and predicted to encode a protein of 555 amino acids. The DJM-1 protein of *Drosophila melanogaster* contains one domain of unknown function DUF812, one homolog of H. sapiens coiled-coil domain-containing protein 22 (CCDC22, coiled-coil domain containing 22), or one SMC (structural maintenance of chromosomes) domain on the C-terminus, which normally binds to DNA and acts in organizing and segregating chromosome (Fig. 6.1). Here, an attempt to use *Drosophila* genetics to firstly address DJM-1 functions was performed, with the final goal to identify cellular and molecular scenarios causally involved in defective brain development of MR patients.

## 6.1 Effect of RNAi versus *djm-1* on fly viability

In a first approach to address DJM-1 function, genomically encoded double-strand RNAs for interference were constructed. Thus, sequences from both N- and C-terminal stretches (CG9951 cDNA (double stranded RNA hairpin, ~400bp) were cloned into pUAST vector and injected into *Drosophila* embryos. The *UAS-DJM-1-RNAi* lines were activated by different driver lines: ubiquitously expressing drivers: actin-Gal4 and tubulin-Gal4; muscle specific drivers: 24B-Gal4; pan-neuronal drivers: Elav-Gal4. The ubiquitous expression of *UAS-DJM-1-RNAi* driven by actin-Gal4 or tubulin-Gal4 results in pupal lethality. Strong pan-neuronal



expression of *UAS-DJM-1-RNAi* (using Elav-Gal4) caused embryonic lethality. Muscle expression of *UAS-DJM-1-RNAi* by 24B-Gal4 provokes later lethality (reduced viability as well). These interference results suggest that DJM-1 might play important roles in development of *Drosophila*, potentially also in the nervous system. However, at this point it cannot be excluded that the defects observed after *djm-1* interference are due to non-specific effects of the RNAi constructs used (“e.g. cross-targeting into other loci”). Therefore, the description of its true loss of function phenotype need to be generated a genuine null mutant for its phenotype and rescue analysis.

## 6.2 Tissue distribution for *djm-1* mRNA

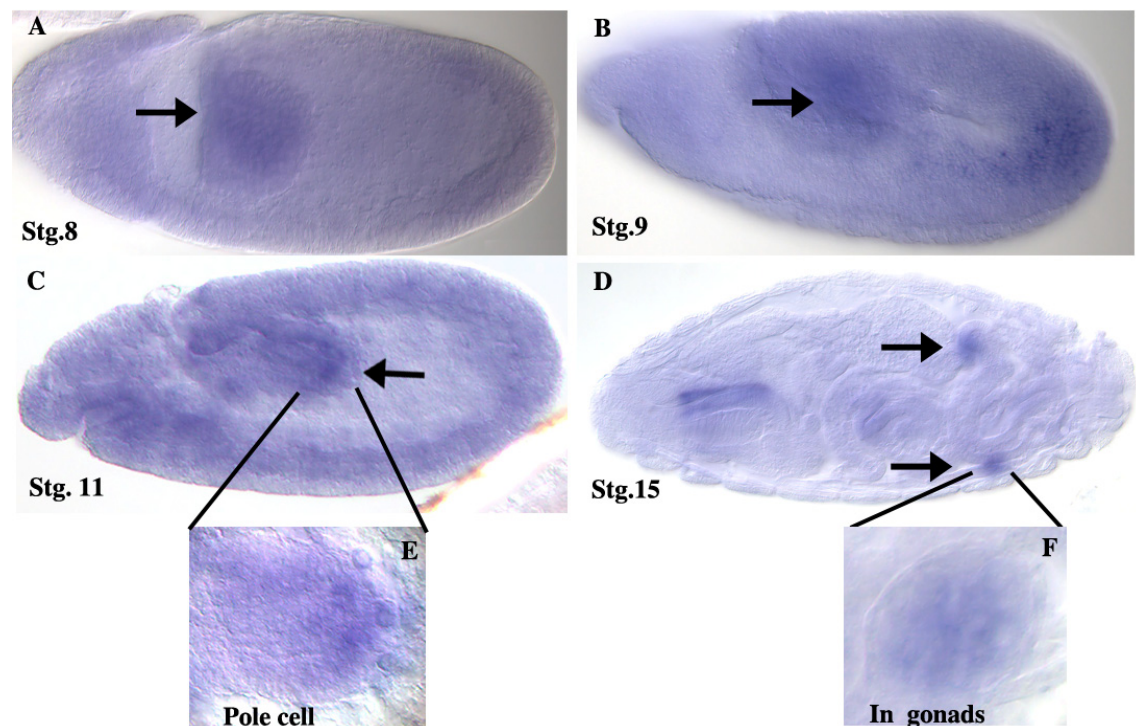


**Figure 6.2** *In situ* hybridization of *djm-1* in *Drosophila* embryos. Specific staining was obtained when an antisense probe of *djm-1* cDNA was used. Sense probes did not produce any label in either experiment (data not shown). *Djm-1* was specifically expressed in the pole cells from stage 8 throughout embryogenesis (A-D, arrows). (E) and (F), respectively, is enlargement of (C) and (D).

To detect the mRNA expression pattern in *Drosophila*, *in situ* hybridizations were performed throughout *Drosophila* embryogenesis until late larvae to investigate the spatio-temporal expression pattern of *djm-1*. A strong specific label of *djm-1* was detected in the pole cells and gonads from stage 8 embryogenesis (Fig. 6.2A-F), and also in *Drosophila* larvae (Fig. 6.3). The gonads are the precursors of the testes in males and ovaries in females. It suggests that *djm-1* exists in pole cells and gonads of *Drosophila melanogaster*, and thus might be involved in the formation and functional regulation of reproductive organs. A strong specific label of

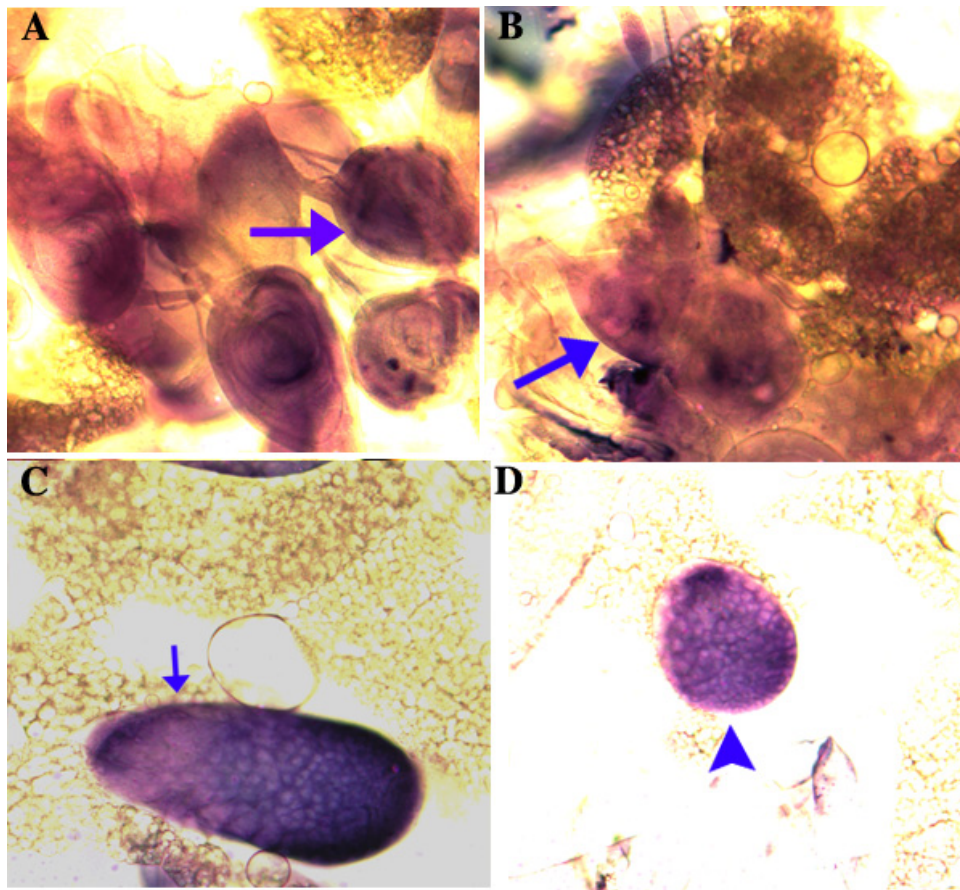


**Figure 6.3** *In situ* hybridization of *djm-1* in *Drosophila* 3<sup>rd</sup> larvae. Specific staining was obtained in eye disc (A, large arrows), wing disc (B, large arrows) and female gonads (C, small arrows) and male gonads (D, arrow heads) of 3<sup>rd</sup> instar larvae. Sense probes did not produce any label in either experiment (data not shown).

*djm-1* was also detected in eye disc and wing disc throughout *Drosophila* larvae stages (Fig. 6.3A-B) but not in the brain, indicating *djm-1* may function in formation and regulation of eye disc and wing disc

## 6.3 Generating mutants for *djm-1*

*Djm-1* deletion mutants were generated by the use of a fly line carrying the P-element P{SUPor-P}KG04920 [BDGP Gene Disruption Project (Bellen, 2004)] located in downstream of 3' UTR of *djm-1* CG9951 on the 3<sup>rd</sup> chromosome (Fig. 6.4). A fruit fly line carrying the  $\Delta 2-3$  transposase on the 2nd chromosome was used to activate P-element mobilization. Adult male flies from lines in which P{SUPor-P}KG04920 might have been mobilized were tested for imprecise and precise excision events via single fly genomic PCR (primer pairs: p-element primer together with genomic primer). For further mapping imprecise excisions, we used 5 genomic primer pairs of *djm-1* and 4 genomic primer pairs of *lmpt* to map whether and how much the genetic locus of *djm-1* or neighbor gene, *lmpt* is imprecisely excised (Fig. 6.4). Single fly genomic PCRs were performed according to Gloor (Gloor, 1993). Finally, two imprecise excisions, *djm-1*<sup>ex253</sup> and *djm-1*<sup>ex416</sup>, were obtained. These two excisions delete the most part of *djm-1* locus but also the first exon of *lmpt* (the parental line,

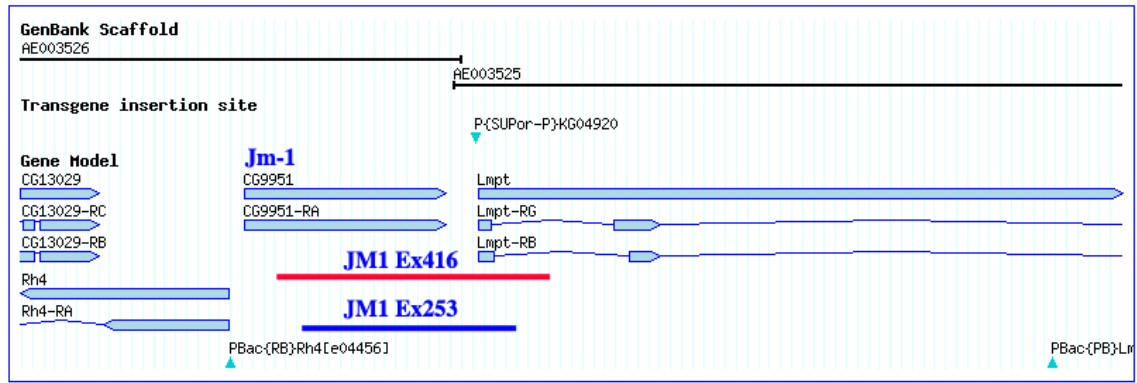


**Figure 6.4** *Drosophila djm-1* imprecise excision scheme using the p-element line P{SUPor-P}KG04920 closed to *djm-1*. The red line and blue line, respectively, represents the genome locus part deletion of *djm-1*<sup>ex416</sup> and *djm-1*<sup>ex253</sup>.

P{SUPor-P}KG04920, is located in the 5'UTR of *lmp1*). Here, Df9003 was used as its large deficiency, which deletes the whole locus of *djm-1* gene completely as well as other neighbor gene of *djm-1*. Even though the homozygote of *djm-1*<sup>ex416</sup> provokes larvae lethality, but homozygote of *djm-1*<sup>ex253</sup> and heterozygote of *djm-1*<sup>ex416/Df9003</sup> are viable and sterile.

## 6.4 Analysis of locomotion abilities deficits of *djm-1* mutants

Though in *djm-1* mutants NMJs appeared rather normal concerning their molecular and morphological organization, the mutant adult flies appeared somewhat sluggish. Thus, walking and negative geotaxis abilities were analyzed in the *djm-1* mutant (*djm-1*<sup>ex416/Df9003</sup>) adult flies in dark. Locomotion activity was reduced in *djm-1*<sup>ex416/Df9003</sup> (Fig. 6.5A-B), but not in *djm-1*<sup>ex253/Df9003</sup> (data not shown). *w*<sup>1118</sup>, control flies crossed about 20 lines within 30 s when walking on a horizontal surface with a 2 × 2 cm square grid, however, *djm-1*<sup>ex416/Df9003</sup> animals only crossed about 12 lines

(Fig. 6.5A). Deficient walking ability in the *djm-1* mutant could not be rescued by re-expression of DJM-1. The rescue flies could walk only about 13 lines. When control flies were tapped to the bottom of a cylindrical vial they immediately started climbing up the walls (negative geotaxis). Within 30 s, *w<sup>1118</sup>* animals as control climbed about 8.3 cm, whereas *djm-1<sup>ex416/Df<sup>9003</sup></sup>* flies only climbed 4.1 cm (Fig. 6.5B). Deficient ability of negative geotaxis (Fig. 6.5B) in *djm-1* mutant could not be rescued by re-expression of DJM-1. It suggests that the deficiency in walking and climbing ability might not due to a lack of *DJM-1*. The mutant *djm-1<sup>ex416/Df<sup>9003</sup></sup>* also deletes the N-terminal locus of *Impt* gene, which might result in the locomotion deficiency. The function and biological processes involved of *djm-1* need further investigation.

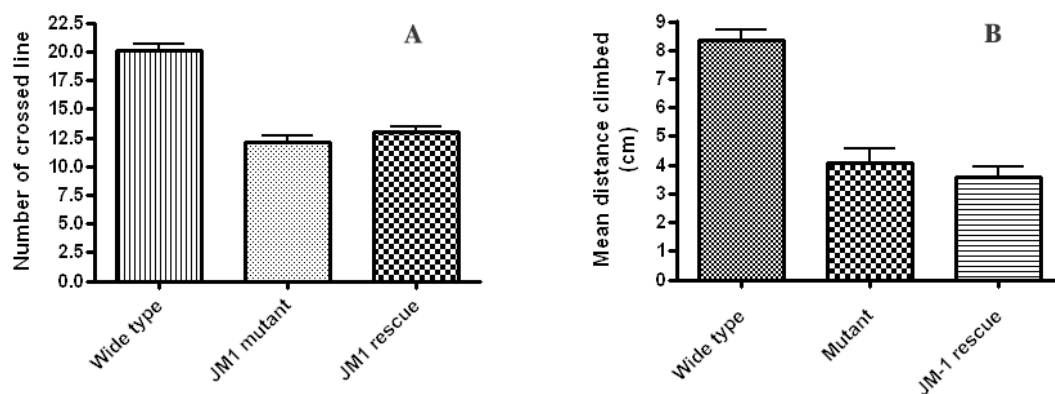


**Figure 6.5 Walking and geotaxis ability in *dgit* mutant.** Locomotion tests including walking ability (A) and negative geotaxis (B) were investigated in control *w<sup>1118</sup>*, the *djm-1* mutant and rescue adult flies after clipping the wings in dark. (A) Spontaneous walking on a horizontal surface of such flies is also reduced as reflected by the number of lines of a  $2 \times 2$  cm grid crossed within a 30 s period ( $n = 15$ ). Deficient walking ability in *djm-1* mutant could not be rescued by re-expression of DJM-1. (B) The mutant fail to show negative geotaxis as quantified by the mean distance climbed vertically in an empty food vial within a period of 30 s ( $n = 15$ ). Deficient negative geotaxis ability in the *djm-1* mutant also could not be restored by re-expression of DJM-1. Mutant *djm-1<sup>ex416/Df<sup>9003</sup></sup>*

and rescue flies *Elav-Gal4/+; djm-I<sup>ex416/Df9003</sup>*; *UAS-DJMI-GFP/+* were used for this locomotion test. Data are mean  $\pm$  SEM

## **7. References**

- Adachi, M., S. Suematsu, et al. (1995) "Targeted mutation in the Fas gene causes hyperplasia in peripheral lymphoid organs and liver." *Nat Genet* 11(3): 294-300.
- Albin, S. D. and G. W. Davis (2004) "Coordinating structural and functional synapse development: postsynaptic p21-activated kinase independently specifies glutamate receptor abundance and postsynaptic morphology." *J Neurosci* 24(31): 6871-9.
- Andlauer T. F. M. and S. J. Sigrist (2010) "*In vivo* Imaging of *Drosophila* Larval Neuromuscular Junctions to Study Synapse Assembly, Cold Spring Harbor Press, *Drosophila* Neurobiology Methods: A Laboratory Manual, Chapter 21"
- Atwood, H. L. and S. Karunanithi (2002) "Diversification of synaptic strength: presynaptic elements." *Nat Rev Neurosci* 3: 497-516.
- Atwood, H. L., C. K. Govind, et al. (1993) "Differential ultrastructure of synaptic terminals on ventral longitudinal abdominal muscles in *Drosophila* larvae." *J Neurobiol* 24:1008-24.
- Audebert, S., C. Navarro, et al. (2004) "Mammalian Scribble forms a tight complex with the betaPIX exchange factor." *Curr Biol* 14(11): 987-95.
- Auld, V. J., R. D. Fetter, et al. (1995) "Gliotactin, a novel transmembrane protein on peripheral glia, is required to form the blood-nerve barrier in *Drosophila*." *Cell* 81(5): 757-67.
- Bagrodia, S. and R. A. Cerione (1999) "Pak to the future. *Trends Cell Biol.*" 9(9): 350-5.

- Barry, M. F. and E. B. Ziff (2002) "Receptor trafficking and the plasticity of excitatory synapses." *Curr Opin Neurobiol* 12: 279-86.
- Bateup H.S., B.L. Sabatini (2010) "For synapses, it's depression not death." *Cell* 141(5):750-2.
- Batlevi Y., D.N. Martin, et al. (2010) "Dynein light chain 1 is required for autophagy, protein clearance, and cell death in *Drosophila*." *Proc Natl Acad Sci U S A*. 107(2):742-7.
- Bellen, H. J., R. W. Levis, et al. (2004) "The BDGP gene disruption project: single transposon insertions associated with 40% of *Drosophila* genes." *Genetics* 167(2): 761-81.
- Bliss, T. V. and G. L. Collingridge (1993) "A synaptic model of memory: long-term potentiation in the hippocampus." *Nature* 361:31-39.
- Blomgren, K., M. Leist, et al. (2007) "Pathological apoptosis in the developing brain." *Apoptosis* 12(5): 993-1010.
- Borgdorff, A.J. and D. Choquet (2002) "Regulation of AMPA receptor lateral movements." *Nature* 417:649-53.
- Brand, A. H. and N. Perrimon (1993) "Targeted gene expression as a means of altering cell fates and generating dominant phenotypes." *Development* 118(2): 401-15.
- Bretscher, M. S. (1996) "Moving membrane up to the front of migrating cells." *Cell* 85(4): 465-7.
- Burton, P. R. and J. L. Paige (1981) "Polarity of axoplasmic microtubules in the olfactory nerve of the frog." *Proc Natl Acad Sci U S A* 78(5): 3269-73.



- Cai, Q. and Z. H. Sheng (2009) "Mitochondrial transport and docking in axons." *Exp Neurol* 218(2): 257-67.
- Cai, Q., P. Y. Pan, et al. (2007) "Syntabulin-kinesin-1 family member 5B-mediated axonal transport contributes to activity-dependent presynaptic assembly." *J Neurosci* 27(27): 7284-96.
- Ceccarelli B., W. P. Hurlbut, et al. (1973) "Turnover of transmitter and synaptic vesicles at the frog neuromuscular junction." *J Cell Biol* 57: 499-524.
- Chauvier, D., H. Lecoecur, et al. (2005) "Upstream control of apoptosis by caspase-2 in serum-deprived primary neurons." *Apoptosis* 10(6): 1243-59.
- Chen, J., T. Nagayama, et al. (1998) "Induction of caspase-3-like protease may mediate delayed neuronal death in the hippocampus after transient cerebral ischemia." *J Neurosci* 18:4914-28.
- Chen, K. and D. E. Featherstone (2005) "Discs-large (DLG) is clustered by presynaptic innervation and regulates postsynaptic glutamate receptor subunit composition in *Drosophila*." *BMC Biol* 3:1.
- Chintapalli, V. R., J. Wang, et al. (2007). Using FlyAtlas to identify better *Drosophila* models of human disease. *Nature Genetics* 39: 715-20.
- Claing, A., W. Chen, et al. (2001) "beta-Arrestin-mediated ADP-ribosylation factor 6 activation and beta 2-adrenergic receptor endocytosis." *J Biol Chem* 276(45): 42509-13.
- Colbourne, F., H. Li, et al. (1999) "Continuing postischemic neuronal death in CA1: influence of ischemia duration and cytoprotective doses of NBQX and SNX-111 in rats." *Stroke* 30(3): 662-8.

- Collingridge, G. L., J. T. Isaac, et al. (2004) "Receptor trafficking and synaptic plasticity." *Nat Rev Neurosci* 5:952-62.
- Cooney, J. R., J. L. Hurlburt, et al. (2002) "Endosomal compartments serve multiple hippocampal dendritic spines from a widespread rather than a local store of recycling membrane." *J Neurosci* 22(6): 2215-24.
- Danial, N. N. and S. J. Korsmeyer (2004) "Cell death: critical control points." *Cell* 116(2): 205-19.
- Davis, G. W., A. DiAntonio, et al. (1998) "Postsynaptic PKA controls quantal size and reveals a retrograde signal that regulates presynaptic transmitter release in *Drosophila*." *Neuron* 20:305-15.
- Deguchi-Tawarada, M., E. Inoue, et al. (2004) "CAST2: identification and characterization of a protein structurally related to the presynaptic cytomatrix protein CAST." *Genes Cells* 9(1): 15-23.
- Depaepe, V., N. Suarez-Gonzalez, et al. (2005) "Ephrin signalling controls brain size by regulating apoptosis of neural progenitors." *Nature* 435(7046): 1244-50.
- Di Cesare, A., S. Paris, et al. (2000) "p95-APP1 links membrane transport to Rac-mediated reorganization of actin." *Nat Cell Biol* 2: 521-30.
- DiAntonio, A., S. A. Petersen, et al. (1999) "Glutamate receptor expression regulates quantal size and quantal content at the *Drosophila* neuromuscular junction." *J Neurosci* 19:3023-32.
- Dick T., K. Ray, et al. (1996) "Cytoplasmic dynein (ddlc1) mutations cause morphogenetic defects and apoptotic cell death in *Drosophila melanogaster*." *Mol Cell Biol* 16:1966–77.

- Dickman D. K., Z. Lu, et al.(2006) "Altered synaptic development and active zone spacing in endocytosis mutants." *Curr Biol* **16**:591–598.
- Dingledine, R., K. Borges, et al. (1999) "The glutamate receptor ion channels." *Pharmacol Rev* **51**:7-61.
- Donaldson, J. G. and C. L. Jackson (2000) "Regulators and effectors of the ARF GTPases." *Curr Opin Cell Biol* **12**: 475-82.
- Donaldson, J.G. (2003) "Multiple roles for Arf6: sorting, structuring, and signaling at the plasma membrane." *J Biol Chem* **278**: 41573–41576.
- Drachman, D. (2005). "Do we have brain to spare?". *Neurology* **64** (12): 2004–5.
- Dresbach, T., B. Qualmann, et al. (2001) "The presynaptic cytomatrix of brain synapses." *Cell Mol Life Sci* **58**(1): 94-116.
- D'Souza-Schorey, C. and P. Chavrier (2006) "ARF proteins: roles in membrane traffic and beyond." *Nat Rev Mol Cell Biol* **7**(5): 347-58.
- D'Souza-Schorey, C., E. van Donselaar, et al. (1998) "ARF6 targets recycling vesicles to the plasma membrane: insights from an ultrastructural investigation." *J Cell Biol* **140**(3): 603-16.
- D'Souza-Schorey, C., G. Li, et al. (1995) "A regulatory role for ARF6 in receptor-mediated endocytosis." *Science* **267**(5201): 1175-8.
- Ducut Sigala, J. L., V. Bottero, et al. (2004) "Activation of transcription factor NF-kappaB requires ELKS, an IkappaB kinase regulatory subunit." *Science* **304**(5679): 1963-7.

- Duncan JE, Goldstein LS. (2006) "The genetics of axonal transport and axonal transport disorders." PLoS Genet, 2(9):e124.
- Enari, M., H. Sakahira, et al. (1998) "A caspase-activated DNase that degrades DNA during apoptosis, and its inhibitor ICAD." Nature 391(6662): 43-50.
- Espindola, F. S., D. M. Suter, et al. (2000) "The light chain composition of chicken brain myosin-Va: calmodulin, myosin-II essential light chains, and 8-kDa dynein light chain/PIN." Cell Motil Cytoskeleton 47(4): 269-81.
- Estes P. S., T. C. Jackson, et al. (2003) "Functional dissection of a eukaryotic dicistronic gene: Transgenic stonedB, but not stonedA, restores normal synaptic properties to *Drosophila* stoned mutants." Genetics **165**:185–196.
- Featherstone, D. and K. Broadie (2002). "Response: meaningless minis?" Trends Neurosci 25(8): 386-387.
- Featherstone, D. E., E. Rushton, et al. (2005) "An essential *Drosophila* glutamate receptor subunit that functions in both central neurosis and neuromuscular junction." J Neurosci 25:3199-3208.
- Fergestad, T., W. S. Davis, et al. (1999) "The stoned proteins regulate synaptic vesicle recycling in the presynaptic terminal." J Neurosci 19(14): 5847-60.
- Freeman, M. R. (2006) "Sculpting the nervous system: glial control of neuronal development." Curr Opin Neurobiol 16(1): 119-25.
- Geppert, M., Y. Goda, et al. (1994) "Synaptotagmin I: a major Ca<sup>2+</sup> sensor for transmitter release at a central synapse." Cell 79:717-27.

- Gillardon, F., B. Bottiger, et al. (1997) "Activation of CPP-32 protease in hippocampal neurons following ischemia and epilepsy." *Brain Res Mol Brain Res* 50:16-22.
- Gillardon, F., I. Kiprianova, et al. (1999) "Inhibition of caspases prevents cell death of hippocampal CA1 neurons, but not impairment of hippocampal long-term potentiation following global ischemia." *Neuroscience* 93:1219-22.
- Gilmore, E. C., R. S. Nowakowski, et al. (2000) "Cell birth, cell death, cell diversity and DNA breaks: how do they all fit together?" *Trends Neurosci* 23(3): 100-5.
- Gloor, G. B., C. R. Preston, et al. (1993) "Type I repressors of P element mobility." *Genetics* 135(1): 81-95.
- Goehler, H., M. Lalowski, et al. (2004) "A protein interaction network links GIT1, an enhancer of huntingtin aggregation, to Huntington's disease." *Mol Cell* 15(6): 853-65.
- Goldstein, L. S. (2001a) "Kinesin molecular motors: transport pathways, receptors, and human disease." *Proc Natl Acad Sci U S A* 98(13): 6999-7003.
- Goldstein, L. S. (2001b) "Molecular motors: from one motor many tails to one motor many tales." *Trends Cell Biol* 11(12): 477-82.
- Goodman, C. S., M. J. Bastiani, et al. (1986) "Growth cone guidance and cell recognition in insect embryos." *Dev Biol (N Y)* 1985 3:283-300.

- Gundelfinger, E. D. and S. tom Dieck (2000) "Molecular organization of excitatory chemical synapses in the mammalian brain." *Naturwissenschaften* 87(12): 513-23.
- Gundelfinger, E. D., M. M. Kessels, et al. (2003) "Temporal and spatial coordination of exocytosis and endocytosis." *Nat Rev Mol Cell Biol* 4(2): 127-39.
- Hall, Z. W. and J. R. Sanes (1993) "Synaptic structure and development: the neuromuscular junction." *Cell* 72 Suppl: 99-121.
- Hao, M. and F. R. Maxfield (2000) "Characterization of rapid membrane internalization and recycling." *J Biol Chem* 275(20): 15279-86.
- Hell, S. W. and J. Wichmann (1994) "Breaking the diffraction resolution limit by stimulated emission: stimulated-emission-depletion fluorescence microscopy." *Optics Letters* 19 (11): 780–782.
- Heuser J. E. and T. S. Reese (1973) "Evidence for recycling of synaptic vesicle membrane during transmitter release at the frog neuromuscular junction." *J Cell Biol* 57:315-44.
- Hille, B. (2001) "Ion Channels of Excitable Membranes." 3rd Edition. Sunderland, Massachusetts: Sinauer Associates, Inc.
- Himi, T., Y. Ishizaki, et al. (1998) "A caspase inhibitor blocks ischaemia-induced delayed neuronal death in the gerbil." *Eur J Neurosci* 10(2): 777-81.
- Hirokawa, N. and R. Takemura (2005) "Molecular motors and mechanisms of directional transport in neurons." *Nat Rev Neurosci* 6:201–14.

- Hoefen, R. J. and B. C. Berk (2006) "The multifunctional GIT family of proteins." *J Cell Sci* 119(Pt 8): 1469-75.
- Horn, C. and E. A. Wimmer (2000). "A versatile vector set for animal transgenesis." *Dev Genes Evol* 210(12): 630-637.
- Inohara, N. and G. Nunez (1999) "Genes with homology to DFF/CIDEs found in *Drosophila melanogaster*." *Cell Death Differ* 6(9): 823-4.
- Inohara, N., T. Koseki, et al. (1998) "CIDE, a novel family of cell death activators with homology to the 45 kDa subunit of the DNA fragmentation factor." *EMBO J* 17(9): 2526-33.
- Jackson, T. R., B. G. Kearns, et al. (2000) "Cytohesins and centaurins: mediators of PI 3-kinase-regulated Arf signaling." *Trends Biochem Sci* 25: 489-95.
- Jaffrey, S. R. and S. H. Snyder (1996) "PIN: an associated protein inhibitor of neuronal nitric oxide synthase." *Science* 274(5288): 774-7.
- Jahn, R., T. Lang, et al. (2003) "Membrane fusion." *Cell* 112:519-33.
- Jeanette, L. N. Sigala, et al. (2004) "Activation of Transcription Factor NF-B Requires ELKS, an IB Kinase Regulatory Subunit." *Science* 304:1963-7.
- Kandel, E. R., J. H. Schwartz, et al. (2000). "Principles of Neural Science (4th ed.)." New York: McGraw-Hill: 178-82.
- Karess, R. E. and G. M. Rubin (1984) "Analysis of P transposable element functions in *Drosophila*." *Cell* 38(1): 135-46.

- Kelly L. E. and A.M. Phillips (2005) "Molecular and genetic characterization of the interactions between the *Drosophila* stoned B protein and DAP-160 (intersectin)." *Biochem J* 388(1):195-204.
- Kim, S., J. Ko, et al. (2003) "The GIT family of proteins forms multimers and associates with the presynaptic cytomatrix protein Piccolo." *J Biol Chem* 278(8) : 6291-300.
- King, S. M., E. Barbarese, et al. (1996) "Brain cytoplasmic and flagellar outer arm dyneins share a highly conserved Mr 8,000 light chain." *J Biol Chem* 271(32): 19358-66.
- Kittel, R. J., C. Wichmann, et al.. (2006) "Bruchpilot promotes active zone assembly, Ca<sup>2+</sup> channel clustering, and vesicle release." *Science* 312(5776): 1051-4.
- Ko, J., M. Na, et al. (2003) "Interaction of the ERC family of RIM-binding proteins with the liprin-alpha family of multidomain proteins." *J Biol Chem* 278: 42377-85.
- Koenig, J. H., K. Yamaoka, et al. (1993) "Calcium-induced translocation of synaptic vesicles to the active site." *J Neurosci* 13(6): 2313-22.
- Koester, H. J. and D. Johnston (2005) "Target cell-dependent normalization of transmitter release at neocortical synapses." *Science* 308:863-66.
- Koh T.W., P. Verstreken, et al. (2004) "Dap160/intersectin acts as a stabilizing scaffold required for synaptic development and vesicle endocytosis." *Neuron* 43:193–205.



- Koh, T. W. and H. J. Bellen (2003) "Synaptotagmin I, a  $\text{Ca}^{2+}$  sensor for neurotransmitter release." *Trends Neurosci* 26: 413-22.
- Kozyrev S.A, V.P. Nikitin, et al. (2007) "synapse-specific plasticity in command neurons during learning of edible snails under the action of caspase inhibitors." 144(6):755-9.
- Kudryashova I. V., M.V. Onufriev, et al. (2009) "Caspase-3 activity in hippocampal slices reflects changes in synaptic plasticity." *Neurosci Behav Physiol* 39(1):13-20.
- Kuromi H. and Y. Kidokoro (1998) "Two distinct pools of synaptic vesicles in single presynaptic boutons in a temperature-sensitive *Drosophila* mutant, shibire." *Neuron* 20:917–25.
- LaMonte B. H., K. E. Wallace, et al. (2002) "Disruption of dynein/dynactin inhibits axonal transport in motor neurons causing late-onset progressive degeneration." 34: 715-27.
- Lee, K. H., S. Lee, et al. (2006) "Dazl can bind to dynein motor complex and may play a role in transport of specific mRNAs." *EMBO J* 25(18): 4263-70.
- Lenzi, D. and H. von Gersdorff (2001) "Structure suggests function: the case for synaptic ribbons as exocytotic nanomachines." *Bioessays* 23:831-40.
- Leu, S. T., S. A. Jacques, et al. (2004) "Integrin  $\alpha 4 \beta 1$  function is required for cell survival in developing retina." *Dev Biol* 276(2): 416-30.

- Linden, D. J. and J. A. Connor (1995) "Long-term synaptic depression." *Annu Rev Neurosci* 18:319-57.
- Locke, F. S. (1894) "Notiz über den Einfluss physiologischer Kochsalzlösung auf dieelektrische Erregbarkeit von Muskel und Nerv." *zbl Physiol* 8: 166-67.
- Loewen, C. A., S. M. Royer, et al. (2006) "*Drosophila* synaptotagmin I null mutants show severe alterations in vesicle populations but calcium-binding motif mutants do not." *J Comp Neurol* 496(1): 1-12.
- Lossi, L., I. Tamagno, et al. (2004) "Molecular morphology of neuronal apoptosis: analysis of caspase 3 activation during postnatal development of mouse cerebellar cortex." *J Mol Histol* 35(6): 621-9.
- Louneva N., J.W. Cohen, et al. (2008) "Caspase-3 is enriched in postsynaptic densities and increased in Alzheimer's disease." *Am J Pathol* 173(5):1488-95.
- Madden, D. R. (2002) "The structure and function of glutamate receptor ion channels." *Nat Rev Neurosci* 3:91-101.
- Malinow, R., R. C. Malenka (2002) "AMPA receptor trafficking and synaptic plasticity." *Annu Rev Neurosci* 25:103-26.
- Manabe, R., L. Whitmore, et al. (2002) "Identification of a novel microtubule-associated protein that regulates microtubule organization and cytokinesis by using a GFP-screening strategy." *Curr Biol* 12(22): 1946-51.

- Marie B., S. T. Sweeney, et al. (2004) "Dap160/intersectin scaffolds the periaxial zone to achieve high-fidelity endocytosis and normal synaptic growth." *Neuron* **43**:207–219.
- Marrus, S. B., S. L. Portman, et al. (2004) "Differential localization of glutamate receptor subunits at the *Drosophila* neuromuscular junction." *J Neurosci* **24**:1406-15.
- Matafora, V., S. Paris, et al. (2001) "Molecular mechanisms regulating the subcellular localization of p95-APP1 between the endosomal recycling compartment and sites of actin organization at the cell surface." *J Cell Sci* **114**(Pt 24): 4509-20.
- Miki, H., M. Setou, et al. (2001) "All kinesin superfamily protein, KIF, genes in mouse and human." *Proc Natl Acad Sci U S A* **98**(13): 7004-11.
- Miller, K. E., J. DeProto, et al. (2005) "Direct observation demonstrates that Liprin-alpha is required for trafficking of synaptic vesicles." *Curr Biol* **15**(7): 684-9.
- Monier, S., F. Jollivet, et al. (2002) "Characterization of novel Rab6-interacting proteins involved in endosome-to-TGN transport." *Traffic* **3**(4): 289-97.
- Mukae, N., H. Yokoyama, et al. (2000) "Identification and developmental expression of inhibitor of caspase-activated DNase (ICAD) in *Drosophila melanogaster*." *J Biol Chem* **275**(28): 21402-8.

- Navarro, C., H. Puthalakath, et al. (2004) "Egalitarian binds dynein light chain to establish oocyte polarity and maintain oocyte fate." *Nat Cell Biol* 6(5): 427-35.
- Neher, E. (1998) "Vesicle pools and Ca<sup>2+</sup> microdomains: new tools for understanding their roles in neurotransmitter release." *Neuron* 20:389-99.
- Ni, B., X. Wu, et al. (1998) "Transient global forebrain ischemia induces a prolonged expression of the caspase-3 mRNA in rat hippocampal CA1 pyramidal neurons." *J Cereb Blood Flow Metab* 18:248-56.
- Ohtsuka, T., E. Takao-Rikitsu, et al. (2002) "Cast: a novel protein of the cytomatrix at the active zone of synapses that forms a ternary complex with RIM1 and munc13-1." *J Cell Biol* 158:577-90.
- Okada, Y., H. Yamazaki, et al. (1995) "The neuron-specific kinesin superfamily protein KIF1A is a unique monomeric motor for anterograde axonal transport of synaptic vesicle precursors." *Cell* 81(5): 769-80.
- Ouyang, Y. B., Y. Tan, et al. (1999) "Survival- and death-promoting events after transient cerebral ischemia: phosphorylation of Akt, release of cytochrome C and activation of caspase-like proteases." *J Cereb Blood Flow Metab* 19:1126-35.
- Paris, S., L. Za, et al. (2002) "Analysis of the subcellular distribution of avian p95-APP2, an ARF-GAP orthologous to mammalian paxillin kinase linker." *Int. J. Biochem. Cell Biol* 34(7): 826-37.
- Parks, A. L., K. R. Cook, et al. (2004) "Systematic generation of high-resolution deletion coverage of the *Drosophila melanogaster* genome."

Nat Genet 36(3): 288-92.

Parks, S. B., B. W. Popovich, et al. (2001). "Real-time polymerase chain reaction with fluorescent hybridization probes for the detection of prevalent mutations causing common thrombophilic and iron overload phenotypes." *Am J Clin Pathol* 115(3): 439-447.

Pazour, G. J., C. G. Wilkerson, et al. (1998) "A dynein light chain is essential for the retrograde particle movement of intraflagellar transport (IFT)." *J Cell Biol* 141:979–92.

Peters, P. J., V. W. Hsu, et al. (1995) "Overexpression of wild-type and mutant ARF1 and ARF6: distinct perturbations of nonoverlapping membrane compartments." *J Cell Biol* 128(6): 1003-17.

Petersen, S. A., R. D. Fetter, et al. (1997) "Genetic analysis of glutamate receptors in *Drosophila* reveals a retrograde signal regulating presynaptic transmitter release." *Neuron* 19:1237-48.

Pfister, K. K., E. M. Fisher, et al. (2005) "Cytoplasmic dynein nomenclature." *J Cell Biol* 171(3): 411-3.

Pfister, K. K., P. R. Shah, et al. (2006) "Genetic analysis of the cytoplasmic dynein subunit families." *PLoS Genet* 2(1): e1.

Phillips, G. R., J. K. Huang, , et al. (2001) "The presynaptic particle web: ultrastructure, composition, dissolution, and reconstitution." *Neuron* 32:63-7.

Phillis, R., D. Statton, et al. (1996) "Mutations in the 8 kDa dynein light chain gene disrupt sensory axon projections in the *Drosophila* imaginal CNS." *Development* 122:2955–63.

- Pinheiro, P. and C. Mulle (2006) "Kainate receptors." *Cell Tissue Res* 326(2):457-82.
- Poisson, N., E. Real, et al. (2001) "Molecular basis for the interaction between rabies virus phosphoprotein P and the dynein light chain LC8, dissociation of dynein-binding properties and transcriptional functionality of P." *J Gen Virol* 82: 2691–6.
- Premont, R. T., A. Claing , et al. (1998) "beta2-Adrenergic receptor regulation by GIT1, a G protein-coupled receptor kinase-associated ADP ribosylation factor GTPase-activating protein.." *Proc Natl Acad Sci U S A* 95(24): 14082-7.
- Premont, R. T., A. Claing, et al. (2000) "The GIT Family of ADP-ribosylation Factor GTPase-activating Proteins." *J Biol Chem* 275: 22373-80.
- Purves, D., R. B. Lotto, et al. (2001) "Why we see things the way we do: evidence for a wholly empirical strategy of vision." *Philos Trans R Soc Lond B Biol Sci* 356(1407), 285-97.
- Puthalakath, H., A. Villunger, et al. (2001) "Bmf: a proapoptotic BH3-only protein regulated by interaction with the myosin V actin motor complex, activated by anoikis." *Science* 293(5536): 1829-32.
- Puthalakath, H., D. C. Huang, et al. (1999) "The proapoptotic activity of the Bcl-2 family member Bim is regulated by interaction with the dynein motor complex." *Mol Cell* 3:287–6.
- Qin, G., T. Schwarz, et al. (2005) "Four different subunits are essential for expressing the synaptic glutamate receptor at neuromuscular junctions of *Drosophila*." *J Neurosci* 25:3209-18.

- Radhakrishna, H., O. Al-Awar, et al. (1999) "ARF6 requirement for Rac ruffling suggests a role for membrane trafficking in cortical actin rearrangements." *J Cell Sci* 112 ( Pt 6): 855-66.
- Ranjan R, Bronk P, Zinsmaier KE (1998) "Cysteine string protein is required for calcium secretion coupling of evoked neurotransmission in *Drosophila* but not for vesicle recycling." *J Neurosci* 18(3):956-64.
- Raoul, C., C. E. Henderson, et al. (1999) "Programmed cell death of embryonic motoneurons triggered through the Fas death receptor." *J Cell Biol* 147(5): 1049-62.
- Rasse, T. M., W. Fouquet, et al. (2005) "Glutamate receptor dynamics organizing synapse formation *in vivo*." *Nature Neuroscience* 8(7): 898-905.
- Raux, H., A. Flamand, et al. (2000) "Interaction of the rabies virus P protein with the LC8 dynein light chain." *J Virol* 74:10212–16.
- Reiff, D. F., P. R. Thiel, et al. (2002) "Differential regulation of active zone density during long-term strengthening of *Drosophila* neuromuscular junctions." *J Neurosci* 22(21): 9399-409.
- Rheuben, M. B., M. Yoshihara, et al. (1999) "Ultrastructural correlates of neuromuscular junction development." *Int Rev Neurobiol* 43: 69-92.
- Ridley, M. (1992) "Swallows and scorpionflies find symmetry is beautiful." *Science* 257(5068): 327-8.
- Rink, A., K. M. Fung, et al. (1995) "Evidence of apoptotic cell death after experimental traumatic brain injury in the rat." *Am J Pathol* 147(6): 1575-83.

- Rizzoli, S. O. and W. J. Betz (2005) "Synaptic vesicle pools." *Nat Rev Neurosci* 6:57-69.
- Roeleveld, N. and G. A. Zielhuis (1997) "The prevalence of mental retardation: a critical review of recent literature." *Dev Med Child Neurol* 39: 125-32.
- Rompolas, P., L. Pedersen, et al. (2007) "Chlamydomonas FAP133 is a dynein intermediate chain associated with the retrograde intraflagellar transport motor." *J Cell Sci* 120:3653–65.
- Rosenmund, C., J. Rettig, et al. (2003) "Molecular mechanisms of active zone function." *Curr Opin Neurobiol* 13:509-19.
- Rosenmund, C., Y. Stern-Bach, et al. (1998) "The tetrameric structure of a glutamate receptor channel " *Science* 280:1596-99.
- Roth, M. G. (1999) "Snapshots of ARF1: implications for mechanisms of activation and inactivation." *Cell* 97(2): 149-52.
- Rozov, A., N. Burnashev, et al. (2001) "Transmitter release modulation by intracellular Ca<sup>2+</sup> buffers in facilitating and depressing nerve terminals of pyramidal cells in layer 2/3 of the rat neocortex indicates a target cell-specific difference in presynaptic calcium dynamics." *J Physiol* 531:807-26.
- Rubin, G. M. and A. C. Spradling (1982) "Genetic transformation of *Drosophila* with transposable element vectors." *Science* 218(4570): 348-53.



- Sakaba, T., and E. Neher (2001) "Calmodulin mediates rapid recruitment of fast-releasing synaptic vesicles at a calyx-type synapse." *Neuron* 32:1119-31.
- Sakahira, H., M. Enari, et al. (1998) "Cleavage of CAD inhibitor in CAD activation and DNA degradation during apoptosis." *Nature* 391(6662): 96-9.
- Sakahira, H., M. Enari, et al. (1999) "Functional differences of two forms of the inhibitor of caspase-activated DNase, ICAD-L, and ICAD-S." *J Biol Chem* 274(22): 15740-4.
- Sambrook, J. and M. J. Gething (1989) "Protein structure. Chaperones, paperones." *Nature* 342(6247): 224-5.
- Schneggenburger, R. and E. Neher (2005) "Presynaptic calcium and control of vesicle fusion." *Curr Opin Neurobiol* 15:266-74.
- Schnorrer, F., K. Bohmann, et al. (2000) "The molecular motor dynein is involved in targeting swallow and bicoid RNA to the anterior pole of *Drosophila* oocytes." *Nat Cell Biol* 2(4): 185-90.
- Schroer, T. A. and R. B. Kelly (1985) "*In vitro* translocation of organelles along microtubules." *Cell* 40(4): 729-30.
- Schuster, C. M., A. Ultsch, et al. (1991) "Molecular cloning of an invertebrate glutamate receptor subunit expressed in *Drosophila* muscle." *Science* 254:112-14.
- Schuster, C. M., G. W. Davis, et al. (1996a) "Genetic dissection of structural and functional components of synaptic plasticity. I. Fasciclin II controls synaptic stabilization and growth." *Neuron* 17:641-54.

- Schuster, C. M., G. W. Davis, et al. (1996b) "Genetic dissection of structural and functional components of synaptic plasticity. II. Fasciclin II controls presynaptic structural plasticity." *Neuron* 17:655-67.
- Schoch S. and E. D. Gundelfinger (2006) "Molecular organization of the presynaptic active zone. " *Cell Tissue Res* 326(2):379-91.
- Seeburg, P. H. (1993) "The TiPS/TINS lecture: the molecular biology of mammalian glutamate receptor channels." *Trends Pharmacol Sci* 14:297-303.
- Sever, S., H. Damke, et al. (2000) "Dynamin:GTP controls the formation of constricted coated pits, the rate limiting step in clathrin-mediated endocytosis." *J Cell Biol* 150(5) :1137-48.
- Shapira, M., R. G. Zhai, et al. (2003) "Unitary assembly of presynaptic active zones from Piccolo-Bassoon transport vesicles." *Neuron* 38(2): 237-52.
- Shi, S., Y. Hayashi, et al. (2001) "Subunit-specific rules governing AMPA receptor trafficking to synapses in hippocampal pyramidal neurons." *Cell* 105:331-43.
- Shin, H., M. Wyszynski, et al. (2003) "Association of the kinesin motor KIF1A with the multimodular protein liprin-alpha." *J Biol Chem* 278(13): 11393-401.
- Shu, X., N. C. Shaner, et al. (2006) "Novel chromophores and buried charges control color in mFruits." *Biochemistry* 45(32): 9639-47.

- Sigrist, S. J., D. F. Reiff, et al. (2003) "Experience-dependent strengthening of *Drosophila* neuromuscular junctions." *J Neurosci* 23:6546-56.
- Sigrist, S. J., P. R. Thiel, et al. (2000) "Postsynaptic translation affects the efficacy and morphology of neuromuscular junctions." *Nature* 405:1062-5.
- Sigrist, S. J., P. R. Thiel, et al. (2002) "The postsynaptic glutamate receptor subunit DGluR-IIA mediates long-term plasticity in *Drosophila*." *J Neurosci* 22:7362-72.
- Sone, M., E. Suzuki, et al. (2000) "Synaptic development is controlled in the periaxial zones of *Drosophila* synapses." *Development* 127:4157-68.
- Stewart, B. A., H. L. Atwood, et al. (1994). "Improved stability of *Drosophila* larval neuromuscular preparations in haemolymph-like physiological solutions." *J Comp Physiol [A]* **175**(2): 179-191.
- Südhof, T. C. (2004) "The synaptic vesicle cycle." *Annu Rev Neurosci* 27:509-47.
- Tai, A. W., J. Z. Chuang, et al. (2001) "Cytoplasmic dynein regulation by subunit heterogeneity and its role in apical transport." *J Cell Biol* 153(7): 1499-509.
- Tajiri, S., S. Yano, et al. (2006) "CHOP is involved in neuronal apoptosis induced by neurotrophic factor deprivation." *FEBS Lett* 580(14): 3462-8.
- Takao-Rikitsu, E., S. Mochida, et al. (2004) "Physical and functional

interaction of the active zone proteins, CAST, RIM1, and Bassoon, in neurotransmitter release." J Cell Biol 164(2) 301-11.

Tanner, C. A., P. Rompolas, et al. (2008) "Three members of the LC8/DYNLL family are required for outer arm dynein motor function." Mol Biol Cell 19(9): 3724-34.

Theodosiou, NA, and T. Xu (1998) "Use of FLP/FRT system to study *Drosophila* development." Methods 14(4):355-65.

Turner, C. E., K. A. West, et al. (2001) "Paxillin–ARF GAP signaling and the cytoskeleton." Curr. Opin. Cell Biol. 13: 593-9.

Turner, C. E., M. C. Brown, et al. (1999) "Paxillin LD4 Motif Binds PAK and PIX through a Novel 95-kD Ankyrin Repeat, ARF-GAP Protein: A Role in Cytoskeletal Remodeling." J Cell Biol 145: 851-63.

Uchida, H., A. Kondo, et al. (2001) "PAG3/Papalpha/KIAA0400, a GTPase-activating protein for ADP-ribosylation factor (ARF), regulates ARF6 in Fcγ receptor-mediated phagocytosis of macrophages." J Exp Med 193(8): 955-66.

Vadlamudi, R. K., R. Bagheri-Yarmand, et al. (2004) "Dynein light chain 1, a p21-activated kinase 1-interacting substrate, promotes cancerous phenotypes." Cancer Cell 5(6): 575-85.

Vale, R.D. (2003) "The molecular motor toolbox for intracellular transport." Cell 112:467–80.

Vallee, R. B., J. C. Williams, et al. (2004) "Dynein: An ancient motor protein involved in multiple modes of transport." J Neurobiol 58(2): 189-200.

- Van Deerlin, V. M., P. M. Sleiman, et al. (2010). "Common variants at 7p21 are associated with frontotemporal lobar degeneration with TDP-43 inclusions." *Nat Genet* 42(3): 234-239.
- von Gersdorff H. and G. Matthews (1994) "Dynamics of synaptic vesicle fusion and membrane retrieval in synaptic terminals." *Nature* 367: 735–9.
- Von Gersdorff, H. (2001) "Synaptic ribbons: versatile signal transducers." *Neuron* 29:7-10.
- Wagh, D. A., T. M. Rasse, et al. (2006) "Bruchpilot, a protein with homology to ELKS/CAST, is required for structural integrity and function of synaptic active zones in *Drosophila*." *Neuron* 49(6): 833-44.
- Wang, Y., M. Okamoto, et al. (1997) "Rim is a putative Rab3 effector in regulating synaptic-vesicle fusion." *Nature*, 388: 593-98.
- Wang, Y., X. Liu, et al. (2002) "A family of RIM-binding proteins regulated by alternative splicing: Implications for the genesis of synaptic active zones." *Proc Natl Acad Sci U S A* 99:14464-69.
- Watanabe-Fukunaga, R., C. I. Brannan, et al. (1992) "Lymphoproliferation disorder in mice explained by defects in Fas antigen that mediates apoptosis." *Nature* 356(6367): 314-7.
- Waterman-Storer, C. M., S. B. Karki, et al. (1997) "The interaction between cytoplasmic dynein and dynactin is required for fast axonal transport." *PNAS* 94: 2212180-185.
- Weigmann, K., R. Klapper, et al. (2003) "FlyMove--a new way to look at development of *Drosophila*." *Trends Genet* 19(6): 310-1.

- Williams, M. E., X. Lu, et al. (2006) "UNC5A promotes neuronal apoptosis during spinal cord development independent of netrin-1." *Nat Neurosci* 9(8): 996-8.
- Wucherpennig, T., M. Wilsch-Bräuninger, et al. (2003) "Role of *Drosophila* Rab5 during endosomal trafficking at the synapse and evoked neurotransmitter release." *J Cell Biol* 161(3): 609-24.
- Wyllie, A. H. (1980) "Glucocorticoid-induced thymocyte apoptosis is associated with endogenous endonuclease activation." *Nature* 284(5756): 555-6.
- Xu, D., Y. Bureau, et al. (1999) "Attenuation of ischemia-induced cellular and behavioral deficits by X chromosome-linked inhibitor of apoptosis protein overexpression in the rat hippocampus." *J Neurosci* 19:5026-33.
- Yakovlev, A. G., S. M. Knoblach, et al. (1997) "Activation of CPP32-like caspases contributes to neuronal apoptosis and neurological dysfunction after traumatic brain injury." *J Neurosci* 17(19): 7415-24.
- Yang, P., D. R. Diener, et al. (2001) "Localization of calmodulin and dynein light chain LC8 in flagellar radial spokes." *J Cell Biol* 153:1315-26.
- Yokoyama, H., N. Mukae, et al. (2000) "A novel activation mechanism of caspase-activated DNase from *Drosophila melanogaster*." *J Biol Chem* 275(17): 12978-86.
- Zekri, L., K. Chebli, et al. (2005) "Control of fetal growth and neonatal survival by the RasGAP-associated endoribonuclease G3BP." *Mol Cell Biol* 25(19): 8703-16.

- Zhai, R. G., H. Vardinon-Friedman, et al. (2001) "Assembling the Presynaptic Active Zone." *Neuron*, 29: 131-43.
- Zhai, R.G. and H. J. Bellen (2004) "The architecture of the active zone in the presynaptic nerve terminal." *Physiology (Bethesda)* 19:262-70.
- Zhang, H., D. J. Webb, et al. (2003) "Synapse formation is regulated by the signaling adaptor." *GIT1. J Cell Biol* 161(1):131-42.
- Zhao, Z. S., E. Manser, et al. (2000) "Coupling of PAK-Interacting Exchange Factor PIX to GIT1 Promotes Focal Complex Disassembly." *Mol Cell Biol* 20(17): 6354-63.
- Zhu, J. J., J. A. Esteban, et al. (2000) "Postnatal synaptic potentiation: delivery of GluR4-containing AMPA receptors by spontaneous activity." *Nat Neurosci* 3:1098-106.
- Ziv, N. E. and C. C. Garner (2004) "Cellular and molecular mechanisms of presynaptic assembly." *Nat Rev Neurosci* 5(5): 385-99.
- Zucker, R. S, and W. G. Regehr (2002) "Short-term synaptic plasticity." *Annu Rev Physiol* 64:355-405.

# 8. Appendix

## 8.1 Table of Figures

<b>Figure 2.1</b> Electrical and chemical synapses.....	12
<b>Figure 2.2</b> Schematic diagram of interactions of CAZ proteins and the resulting network at the active zone.....	15
<b>Figure 2.3</b> Schematic diagram of the organization of the PSD at a mammalian excitatory synapse.....	19
<b>Figure 2.4</b> The targeted transport of synaptic cargoes and organelles from the soma to synapses.....	23
<b>Figure 2.5</b> The microtubule (MT)-based axonal transport contributes to the new synapse formation and presynaptic plasticity.....	24
<b>Figure 2.6</b> Schematic representation of the three mechanisms converging on caspase-3.....	29
<b>Figure 2.7</b> Life cycle of <i>Drosophila Melanogaster</i> .....	31
<b>Figure 2.8</b> Organization and development of <i>Drosophila</i> NMJ synapses.....	33
<b>Figure 2.9</b> Summary of GIT1 protein interactions and functions.....	37
<b>Figure 3.1</b> LR reaction... ..	44
<b>Figure 3.2</b> UAS/Gal4 system.....	56
<b>Figure 3.3</b> Schematics for deficiency generation.....	58
<b>Figure 4.1</b> DREP-2 interacts with Brp.....	71
<b>Figure 4.2</b> Schematic structure of DREP and DFF proteins.....	72
<b>Figure 4.3</b> <i>In situ</i> hybridization of <i>drep-2</i> in <i>Drosophila</i> embryos.....	75
<b>Figure 4.4.1</b> Genetic scheme used for FLP-FRT-based <i>drep-2</i> deletions.....	76
<b>Figure 4.4.2</b> <i>Drosophila drep-2</i> mutantgenesis.....	76
<b>Figure 4.4.3</b> DREP-2 antibody staining in immunoblot and immunofluorescence.....	79
<b>Figure 4. 5.1</b> DREP-2 colocalizes with Brp in CNS of <i>w<sup>1118</sup> Drosophila</i> 3 <sup>rd</sup> instar larvae.....	81
<b>Figure 4.5.2</b> DREP-4 staining in synapse.....	82
<b>Figure 4.6</b> NMJ morphological phenotype in 3 <sup>rd</sup> instar larvae of the <i>drep-2</i> mutant....	83
<b>Figure 4.7</b> Strawberry tagged DREP-2 molecules show bidirectional axonal transports in <i>Drosophila</i> 3 <sup>rd</sup> instar larvae.....	84



<b>Figure 4.8</b> An accumulation of large size vesicles and floating electron dense structure in <i>digit</i> mutant by EM.....	85
<b>Figure 5.1</b> Schematic overview of GIT protein structure and <i>digit</i> mutantgenesis ....	93
<b>Figure 5.2</b> <i>DGIT</i> is expressed at boutons of L3 NMJ.....	95
<b>Figure 5.3</b> <i>Drosophila</i> GIT interacts with StnB <i>in vivo</i> .....	96
<b>Figure 5.4</b> Loss of glutamate receptor at glutamatergic boutons of <i>digit</i> mutants.....	97
<b>Figure 5.5</b> Reduction in StnB level at <i>digit</i> mutant NMJs.....	98
<b>Figure 5.6</b> A depletion of synaptic vesicles and accumulation of large size vesicles and membrane recycling intermediates in <i>digit</i> mutant by EM.....	99
<b>Figure 5.7</b> Walking and geotaxis ability in <i>digit</i> mutants.....	103
<b>Figure 6.1</b> Schematic overview of protein structures of DJM-1.....	110
<b>Figure 6.2</b> <i>In situ</i> hybridization of <i>djm-1</i> in <i>Drosophila</i> embryos.....	112
<b>Figure 6.3</b> <i>In situ</i> hybridization of <i>djm-1</i> in <i>Drosophila</i> 3 <sup>rd</sup> larvae.....	112
<b>Figure 6.4</b> <i>Drosophila jm-1</i> imprecise excision scheme using the p-element line P{SUPor-P}KG04920 closed to <i>djm-1</i> .....	114
<b>Figure 6.5</b> Walking and geotaxis ability in <i>digit</i> mutant.....	115
 <b>Table 4.1</b> The <i>drep-2</i> mRNA enrichment in different tissues of adult flies and larvae detected by RT-PCR.....	74
 <b>Table 5.1</b> Rescue of <i>digit</i> mutant lethality by tissue-specific expression of <i>digit</i> .....	94
 <b>Table 5.2</b> The <i>digit</i> mRNA enrichment in different tissues of adult flies and larvae detected by RT-PCR.....	95

## **8.2 Abbreviations**

**ABP:** AMPA RECEPTOR-BINDING PROTEIN

**AEL:** AFTER EGG-LAYING

**AKAP79:** A-KINASE ANCHOR PROTEIN 79

**AMPA:** A-AMINO-3-HYDROXYL-5-METHYL-4-ISOXALONE  
PROPIONIC ACID

**ANK:** ANKYRIN REPEATS

**AP:** ACTION POTENTIAL

**ARF:** ADP-RIBOSYLATION FACTOR

**ARFGAPs:** ADP-RIBOSYLATION FACTOR (ARF)-DIRECTED  
GTPASE ACTIVATING PROTEINS (GAPs)

**AZ:** ACTIVE ZONE

**Brp:** BRUCHPILOT

**Cac:** CACOPHONY

**CAD:** CASPASE-ACTIVATED DNASE

**CAST:** CYTOMATRIX AT THE ACTIVE ZONE-ASSOCIATED  
STRUCTURAL PROTEIN

**CAZ:** CYTOMATRIX AT THE ACTIVE ZONE

**CIDE:** Cell death-inducing DFF45-like effector

**CNS:** CENTRAL NERVOUS SYSTEM

**CNTF:** CILIARY NEUROTROPHIC FACTOR

**CSP** Cysteine string protein

**DAG:** DIACYLGLYCEROL

**DFF40:** DNA FRAGMENTATION FACTOR 40 KDa

**DGLUR:** *DROSOPHILA* GLUTAMATE RECEPTOR SUBUNIT

**DHC:** DYNEIN HEAVY CHAIN

**DLC:** DYNEIN LIGHT CHAIN

**DLG:** DISCS-LARGE

**DREP:** DFF RELATED PROTEIN

**ECL:** ENHANCED CHEMI-LUMINESCENCE

**ECM:** EXTRACELLULAR MATRIX

**EE:** EARLY ELIMINATION

**EGTA:** THYLENEGLYCOL-*BIS*(B-AMINOETHYL)-N,N,N',N'-TETRAACETIC ACID

**EM:** ELECTRON MICROSCOPY

**ER:** ENDOPLASMATIC RETICULUM

**ERC:** ELKS/RAB6-INTERACTING PROTEIN/CAST

**Ex:** EXCISION

**FAK:**  $\beta$ PIX ADHESION KINASE

**FAS:** *DROSOPHILA* NCAM HOMOLOGUE FASCICLIN I

**FA:** FOCAL ADHESION

**FE:** FOCAL ELECTRODE

**FLP:** FLIPPASE RECOGNITION TARGET

**FRAP:** FLUORESCENCE RECOVERY AFTER PHOTOBLEACHING

**FRT:** FLIPPASE RECOGNITION TARGET

**GABA:**  $\Gamma$ -AMINOBUTYRIC ACID

**GAPs:** GTPASE ACTIVATING PROTEINS

**GDNF:** GLIAL CELL-DERIVED NEUROTROPHIC FACTOR

**GEF:** GUANINE NUCLEOTIDE EXCHANGE FACTOR

**GFP:** GREEN FLUORESCENT PROTEIN

**GIT:** *G-PROTEIN* COUPLED RECEPTOR KINASE INTERACTING PROTEIN

**GluRIID:** GLUTEMATE RECEPTOR IID

**GPCR:** (AG)-RECEPTOR G-PROTEIN-COUPLED RECEPTOR

**GRIP:** GLUTAMATE RECEPTOR INTERACTING PROTEIN

**GRKBD:** G-PROTEIN-COUPLED RECEPTOR KINASE-BINDING DOMAIN

**HL-3:** HEMOLYMPH-LIKE 3

**HRP:** HORSE RADISH PEROXIDASE

**ICAD:** INHIBITOR of CAD

**IKK:** I $\kappa$ B KINASE

**IQ:** INTELLIGENCE QUOTIENT

**KA:** KAINATE

**KCA CHANNEL** CALCIUM-ACTIVATED POTASSIUM CHANNEL

**KHC:** KINESIN HEAVY CHAIN

**KLC:** KINESIN LIGHT CHAIN

**LiAc:** LITHIUM ACETATE

**LTD:** LONG-TERM DEPRESSION

**LTP:** LONG-TERM POTENTIATION

**M:** MOUSE

**MAB:** MONOCLONAL ANTIBODY

**mEJC:** MINIATURE EVOKED JUNCTIONAL CURRENT

**MR:** MENTAL RETARDATION

**MRFP:** MONOMERIC RED FLUORESCENT PROTEIN

**MS:** MASS SPECTROMETRY

**MStraw:** MONOMERIC STRAWBERRY

**MT:** MICROTUBULIN

**MUNC13:** MAMMALIAN HOMOLOGUE of UNC13

**MVB:** MULTIVESICULAR BODIES

**NCAM:** NEURONAL CELL ADHESION MOLECULE

**NF- $\kappa$  B:** NUCLEAR FACTOR-KAPPA B

**NGF:** NERVE GROWTH FACTOR

**NGS:** GOAT SERUM

**NMDA:** *N*-METHYL-D-ASPARTATE

**NMJ:** NEUROMUSCULAR JUNCTION

**ORF:** OPEN READING FRAME

**PAK:** P21-ASSOCIATED KINASE

**PARP:** POLY ADENOSINE 5-DIPHOSPHATE–RIBOSE POLYMERASE

**PBS:** PAXILLIN-BINDING SUBDOMAIN (IN THE CHAPTER OF GIT)

**PBS:** PHOSPHATE-BUFFERED SALINE (IN THE CHAPTER OF MATERIALS AND METHODS)

**PBT:** PHOSPHATE-BUFFERED SALINE WITH TRITON

**PCD:** PROGRAMMED CELL DEATH

**PCR:** POLYMERASE CHAIN REACTION

**PEG:** POLYETHYLENE GLYCOL

**PFA:** PARAFORMALDEHYDE

**PIX:** PAK-INTERACTIVE EXCHANGE FACTOR

**PNS:** PERIPHERAL NERVOUS SYSTEM

**PSD:** POSTSYNAPTIC DENSITY

**PTDINS(3,4,5)P3:** PHOSPHATIDYLINOSITOL (3,4,5)-TRISPHOSPHATE

**PTDINS(4,5)P2:** PHOSPHATIDYLINOSITOL 5-PHOSPHATE, PHOSPHATIDYLINOSITOL (4,5)-BISPHOSPHATE

**PTV:** PICCOLO-BASSOON TRANSPORT VESICLE

**RB:** RABBIT

**RIM:** RAB3-INTERACTING MOLECULE

**RNAi:** RNA INTERFERENCE

**R<sub>s</sub>:** SERIES RESISTANCE

**RT:** ROOM TEMPERATURE

**SAP-97:** SYNAPSE-ASSOCIATED PROTEIN

**SD:** *STANDARD* DEVIATIONS

**SEM:** *STANDARD* ERROR OF THE MEAN

**SHD:** SPA2 HOMOLOGY DOMAIN

**SNAP:** SOLUBLE *N*-ETHYLMALEIMIDE-SENSITIVE FACTOR  
**SNARE:** SNAP RECEPTOR  
**SSR:** SUBSYNAPTIC RETICULUM  
**STED:** STIMULATED EMISSION DEPLETION FLUORESCENCE  
MICROSCOPY  
**StnB:** STONED B  
**SV:** SYNAPTIC VESICLE  
**SVs:** SYNAPTIC VESICLES  
**Syn:** SYNAPSIN  
**Syt:** SYNAPTOTAGMIN  
**TARP:** TRANSMEMBRANE AMPA RECEPTOR REGULATORY  
PROTEIN  
**TBI:** TRAUMATIC BRAIN INJURY  
**TE:** TRIS-EDTA  
**TGN:** TRANS-GOLGI NETWORK  
**TNF:** TUMOR NECROSIS FACTOR  
**TRK:** TYROSINE KINASE RECEPTOR  
**Tx:** TRITON X  
**UAS:** UPSTREAM ACTIVATING SEQUENCE  
**UNC13:** UNCOORDINATED PROTEIN-13  
**UTR** UNTRANSLATED REGION  
**VLM:** VENTRAL LONGITUDINAL MUSCLE  
**XLMR:** X-LINKED MENTAL RETARDATION  
**Y2H:** YEAST-TWO-HYBRID  
**YPDA:** YEAST, PEPTONE, DEXTROSE, ADENINE MEDIUM

## **8.3 Publications**

- Daniel Banovic, Omid Korramshahi, David Oswald, Carolin Wichmann, Tamara Riedt, Wernhner Fouquet, **Rui Tian**, Stephan Sigrist, and Hermann Aberle (2010) *Drosophila* neuroligin 1 promotes growth and postsynaptic differentiation at glutamatergic neuromuscular junctions, *Neuron*, 66( 5): 724-738
- **Rui Tian**, Sheng-Jian Li, Dong-Liang Wang, Zhen Zhao, Ying Liu, Rong-Qiao He (2004) The acidic C-terminal domain stabilizes the chaperone function of protein disulfide isomerase. *J. Biol. Chem.*, 279(47): 48830-5
- **Rui Tian**, Chun-Lai Nie, Rong-Qiao He (2004) Chaperone-like manner of human neuronal tau toward lactate dehydrogenase. *Neurochemical Research*, 29(10): 1863-72
- **Rui Tian**, Mei-Hua Qu, Ying Liu, Rong-Qiao He (2004) Aggregated tau induces the inactivation and conformational changes of lactate dehydrogenase. *Progress in Biochemistry and Biophysics*, 31(7):596-9
- Mei-Hua Qu, Hui Li, **Rui Tian**, Chun-Lai Nie, Bao-Shan Han, Rong-Qiao He (2004) Neuronal tau induces DNA conformational changes observed by atomic force microscopy. *Neuroreport*, 15(18):2723-7